

8-2024

Exploring Overbank Sediment Deposition Variation in Heavily Modified Floodplains of the Lower Mississippi River: A Sedimentological and Geophysical Analysis

Seth Fradella

Follow this and additional works at: https://aquila.usm.edu/masters_theses



Part of the [Geology Commons](#), [Geomorphology Commons](#), [Geophysics and Seismology Commons](#), [Sedimentology Commons](#), and the [Soil Science Commons](#)

Recommended Citation

Fradella, Seth, "Exploring Overbank Sediment Deposition Variation in Heavily Modified Floodplains of the Lower Mississippi River: A Sedimentological and Geophysical Analysis" (2024). *Master's Theses*. 1056. https://aquila.usm.edu/masters_theses/1056

This Masters Thesis is brought to you for free and open access by The Aquila Digital Community. It has been accepted for inclusion in Master's Theses by an authorized administrator of The Aquila Digital Community. For more information, please contact aquilastaff@usm.edu.

EXPLORING OVERBANK SEDIMENT DEPOSITION VARIATION IN HEAVILY
MODIFIED FLOODPLAINS OF THE LOWER MISSISSIPPI RIVER: A
SEDIMENTOLOGICAL AND GEOPHYSICAL ANALYSIS

by

Seth M. Fradella

A Thesis
Submitted to the Graduate School,
the College of Arts and Sciences
and the School of Biological, Environmental, and Earth Sciences
at The University of Southern Mississippi
in Partial Fulfillment of the Requirements
for the Degree of Master of Science

Committee:

Dr. Franklin T. Heitmuller, Committee Chair
Dr. T. Mark Puckett
Dr. David H. Holt

August 2024

COPYRIGHT BY

Seth M. Fradella

2024

Published by the Graduate School



ABSTRACT

Since the 1930s, the Lower Mississippi River (LMR) has experienced large-scale modifications to the channel profile and surrounding floodplains through dams, dikes, revetments, dredging, and channel cutoffs. Although these changes have improved navigation and reduced flood risk, unanticipated changes to the major flood return period, individual flood severity and duration, and sediment regime have become increasingly apparent and sometimes problematic, such as the 2011 and 2018-2020 floods. Flood control levees along the LMR have reduced the natural floodplain area by 70-90%, resulting in heavily restricted overbank storage capacity of water and sediment. For the same flood events in recent history, Natchez, MS, has experienced record high flood stages and much longer and more severe inundation compared to Vicksburg, MS. This research focuses on integration of clastic sedimentary characteristics and ground-penetrating radar (GPR) data from overbank profiles at Shipland WMA (48 km northwest of Vicksburg) and St. Catherine Creek NWR (18 km southwest of Natchez) using five 6-meter floodplain sediment cores from both locations in meander scroll and backswamp depositional environments. Through analyzing systematic depositional changes through time and testing the capabilities of GPR in delineating subsurface wetland facies, probable event markers for the historic 1973, 2011, and 2018-2020 floods were defined and correlated across each site. These events only remain distinctive due to ^{14}C temporal estimates; without a scale for time, these flood deposits would be no more distinctive than frequent, minor flood events. GPR is limited to correlation between boreholes and cannot be used to identify flood events alone.

ACKNOWLEDGMENTS

This project would not have been possible without a multitude of collaborators and friends. Foremost, I would like to thank Dr. Frank Heitmuller for his guidance throughout this process and willingness to answer any questions. Dr. Mark Puckett and Dr. David Holt have also been instrumental in shaping this research, and I am especially thankful for Dr. Holt's guidance with GPR.

My biggest collaborator and good friend, Chantz Black, was essential to the development and interpretation of this project, whether he was helping process cores or just someone to complain with. Jessica Prince also helped around the lab in these aspects. Guidance from Dr. Davin Wallace and Shara Gremillion is much appreciated, having assisted through various steps (core processing, data logging, ^{14}C , grain size) and allowing me to utilize their lab space.

Sediment core collection was courtesy of the gentlemen from Walker-Hill Environmental Inc., with help on site from Marshall and his team as well as Loren Stearman, Saysha Sebren, and Mary Woodhall. I would like to recognize Dr. Carlton Anderson and Michael Amelunke's contributions to this project by providing spatial data and GPS hardware.

Finally, I would like to thank the U.S. Army Corps of Engineers Vicksburg District for funding this project and allowing me to dive into such an interesting and multi-faceted field of study.

DEDICATION

Dedicated to my lovely wife, Morgan, whose support and encouragement made this project possible.

TABLE OF CONTENTS

ABSTRACT iii

ACKNOWLEDGMENTS iv

DEDICATION v

LIST OF TABLES ix

LIST OF ILLUSTRATIONS x

LIST OF ABBREVIATIONS xii

CHAPTER I – INTRODUCTION 1

 1.1 Floodplain Processes 2

 1.2 Effects of River Engineering on Flood and Sedimentation Dynamics 3

 1.2.1 U.S. Army Corps of Engineers LMR Legacy Projects 3

 1.2.2 Embanked Floodplains of the Lower Mississippi River 4

 1.3 Flooding 7

 1.4 Research Questions and Hypotheses 8

CHAPTER II – GEOLOGIC SETTING 11

 2.1 Geomorphic Background and Evolution 11

 2.2 Meandering River Facies and Typical Sedimentation 12

 2.2.2 Point Bar and Meander Scroll Sedimentation 13

 2.2.3 Natural Levee and Backswamp Sedimentation 15

CHAPTER III – LITERATURE REVIEW 16

CHAPTER IV – METHODS.....	22
4.1 Assessment for Anthropogenic Fluvial Change	22
4.2 Study Areas.....	22
4.2.1 Shipland WMA near Mayersville, MS (SWMA)	22
4.2.2 St. Catherine Creek NWR near Natchez, MS (SCC).....	24
4.3 Sediment Cores	25
4.4 Isotopic Dating.....	26
4.5 Grain Size Analyses	27
4.6 Ground-Penetrating Radar	27
CHAPTER V – RESULTS	36
5.1 Sediment Cores and Grain Size	36
5.1.1 Sediment Characteristics.....	37
5.1.1.1 Shipland WMA.....	37
5.1.1.2 St. Catherine Creek NWR.....	37
5.2 ¹⁴ C Dating.....	45
5.3 GPR.....	46
5.3.2 Shipland WMA	48
5.3.3 St. Catherine Creek NWR.....	48
CHAPTER VI – DISCUSSION.....	51
6.1 Sedimentary Structures and Depositional Trends.....	51

6.1.1 Shipland WMA	53
6.1.2 St. Catherine Creek NWR.....	54
6.2 GPR Interpretation	55
6.2.1 Shipland WMA	56
6.2.2 St. Catherine Creek NWR.....	56
6.3 Flood Event Interpretations.....	59
6.3.1 1973 Flood	59
6.3.1.1 Shipland WMA	59
6.3.1.2 St. Catherine Creek NWR.....	59
6.4 2011 Flood	60
6.4.1.1 Shipland WMA	60
6.4.1.2 St. Catherine Creek NWR.....	60
6.5 2018-2019 and 2020 Floods.....	61
6.5.1.1 Shipland WMA	61
6.5.1.2 St. Catherine Creek NWR.....	62
CHAPTER VII – CONCLUSIONS.....	67
APPENDIX A – Data Tables.....	71
APPENDIX B – Sediment Core Data.....	73
WORKS CITED	83

LIST OF TABLES

Table 3.1 Literature addressing the effects of human interaction on the Lower Mississippi River..... 17

Table 3.2 Literature addressing general and flood sedimentation in the Lower Mississippi River..... 18

Table 3.3 Fundamental literature and applications of ground-penetrating radar to subsurface floodplain analysis of the Lower Mississippi River. 21

Table 5.1 GPR parameters chosen for data processing at Shipland WMA and St. Catherine Creek NWR. 47

Table A.1 The 50 highest flood crests recorded at Vicksburg and Natchez, MS 71

Table A.2 ¹⁴C data collected from all cores. 72

Table B.1 Shipland WMA Core 1 grain size data 73

Table B.2 Shipland WMA Core 2 grain size data 74

Table B.3 Shipland WMA Core 3 grain size data 75

Table B.4 Shipland WMA Core 4 grain size data 76

Table B.5 Shipland WMA Core 5 grain size data 77

Table B.6 St. Catherine Creek NWR Core 1 grain size data 78

Table B.7 St. Catherine Creek NWR Core 2 grain size data 79

Table B.8 St. Catherine Creek NWR Core 3 grain size data 80

Table B.9 St. Catherine Creek NWR Core 4 grain size data 81

Table B.10 St. Catherine Creek NWR Core 5 grain size data 82

LIST OF ILLUSTRATIONS

Figure 1.1 Floodplain Map 5

Figure 1.2 Historical Flood Variance Between Vicksburg and Natchez, MS 8

Figure 2.1 Divisions of the Lower Mississippi River 12

Figure 2.2 Overview map of the Shipland WMA and St. Catherine Creek NWR study sites along the Lower Mississippi River 13

Figure 2.3 Idealized point bar stratification sequence 14

Figure 2.4 General cross section of a point bar and cut bank of a meandering stream 15

Figure 3.1 GPR radar facies of low-gradient floodplains 20

Figure 4.1 Shipland WMA study site with core collection points 23

Figure 4.2 Buried tree bases and limb accumulation at Shipland WMA..... 24

Figure 4.3 St. Catherine Creek NWR study site with core collection points..... 25

Figure 4.4 Parabolic reflectors in GPR..... 29

Figure 4.5 Strata reflectors in GPR..... 29

Figure 4.6 Subsurface mapping using GPR..... 30

Figure 4.7 GPR correlation between sediment cores..... 32

Figure 4.8 Composite overview image of Shipland WMA 34

Figure 4.9 Composite overview image of St. Catherine Creek NWR 35

Figure 5.1 Sediment core photos from Shipland WMA 39

Figure 5.2 Sediment core photos from St. Catherine Creek NWR..... 40

Figure 5.3 Shipland WMA sand/silt/clay graphs 41

Figure 5.4 St. Catherine Creek NWR sand/silt/clay graphs..... 42

Figure 5.5 Shipland WMA grain size percentile trends..... 43

Figure 5.6 St. Catherine Creek NWR grain size percentile trends	44
Figure 5.7 Processed GPR transect A-A' at Shipland WMA	49
Figure 5.8 Processed GPR transect B-B' at Shipland WMA.....	49
Figure 5.9 Processed GPR transect A-A' at St. Catherine Creek NWR.....	50
Figure 5.10 Processed GPR transect B-B' at St. Catherine Creek NWR	50
Figure 6.1 GPR interpretations of Shipland WMA transect A-A'	57
Figure 6.2 GPR interpretations of Shipland WMA transect B-B'	57
Figure 6.3 GPR interpretations of St. Catherine Creek NWR transect A-A'	58
Figure 6.4 GPR interpretations of St. Catherine Creek NWR transect B-B'	58
Figure 6.5 Overbank profile interpretations of Shipland WMA transect A-A'	63
Figure 6.6 Overbank profile interpretations of Shipland WMA transect B-B'	64
Figure 6.7 Overbank profile interpretations of St. Catherine Creek NWR transect A-A'	65
Figure 6.8 Overbank profile interpretations of St. Catherine Creek NWR transect B-B'	66

LIST OF ABBREVIATIONS

<i>GNSS</i>	Global Navigation Satellite System
<i>GPR</i>	Ground-Penetrating Radar
<i>GPS</i>	Global Positioning System
<i>LMR</i>	Lower Mississippi River
<i>RTK</i>	Real Time Kinematics
<i>SCC</i>	St. Catherine Creek NWR
<i>SWMA</i>	Shipland WMA
<i>USACE</i>	U.S. Army Corps of Engineers

CHAPTER I – INTRODUCTION

River floodplains are essential components of natural ecosystems and play a central role in numerous human endeavors, including agriculture, flood mitigation, and contaminant sequestration. Throughout the last century, floodplain areas have been reduced through construction of artificial levees (dikes) or otherwise affected by upstream activities such as dam construction, channelization, and urbanization (Remo and others, 2009). Among major river-floodplain systems of the world, the Lower Mississippi River (LMR) is one of the most heavily impacted by a legacy of engineering and land use in the basin (Kesel, 2003; Remo and others, 2009). Flooding of the Lower Mississippi River (LMR) potentially threatens thousands of inhabitants across millions of acres containing cities and highly productive, economically viable farmland. Understanding, controlling, and mitigating the effects of human-induced changes in land use and river and flood mechanisms can save money and lives for those in flood-prone areas.

In a river as heavily trafficked as the Mississippi River, management and restoration projects are vital in maintaining safe and stable ecosystems. By analyzing flood dynamics and historical floodplain sedimentation in a down-gradient, heavily modified segment of the Mississippi River, assessments can be made of morphological and sedimentological changes through time that may induce further changes in flood and sediment regime that could become problematic for society and ecosystems.

This research seeks to analyze the overbank record near Vicksburg and Natchez, MS, to find evidence of systematic changes in flood sedimentation dynamics.

1.1 Floodplain Processes

Meandering stream geomorphology includes a variety of depositional environments (e.g., channel, point bar, natural levee, backswamp, crevasse splay, etc.). Sedimentological and hydrological processes affect deposition styles and morphologies of these sedimentary facies, and disruptions to the natural, self-regulating balance of these controls can alter the sediment regime, flood processes, and storage mechanics of a meandering river (Saucier, 1994; Meade and Moody, 2010). Lateral point bar accretion, overbank vertical accretion, and braid-channel accretion are the primary floodplain depositional processes (Nanson and Croke, 1992). Point bar and overbank accretion are of greater concern when analyzing geomorphology of the Lower Mississippi Valley. Point bar migration can be surficially expressed as low-relief to well-developed meander scrolls capped by overbank sediments on the convex bank of a meander bend (Nanson and Croke, 1992). Overbank sedimentation is observed along natural levees, crevasse splays, and backswamps of low gradient streams that occur during high stage flow conditions that overtop the channel banks (Nanson and Croke, 1992). Floodplains can be classified by sediment constituents and flow conditions to define stream power and erosional resistance (*non-cohesive* sand and gravel vs. *cohesive* silt and clay; *high-*, *medium-*, and *low-energy* depositional environments) (Nanson and Croke, 1992). Low gradient meandering stream floodplains such as those of the Lower Mississippi River are classified as medium-energy non-cohesive to low-energy cohesive floodplains (Nanson and Croke, 1992).

Floodplains form by both lateral (channel migration, ridges and swales, bedload) and vertical (overbank flooding, horizontal bedding/lamination, fine sediment) accretion

processes (Brierley and Fryirs, 2005). Overbank deposition occurs in zones of hydrologic deceleration that enable suspended load to settle, resulting in generally flattened, low-relief floodplains (Bridge, 2003). Low elevation locations proximal to the channel are expected to experience higher deposition rates of coarser sediments compared to higher elevations and/or locations farther from the main channel (Bridge, 2003). Generally, major flood events deposit millimeters to centimeters of fine sediments, and the average sedimentation rate is inversely related to flood duration (Bridge, 2003). Erosion of the floodplain is minimal and constrained to areas with sparse vegetation and locations that accelerate the flow of flood waters; therefore, preservation potential of overbank deposits is highest in topographically low areas of the floodplain (Bridge, 2003). These progressive accumulations of fine flood sediments account for the strata observed in floodplain sequences. Distal from the channel, fine sediment accumulation may result in vertical uniformity through the sedimentary profile (Bridge, 2003; Brierley and Fryirs, 2005).

1.2 Effects of River Engineering on Flood and Sedimentation Dynamics

1.2.1 U.S. Army Corps of Engineers LMR Legacy Projects

The Mississippi River Commission was created in 1879 under the U.S. Army Corps of Engineers (USACE) to bolster river navigation as well as mitigate floods and flood-incurred damages (USACE, 2023a). The Great Mississippi Flood of 1927 resulted in an overhaul of flood control projects, resulting in the Flood Control Act of 1928 and, consequently, the foundation of the Mississippi River and Tributaries Project, which includes constructed levees, floodwalls, and floodways as well as channelization efforts and tributary improvements (USACE, 2023b). Flood control efforts have contributed to

reduce inundation impacts for nearly a century, but changes in flood regime and sediment dynamics in the wake of long-term channel engineering have become apparent – such as increased frequency of severe, long-duration flood events, gradual increases in bedload, and shifts from transport zones to aggradational sequences (Kesel, 2003; Pinter and others, 2006; Remo and others, 2009; Heitmuller and others, 2017; Munoz and others, 2018).

1.2.2 Embanked Floodplains of the Lower Mississippi River

The Lower Mississippi River has an extensive history of channel engineering to promote navigation and protect inhabited land along the floodplains. These legacy projects have disrupted the natural equilibrium of the fluvial system, resulting in unexpected changes in sedimentation and flood regime, such as alterations to overbank sediment regime and systemic changes driving bank erosion (Heitmuller and others, 2017; Kesel, 2003). The lowermost Mississippi River floodplains are heavily modified and restricted compared to their natural bounds (Fig. 1.1) (Kesel, 2003; Remo and others, 2009; Horowitz, 2010; Meade and Moody, 2010; Hudson and others, 2013). Other human interactions further complicate the dynamics of hydrology and sedimentation in the Mississippi River, including climate change, land use (e.g., urbanization, agriculture, deforestation, etc.), mineral and hydrocarbon extraction, and water use (Horowitz, 2010; Russell and others, 2021).



Figure 1.1 *Floodplain Map*

Map comparing natural floodplain extent to modern floodways with notable engineered structures in the Vicksburg District of the LMR (adapted from Remo and others, 2009).

Recently, the Lower Mississippi River has experienced extensive and unprecedented floods – such as those from 2011 and 2018-2020. These flood events are problematic and dangerous because artificial levees and other flood prevention structures alter sedimentation mechanics and disrupt available overbank storage capacity, resulting in restricted sediment supply, channel deterioration, and reduced bank erosion. These changes result from reducing the size of the natural floodplain and limiting channel-floodplain connectivity with cutoffs, dikes, revetments, etc., as well as by artificially

controlling water and sediment flow that disrupts the natural equilibrium (Kesel, 2003; Heitmuller and others, 2017). Major flood events (100-year return period) have become 20% more frequent over the last 500 years; 75% of this change is attributed to channel modification (Pinter and others, 2006; Munoz and others, 2018). Although the Mississippi River overbank sedimentary record is often regarded as the "textbook" meandering stream depositional facies (Fisk, 1944; Saucier, 1994; Russell and others, 2021), the question remains whether historical understanding of fluvial sedimentation is still applicable to the embanked floodplains of the LMR after decades of artificial engineering and systemic imbalance. Some scientists believe human interference has drastically changed – and will continue to change – the natural equilibrium beyond typical idealized models (Russell and others, 2021). Several researchers have noted that historical river engineering has altered flood and sediment dynamics from the natural equilibrium (Kesel, 2003; Pinter and others, 2006; Remo and others, 2009; Heitmuller and others, 2017; Kesel, 2003; Munoz and others, 2018).

Floods can be preserved in the overbank sedimentary record and may be used to infer flood frequency and severity at a given location. By analyzing the overbank sedimentary record at multiple sites, constructing an historical record of flood-related sedimentation may be possible in order to determine spatial and temporal variation of flood history between locations. Variations may be assessed for artificial/accelerated changes in the fluvial system not expected from typical sedimentary sequence development. This study seeks to analyze any changes in flood patterns in overbank sediment cores at Shipland Wildlife Management Area near Mayersville, MS (50 km north of Vicksburg) and St. Catherine Creek National Wildlife Refuge near Natchez, MS.

1.3 Flooding

Although the Mississippi River is heavily managed by the U.S. Army Corps of Engineers near Vicksburg (Steele Bayou Control Structure and Muddy Bayou Control Structure on the Yazoo River) and Natchez (Old River Control Structure), MS, by water control structures and artificial levees, inundation has still continued to be problematic in recent history (Fig. 1.2, Appendix A.1). This trend may correlate with river engineering legacy projects altering the flood and sediment regime (Heitmuller and others, 2017; Kesel, 2003; Munoz and others, 2018; Pinter and others, 2006; Remo and others, 2009). Given the recent outlier of historically high flood crests – and the consideration that Natchez has recently experienced higher and longer-duration inundation than Vicksburg for the same flood – the location at St. Catherine Creek NWR is expected to experience more frequent and potentially more severe flood events (not considering the effects of sediment translations regarding upstream cutoffs nor the influence of the Old River Control Complex). Furthermore, flood control structures downstream of Shipland WMA may reduce the potential for backwater flood effects along the Mississippi River in that region.

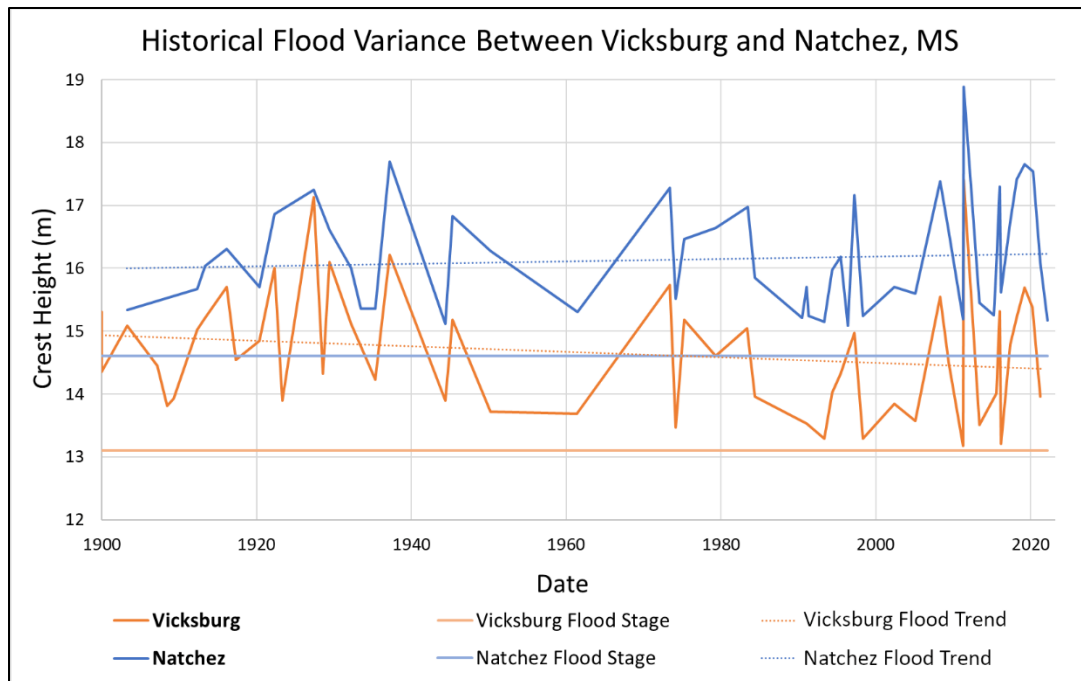


Figure 1.2 *Historical Flood Variance Between Vicksburg and Natchez, MS*

Historical variance in river crest height from the 50 highest flood crests recorded at Vicksburg and Natchez, MS reported by NOAA, including flood crest trends over time and flood stage (Vicksburg: 13.1 m/43 ft; USACE, 2023d; Natchez: 14.6 m/48 ft; USACE, 2023c). Values reported in Appendix A, Table A.1.

1.4 Research Questions and Hypotheses

(1) *Do overbank sedimentary deposits of major floods remain distinctive with progressive burial, and are major flood deposits more distinctive than minor flood deposits with progressive burial?*

Identifying major flood events in the sedimentary record could provide spatial correlation points across boreholes and study sites at a discrete temporal marker. Due to assumed greater extent, energy, and/or duration of major flood events, major flood deposits will assumedly be distinctly identifiable with greater stratal thickness and potentially coarser basal grain size than smaller duration or minor floods. Individual

floods may be differentiated by differences in grain size, sedimentary structures such as laminations, or by interruptions of typical sedimentation (i.e., mud drapes observed between sands in a point bar sequence).

(2) How can sediment cores and ground-penetrating radar reveal how river management practices, modifications, and land use changes have affected sediment dynamics and floodplain evolution of the Mississippi River floodplains at Shipland WMA and St. Catherine Creek NWR?

If river management, channel engineering, and land use practices have altered flood dynamics and sediment regime through time, then changes in the sedimentary record should be reflected in cores collected along the floodplains at both sites that are not reflective of a natural facies progression in a meandering system, assuming sediment cores penetrate to historically relevant depths. These changes may be observed as anomalies in grain size or structures more common/apparent at shallow depths in core profiles compared to deeper strata. However, point bar sequences are expected to fine upward, which may obscure implications related to artificial controls – depositional controls such as variation in sedimentation rate may account for this. Grain size is only expected to fluctuate between sand to clay, so GPR resolution may be limited in this aspect to correlate strata across boreholes at each site. Furthermore, point bar sequences typically fine-upward, which may obscure flood events among general depositional trends.

(3) What are the temporal and spatial relationships between sediment composition and grain size distribution in the Mississippi River floodplains at Shipland

WMA and St. Catherine Creek NWR, and how can sediment cores and ground-penetrating radar contribute to understanding this relationship?

Sediments at Shipland WMA north of Vicksburg, MS are expected to be coarser-grained and less homogeneous than those of St. Catherine Creek NWR near Natchez, MS. The Shipland study site is a point bar, which is associated with sands interrupted by fine-grained flood sediments compared to the predominantly silt and clay expected at the natural levee/backswamp of the St. Catherine Creek location. Grain size distribution through depth is expected to be more variable at Shipland compared to St. Catherine Creek. Much fluvial GPR literature, including research investigating flood frequency with GPR (Okazaki and others, 2015; Sambrook Smith and others, 2015), has focused on braided systems or meandering streams containing gravels/boulders overlying bedrock (Dara and others, 2019). Seemingly, not much GPR research has focused on meandering stream floodplain sedimentation, especially in the LMR. Using GPR to correlate floodplain deposits across a study area could incite more versatility for the method in fluvial geomorphology in the Lower Mississippi Valley.

CHAPTER II – GEOLOGIC SETTING

2.1 Geomorphic Background and Evolution

The Mississippi River drains a catchment of over 3,100,000 km² along 3,700 km between the headwaters in Minnesota to the Gulf of Mexico (Kesel, 2003). The Lower Mississippi River (LMR) refers to the basin south of the confluence with the Ohio River in Cairo, Illinois (Fig. 2.1). Prior to major channel modification efforts in the 1930s, the LMR from Cairo, IL, to Red River Landing near Angola, MS, was an aggrading meandering system that contributed a major proportion of sediment to the river through bank erosion; the remaining distance to the Gulf of Mexico depocenter served as a sediment transport and sequestration route through channel transport and overbank deposition (Aslan and Autin, 1999; Kesel, 2003). Levee construction has restricted sediment pathways and removed an estimated 90% of storage capacity in the Lower Mississippi floodplains (Kesel, 2003). Major flood control structures and channelization endeavors since the 1920s have decreased bank erosion and sediment supply, altered the sediment regime in the river and associated wetlands, and removed sediment caches from the river entirely via chute cutoffs (Kesel, 2003). Due to channel engineering, the lower segment past Red River Landing has transitioned to an aggrading system due to greater bedload sediment supply and limited channel and overbank storage capacity because of cutoffs and artificial structures (Kesel, 2003).

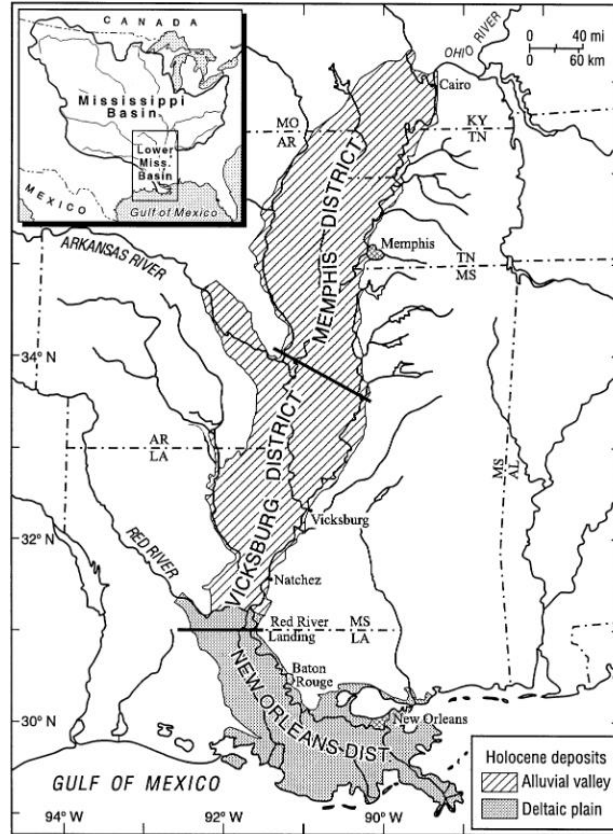


Figure 2.1 *Divisions of the Lower Mississippi River*

Geomorphic divisions of the Lower Mississippi River by the U.S. Army Corps of Engineers (Kesel, 2003).

2.2 Meandering River Facies and Typical Sedimentation

Two typical sedimentary facies are considered to assess Shipland WMA and St. Catherine Creek NWR: point bar / meander scroll (notably at Shipland WMA) and natural levee / backswamp (notably at St. Catherine Creek NWR) deposits (Fig. 2.2).



Figure 2.2 Overview map of the Shipland WMA and St. Catherine Creek NWR study sites along the Lower Mississippi River

(Accessed at Google Earth, 2023).

2.2.2 Point Bar and Meander Scroll Sedimentation

Point bars are located on the convex side of a meander loop and often record the greatest sediment accumulation in a meandering system (Davis, 1983). Large point bars can record the history of point bar migration and flood history through ridges (positive relief) and swales (negative relief) (Davis, 1983). Point bar deposits are typically well-sorted sands but can contain pebbles and silt; the point bar often exhibits gradational upward fining from a channel lag at the base and is sometimes capped by thin mud drapes

(Davis, 1983). At the base of a sequence, often above or interbedded with coarse grains, is large cross-stratification from megaripples. Smaller cross-stratification and horizontal laminations are also typical and indicate lower energy flow or flat bed conditions (Fig. 2.3 and 2.4; Davis, 1983).

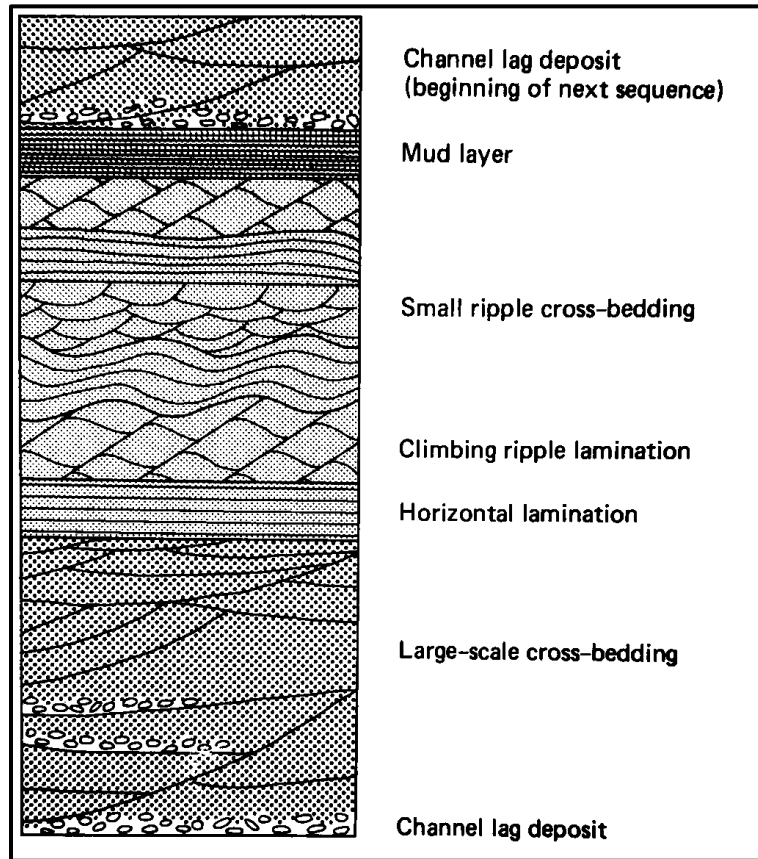


Figure 2.3 *Idealized point bar stratification sequence*

(Davis, 1983).

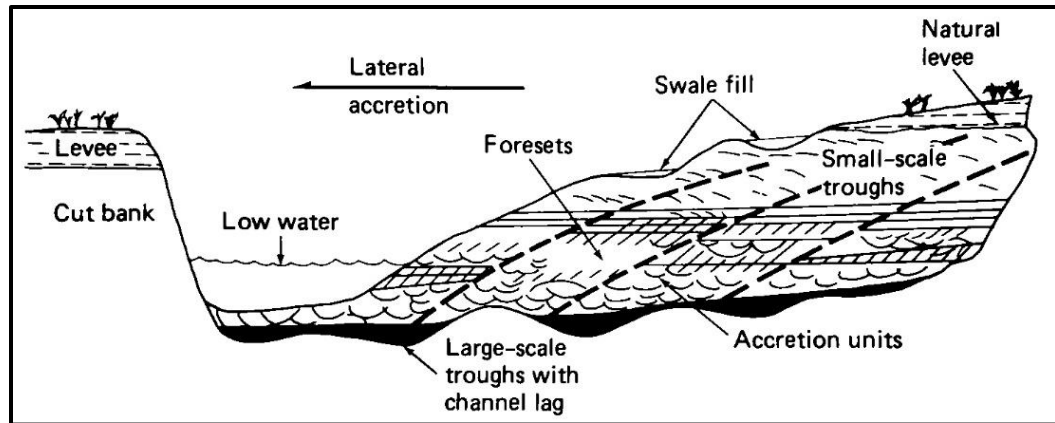


Figure 2.4 *General cross section of a point bar and cut bank of a meandering stream*
(Davis, 1983).

2.2.3 Natural Levee and Backswamp Sedimentation

Overbank (levee/backswamp/flood basin) sedimentation occurs during high-magnitude discharge events when stream level (i.e., stage) rises above the bank, resulting in distinct vertical sequences of fine-grained suspended load sediments (Davis, 1983). Natural levees are well-developed on the concave side of a meander bend, opposite of the point bar, and are characterized by thinly stratified sands and laminated muds with abundant vegetation (Davis, 1983; Hudson and Heitmuller, 2003). The backswamp/flood basin is distal from the natural levee in relation to the channel, characterized by low relief, poor drainage, a slow sedimentation rate, and abundant fine-grained and organic-rich sediment – often fine silt to clay settled from suspension during floods (Davis, 1983). Individual flood events may deposit up to 1 cm of sediment depending on the environment: swampy settings may trap more sediments than a broad, widely dispersed plain (Davis, 1983). A generalized meandering stream cross section is shown in Figure 2.4. Sedimentation in the St. Catherine Creek NWR region may be more complex regarding the effects of crevassing and stream avulsion (Aslan and Autin, 1999).

CHAPTER III – LITERATURE REVIEW

Principal workers have mapped (Fisk, 1944) and analyzed (Fisk, 1944; Saucier, 1994) floodplains, depositional facies, and processes of the Lower Mississippi River for decades. The effects of human interaction on the LMR have been an increasingly important topic of interest over the last 20 years, especially in the wake of recent, severe flood events. Fisk (1944) laid the fundamental framework for mapping and interpretation of the LMR and associated overbank deposits, which was later expanded, refined, and updated by Saucier (1994).

Many researchers have noted that human interaction has altered hydrologic and sedimentary characteristics of the LMR (Kesel, 2003; Horowitz, 2010; Hudson and others, 2013; Munoz and others, 2018; Russell and others, 2021). Not only have engineering and land use changes shifted depositional dynamics of the river at an observable scale (Kesel, 2003), but compounding effects of population growth, urbanization, and climate change will continue to alter the equilibrium of the LMR in the future (Russell and other, 2021). These are important considerations when assessing the history and potential changes through the floodplain profile. Distinct or unexpected facies changes in the subsurface might correlate temporally to river modifications and human interaction through time. Any potentially detrimental changes through time that correlate to artificial causes can be viable for restoration and stabilization projects.

Overbank sedimentation from flood events has also been subject to change due to human influence. Deposition from major historical floods has been analyzed by various researchers (Kesel and others, 1974; Heitmuller and others, 2017) to denote the mechanisms and controls on flood sedimentation. Over the last century, artificial changes

to the river have altered sediment regime, overall decreasing the suspended sediment load due to dams, construction, and erosion prevention measures that reduce the available sediment cache for overbank deposition (Horowitz, 2010; Meade and Moody, 2010).

Table 3.1 *Literature addressing the effects of human interaction on the Lower Mississippi River.*

PAPER	TOPIC	IMPORTANCE
Kesel (2003)	Effects of human interaction on LMR overbank sedimentation	Utilizes historical data to assess sedimentary and morphological changes through time in relation to anthropogenic influences
Horowitz (2010)	Changes in sediment regime through time on the Mississippi River	Analyzes the progressive decline in suspended sediment in Mississippi River floods attributed to construction limiting erosion and dispersion
Munoz and others (2018)	Human interference and climate effects on Mississippi River flooding	Highlights importance of human interference and climate controls on increasing flood severity through time
Russell and others (2021)	Evolution of the Mississippi River into the Anthropocene	Highlights the ongoing impacts humans have created that will continue to artificially change the dynamics of the Mississippi River

Table 3.2 *Literature addressing general and flood sedimentation in the Lower Mississippi River.*

PAPER	TOPIC	IMPORTANCE
Kesel and others (1974)	1973 flood sedimentation	Documents deposition mechanics of the historic 1973 Mississippi River flood south of Natchez, MS
Horowitz (2010)	Changes in sediment regime through time on the Mississippi River	Analyzes the progressive decline in suspended sediment in Mississippi River floods attributed to construction limiting erosion and dispersion
Meade and Moody (2010)	Decline of suspended sediment load in the Mississippi River	Notes various human constructions and practices that have resulted in lower suspended sediment loads through time
Heitmuller and others (2017)	2011 flood sedimentation	Documents deposition mechanics of the historic 2011 Mississippi River flood south of Natchez, MS

While methodologies explaining applications of ground-penetrating radar (Hugenschmidt, 2010; Dong and Ansari, 2011; Benedetto and Benedetto, 2014) are abundant, uses in fluvial sedimentation and geomorphology (Nobes and others, 2001; Okazaki and others, 2015; Dara and others, 2019) are less extensive, with little to no application in low gradient meandering stream floodplains such as the Lower Mississippi River – most available GPR research in fluvial settings has been performed on braided streams with coarser-grained bedform migration (Okazaki and others, 2015) or higher-gradient floodplain subsurface profiling (Dara and others, 2019). Dara and others (2019) generated a comprehensive assessment of several subsurface floodplain radar facies of

the River Tern in central England (Fig. 3.1) that may serve as a fundamental reference for the geophysical interpretations of this research to develop a stratigraphic profile of the Shipland WMA and St. Catherine Creek NWR floodplains. Because of small-scale heterogeneity in floodplain sediments, these radar facies are indicative of general sedimentary trends, not individual layers or deposits (Dara and others, 2019). Roudi and others (2012) had some success correlating sediment cores to GPR imagery to differentiate lithologies of estuarine deposits on the coast of the Oman Sea; however, radar imagery was susceptible to distortion by the water table, which is an important consideration in floodplain applications, as well. Observing GPR at Shipland WMA and St. Catherine Creek NWR contributes to exploring the utility of radar imagery for low gradient floodplains to assess for subsurface flood events.

Of the radar facies detailed by Dara and others (2019), five are applicable to low gradient floodplains of the LMR (facies 1, 2, 3, 5, and 8; Fig. 3.1). St. Catherine Creek NWR is expected to exhibit vertical accretion, which may be represented as horizontal reflectors (facies 1); however, if the depositional environment is very low energy, structures may not be visible (facies 8). At Shipland WMA and St. Catherine Creek NWR, any inclined or clinoform reflectors observed likely represent interbedded sand/mud (facies 2) or higher-energy bedding structures/lateral accretion (facies 3). No sediment larger than sand is expected at either site. Therefore, hard parabolic reflectors are not anticipated; any observed may represent buried organics such as root structures (facies 5).

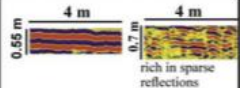

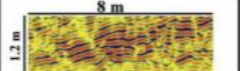



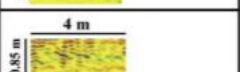



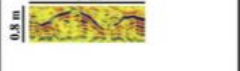

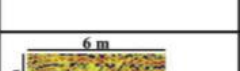



Radar facies	GPR example image	Core section	Lithology	Interpretation	Permeability class
Radar facies type 1 Horizontal-to-subhorizontal reflections			Fine muddy sand, plant remains, clay nodules, as well as some isolated pebbles	Overbank vertical accretion deposits	Intermediate
Radar facies type 2 Sigmoidal to divergent clinoform reflections			Sand layers interbedded with dark silt	Overbank flooding (modern floodplain)	High
Radar facies type 3 Wavy and Inclined reflections			Sand sediment	Lateral or downstream accretion and lateral migration of the river	High
Radar facies type 4 Faint subhorizontal, undular, variable dip, and structureless reflections			Muddy sand rich in organic matter, peat, and clay	Channel fill elements	Low
Radar facies type 5 Curved, concave-upward reflections associated with dipping and small hyperbolic reflections			Sand with organic fragments	Erosional surface	High
Radar facies type 6 Discontinuous, chaotic or irregular rich in macro scale abundant stacked hyperbolic reflections			Big boulders or bedrock surface	Deposits of submerged palaeomeander or bedrock	Low-High
Radar facies type 7 Hummocky, dipping and chaotic reflections including micro-scale hyperbolic diffractions.			Small boulders within sand deposits	Surrounding the older channels represent point bar sediment.	High
Radar facies type 8 Structureless, reflection free zone.			Clay layers	May correspond to swamp deposits	Low

Figure 3.1 *GPR radar facies of low-gradient floodplains*

Data collected from the River Tern, UK (Dara and others, 2009).

Table 3.3 *Fundamental literature and applications of ground-penetrating radar to subsurface floodplain analysis of the Lower Mississippi River.*

PAPER	TOPIC	IMPORTANCE
Nobes and others (2001)	GPR analysis of Holocene floodplains in New South Wales, Australia	Provides a reference of utility of GPR imaging in a floodplain depositional environment
Sambrook Smith and others (2010)	Subsurface imaging of flood events in South Saskatchewan River, Canada	Displays utility of GPR imaging of fluvial landforms in braided streams
Benedetto and Benedetto (2014)	Field application of GPR imaging	Details fundamental utilities and techniques of GPR subsurface imaging
Okazaki and others (2015)	GPR analysis of braided stream bedforms in Abe River, Japan	Provides a reference of utility of GPR imaging to visualize flood events in the subsurface sedimentological record of a braided stream
Dara and others (2019)	GPR analysis of floodplain and bedform sedimentology on River Tern, UK	Provides a baseline reference of fluvial subsurface radar facies and corresponding depositional facies in a lowland meandering stream for research comparison

CHAPTER IV – METHODS

4.1 Assessment for Anthropogenic Fluvial Change

Patrick and others (1982) note three necessary methods for evaluating artificial fluvial change: (1) techniques for determining the nature of local and basin parameters and their spatial variability, (2) techniques for determining the temporal variability of spatial parameters, and (3) a method of analyzing the mechanics of the fluvial system. To assess local spatial variation, this study observes and compares sedimentation and stage-discharge relations between Shipland WMA north of Vicksburg, MS and St. Catherine Creek NWR near Natchez, MS. To assess for temporal variability and the mechanics of the Mississippi River, overbank sediment cores and ground-penetrating radar (GPR) profiles will be collected at Shipland WMA and St. Catherine Creek NWR to potentially delineate flood events in the overbank record and historical changes in sedimentation and flood dynamics.

4.2 Study Areas

Borehole locations at both study sites were recorded using a combination of total-station surveying and traditional GNSS methods corrected using the University of Southern Mississippi Gulf Coast Geospatial Center's RTK network, as detailed by Anderson and others (2022) and Provost and others (2022).

4.2.1 Shipland WMA near Mayersville, MS (SWMA)

The site selected at Shipland WMA (SWMA; Fig. 4.1) near Mayersville, MS, is roughly 48 km northwest of Vicksburg, MS. The site is on the point bar side of the Mississippi River and contains point bar and meander scroll deposits at the surface (Saucier, 1994). Assuming the point bar deposits record Mississippi River bedload,

predominantly sands, minor gravels, and lesser amounts of overbank-silts are expected to be observed in floodplain core profiles (Keown and others, 1986). This site is near a chute channel of the main river. Trees at SWMA appear to be buried rapidly, with no visible root buttresses or exposed trunk bases; fallen limbs are also accumulated in zones, possibly due to flood mobilization (Fig. 4.2).



Figure 4.1 *Shipland WMA study site with core collection points*

(Accessed at Google Earth, 2023). Date of imagery: Aug. 26, 2015.



Figure 4.2 *Buried tree bases and limb accumulation at Shipland WMA*

4.2.2 St. Catherine Creek NWR near Natchez, MS (SCC)

The site selected at St. Catherine Creek NWR (Fig. 4.3) is roughly 18 km south of the city of Natchez, MS. The site is on the cut bank side of the Mississippi River near the outlet of Old St. Catherine Creek and minor tributaries of the Mississippi River. At the surface, the site appears to contain natural levee and backswamp depositional environments. In this region, natural levee sands/silts and backswamp muds are expected in the subsurface between discrete 100-foot-thick meander belt sands deposited during the Late Holocene (Aslan and Autin, 1999). Sandy splays in the sediment profile of this region may derive from crevassing and avulsion rather than exclusively overbank sedimentation (Aslan and Autin, 1999).



Figure 4.3 *St. Catherine Creek NWR study site with core collection points*

(Accessed at Google Earth, 2023). Date of imagery: Nov. 24, 2012.

4.3 Sediment Cores

Five sediment cores were collected in a plus-shaped pattern at floodplain locations adjacent to the Mississippi River at Shipland WMA and St. Catherine Creek NWR. The core tube dimensions are 1.25 in. (3.18 cm) diameter by 48 in. (122 cm) long; 20 feet (6.1 m) of core were collected at each borehole, resulting in five core sections per borehole. Distinctive sedimentary characteristics or structures were correlated between cores across each study site to interpret continuity or discontinuity within the subsurface.

Core sections were halved along the length, photographed, and documented based on lithology, color, and structures. A sample plan was created to collect teaspoon portions of sediment at distinct changes in lithology throughout the core.

One issue with floodplain coring is artificial core shortening. Preferential retention, mixing, thinning, or compaction may occur within short sediment cores, resulting in a warped sediment profile – this is especially problematic in water-saturated, organic-rich muds (Morton and White, 1997). Due to the nature of floodplains and proximity to the channel, core shortening must be considered. Thick-walled, small-diameter core tubes increase the potential for core shortening (Morton and White, 1997); however, inaccessibility of the study sites restricted the use of core tubes greater than 1.25” (3.18 cm) diameter. Calculated sedimentation rates from shortened cores may be two to three times slower than the true rate (Morton and White, 1997), so radiocarbon and Cs/Pb dating are commonly used as temporal proxies for sedimentation rate. In lieu of recording true drilled depth at the borehole on-site to compare with recovered sediment, the total compressed length of sediment in the cores is assumed as the total recovered length. The recovered sediment was extruded by a coefficient to assume the total 48 inches (1.22 m) of each section is present. This method assumes each core section will be uniformly shortened across each 48-inch (1.22 m) interval.

4.4 Isotopic Dating

Due to the argillaceous and saturated nature of floodplain deposits, some buried vegetation has been preserved (Farrell, 1987). Buried vegetation could provide an age proxy for sedimentation rate through ^{14}C radiometric dating. Viable samples were collected in 20 mL scintillation vials, rinsed with deionized water to remove excess sediment, and dried in a desiccation chamber for several weeks with a CaSO_4 desiccant. Once sufficiently dried and preserved, these samples were analyzed and dated at an unaffiliated laboratory, NOSAMS, at the Woods Hole Oceanographic Institution. All

carbon results received from NOSAMS were calibrated via CALIBomb, an online database that references carbon isotopes in various spatial zones through atomic bomb isotope data (Reimer and others, 2004.) Resolution of ^{14}C dating can determine intervals below 50 years – ideally below 25 years – for samples less than 3000 years old (Svetlik and others, 2019). The scale of the Mississippi River results in frequent reworking of older organic material; ^{14}C dates that appeared anomalous were scrutinized to determine the chronology of sediment deposition at both study sites.

4.5 Grain Size Analyses

Sediment samples were assessed for grain size distribution using a Malvern Panalytical Mastersizer 3000 particle size analyzer. Grain size distribution provides a quantitative measure to delineate differences between different strata or facies on a scale of individual flood events to more comprehensive overbank depositional histories between both sites. Grain size results were imported into Gradistat v. 9.1 to view grain size distribution and perform statistical analyses for each sample (Blott and Pye, 2001). Gradistat computes grain size statistics based on the methods conducted by Folk and Ward (1957) on fluvial sediments from the Brazos River. These data were plotted through depth in each core to visualize systematic shifts in sedimentation and provide a basis for determining flood layers.

4.6 Ground-Penetrating Radar

Ground penetrating radar (GPR) is a remote sensing system that utilizes variability in microwave reflectance of substrate materials to construct a cross-sectional profile of the subsurface. GPR typically emits radiation from a range between 10-10,000 Hz and relies on reflection of microwaves through different levels of the subsurface to

visualize variation between different materials, strata, or objects beneath the ground. A typical GPR instrument setup consists of a microwave transmitter, receiving antenna, and processing/display unit (Dong and Ansari, 2011).

The main benefit of GPR is its non-destructive nature, allowing for surveying without excavation (Mahmoodian, 2018), and its comparably low cost, ease of access, and high resolution outcompetes seismic methods for shallow subsurface imaging. GPR's ability to detect changes in strata through depth allows for applications in sedimentological analyses and can be especially useful in interpreting fluvial and floodplain deposition (Dara and others, 2019).

A GPR unit is operated by moving the microwave emitter across the ground surface, typically either by dragging the unit in a harness or pushing using a stroller-like apparatus. If an object or anomalous section is present below the scanned area, it will appear in the data as a disruption in the radar profile, often as a hyperbolic reflector or disruption. The diameter of the object will determine the angle of the reflector (Fig. 4.4). Differences in stratum composition can also be observed as lateral anomalies in the radar signal due to variation in dielectric properties and, consequently, reflectance (Fig. 4.5) (Benedetto and Benedetto, 2014).

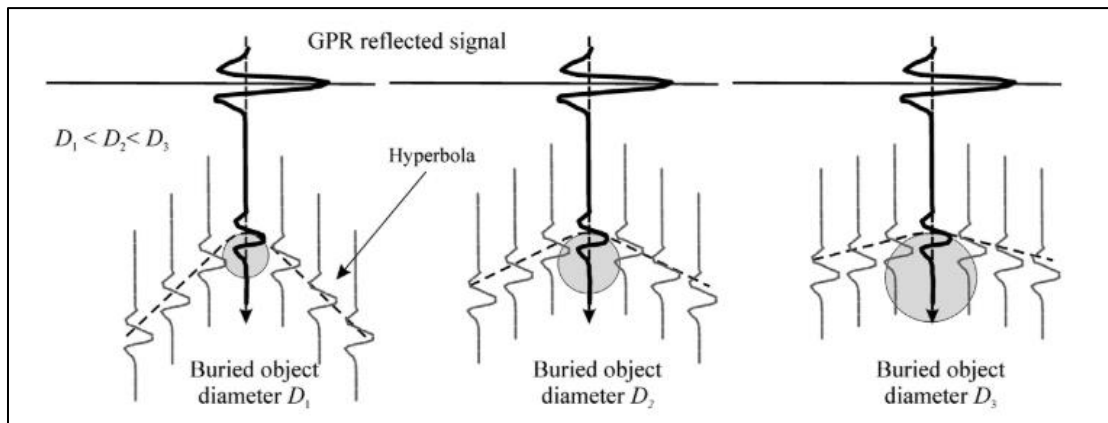


Figure 4.4 *Parabolic reflectors in GPR*

Parabolic artifacts created in a GPR profile when passing a buried object (Benedetto and Benedetto, 2014).

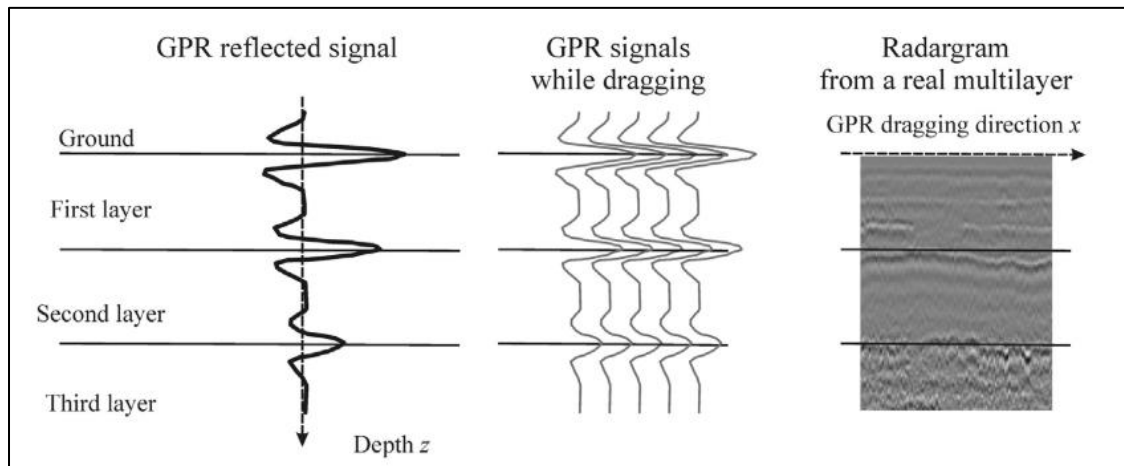


Figure 4.5 *Strata reflectors in GPR*

Layering of strata depicted in a GPR profile due to differences in reflectance (Benedetto and Benedetto, 2014).

GPR is limited to two-dimensional profiles created by individual transects; however, an approximated three-dimensional profile can be generated by recording closely spaced transects across a survey area grid, known as a time-slice. The data collected from each transect can be formatted to define points that meet certain criteria, such as object reflectors or stratal layers, to generate a map of the subsurface (Fig. 4.6). Closely spaced transects across a plotted study area may be compiled into a 3D subsurface profile of the study area to observe changes through depth, as well (Hugenschmidt, 2010); however, 3D profiling was not feasible given the wooded nature of the study sites. Instead, GPR scans were taken in single transects over all aligned boreholes, with scans intersecting at the center core location.

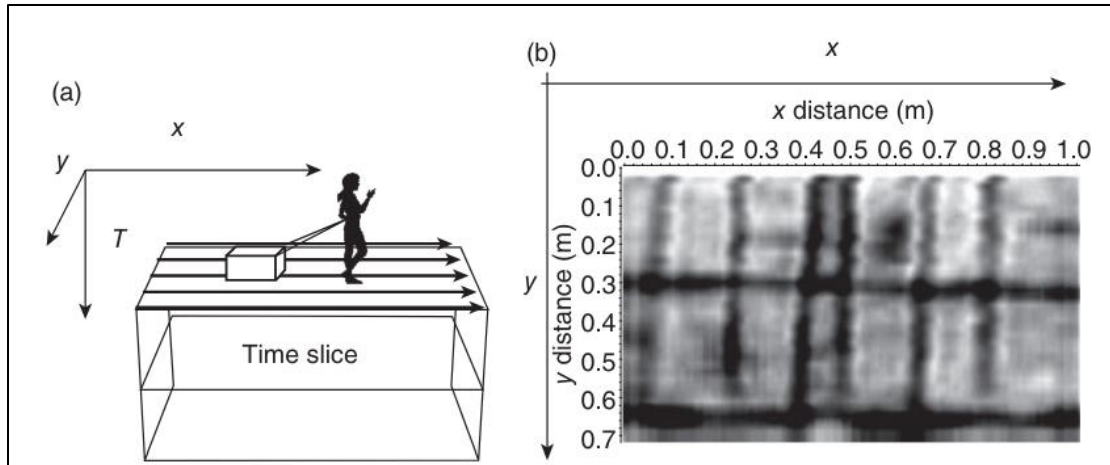


Figure 4.6 *Subsurface mapping using GPR*

Multiple GPR transects across a grid compiled to create a map of subsurface objects (Hugenschmidt, 2010).

Different depositional environments along a floodplain possess different sedimentary characteristics. The main variable considered regarding GPR is change in grain size. For example, point bar deposits are commonly composed of small gravel to sands, whereas levees are commonly fine sand and silt, and backswamps are silt and clay. Because of differences in dielectric properties between grain sizes and compositions, GPR scanning can detect changes in substrate that might result from a flood event (Dara and others, 2019) or differences in sedimentary facies (Okazaki and others, 2015; Dara and others, 2019). Unfortunately, high water or clay content can disrupt GPR quality (Benedetto and Tosti, 2013), which may be problematic in assessing floodplain sedimentation near the water table. According to some sources, GPR penetration may be limited to 50 cm in very fine, saturated soils due to energy dissipation (Doolittle and Butnor, 2009).

GPR has proven useful in assessing subsurface sedimentary structures in meandering river floodplains (Nobes and others, 2001; Sambrook Smith and others, 2010; Dara and others, 2019). Radar profiles can show connectivity between sedimentary units and internal structures across a floodplain. GPR is especially useful when done in tandem with systematic sedimentological analyses to observe finer-scale patterns or phenomena not immediately observable in radar (Nobes and others, 2001), such as lithological assessments derived from sediment cores.

Ground-penetrating radar was used in this study to interpolate and correlate reflectors across the study areas to create a composite image of the subsurface. Distinct reflectors may be related to phenomena seen in the sediment cores, allowing for better resolution and interpretation of the subsurface profile (Fig. 4.7). GPR transects were planned systematically across the study area, intersecting the approximate borehole surfaces, and covering as much of the study site as strategically possible. A well-defined grid was not possible to scan at Shipland WMA nor St. Catherine Creek NWR due to tree cover, so transects were aligned across each borehole to create lines approximately perpendicular and parallel to the Mississippi River channel to best visualize any subsurface phenomena.

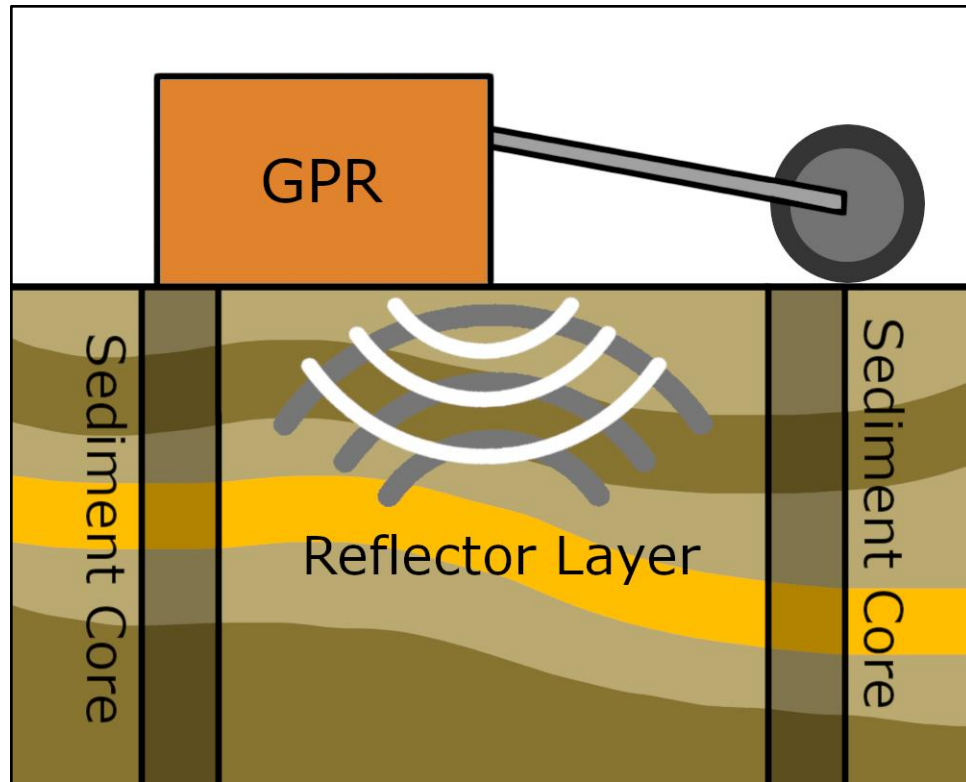


Figure 4.7 *GPR correlation between sediment cores*

Correlation potential between distinct reflectors seen in the subsurface recorded in ground-penetrating radar and sediment cores.

Ground penetrating radar data was assessed using GPR Insights software by Screening Eagle Technologies. GPR Insights utilizes machine learning to analyze data and plot transects geospatially, especially when GPS transects are recorded simultaneously. This program excels in data manipulation, but utilizing artificial intelligence capabilities will not be satisfactory to interpret the subsurface into a three-dimensional model if the transects are not collected in a systematic grid spaced within 30 cm transects. Given the wooded nature of the chosen research sites, these programs are best utilized to create individual subsurface profiles up to 5 meters resolution around and between boreholes without interpolating extra data between surface transects (Fig. 4.8

and 4.9). To supplement this drawback, 400 and 200 MHz GPR data were compared at each site for fine-resolution/shallow and coarse-resolution/deep imaging, respectively. Comparing multiple GPR frequencies is important in profiling different sedimentary facies (Bridge, 2009).

Filters used in GPR post-processing include dewow, time zero, bandpass, background removal, time gain, and migration. Dewow (high-loss temporal filter), time zero (ground surface correction), and background removal parameters were automatically applied by GPR Insights. Time gain equalizes signal amplitudes to account for signal loss with depth (Annan, 2009). The auto gain applied by GPR Insights was sufficient for most scans, but fine adjustments were made where necessary using a time gain filter.

Migration removes source and receiver directionality from the data, generating more defined subsurface geometry (Annan, 2009). Migration was applied when necessary to identify buried objects such as roots but was not necessary to define sedimentary layers.

GPS data was live-tracked with GPR transects using a Trimble R-12 mounted directly to the radar antenna apparatus. GNSS data was corrected using the University of Southern Mississippi Gulf Coast Geospatial Center's RTK satellite network to produce spatial resolution within 10 cm both horizontally and vertically, as detailed by Anderson and others (2022). When ported into GPR Insights, radar transects were automatically aligned to spatial start and end points (Fig. 4.8 and 4.9).



Figure 4.8 *Composite overview image of Shipland WMA*

Displaying borehole locations, cross section transects (A-A' and B-B'), and GPR transects (accessed at Google Earth, 2024). Date of imagery: Nov. 27, 2023.



Figure 4.9 *Composite overview image of St. Catherine Creek NWR*

Displaying borehole locations, cross section transects (A-A' and B-B'), and GPR transects (accessed at Google Earth, 2024). Date of imagery: Nov. 27, 2023.

CHAPTER V – RESULTS

5.1 Sediment Cores and Grain Size

Five cores were analyzed from both study sites. From Shipland WMA, 178 samples were processed (Core 1: 33, Core 2: 37, Core 3: 29, Core 4: 34, Core 5: 45), and 172 samples were processed from St. Catherine Creek NWR (Core 1: 34, Core 2: 39, Core 3: 27, Core 4: 29, Core 5: 43). Individual sample intervals and grain size statistics are reported in Appendix B. All cores from Shipland WMA are dominated by sand; however, distinct compositional changes are apparent as lenses of finer-grained sediment (Fig. 5.1 and 5.3). Cores located closer to the river are more variable compared to points of higher elevation or locations distal from the river (Fig. 5.5).

The cores from St. Catherine Creek NWR are primarily silt with minor layers of very fine sand or clays (Fig. 5.2 and 5.4). The sedimentary record from Core 3 is missing between 244-415 cm due to the collection of a branch buried vertically at depth, which was cored through. Therefore, this interval contains no recovered sediment. Cores at this site reveal no general trends in grain size in relation to channel proximity (Fig. 5.6).

Logarithmic trends recorded from all cores vary among both research sites (Fig. 5.5 and 5.6). At Shipland WMA, Cores 2, 3, and 5 display a coarsening trend through time, whereas Cores 1 and 4 indicate a fining trend in sedimentation. At St. Catherine Creek NWR, Cores 1, 2, and 3 present a fining trend, whereas Cores 4 and 5 coarsen upward. When laid in the context of elevation in a cross-sectional view, grain size changes can be correlated across the cores at both sites along transects perpendicular and parallel to the thalweg.

5.1.1 Sediment Characteristics

5.1.1.1 Shipland WMA

SWMA is sand-dominant with concentrated zones of mud accumulation. The uppermost sediments of all cores from SWMA contain fine sand directly overlying organic-rich, muddy deposits. These muds vary between finely laminated (Cores 2 and 5) to structureless/peaty (Core 3).

Sand units are generally massive, sporadically interrupted by potential bedding surfaces (Core 4). Muddy deposits in all cores at SWMA become increasingly low-chroma with increasing depth. Near the surface, organic-rich layers are very dark brown (10YR 2/2). Most of these cores are comprised of brown (10YR 5/3) clean sand. In cores with basal muds, such as Core 1, reduced dark gray (10YR 4/1) colors are prevalent. Soil horizon differentiation was not observed at this site – no evidence of leaching nor subsurface grain remobilization was observed.

5.1.1.2 St. Catherine Creek NWR

SCC is dominated by silt with secondary components of sand and minor clay. Fine sand varies between 10-50% of total composition in some intervals (Core 5). All cores are comprised of nearly homogeneous zones of mud interrupted by small (< 1 cm) lenses of coarser grained inclusions, often observed as laminae. All cores gradually transition on average from dark yellowish brown (10YR 4/4) near the surface to grayish brown (10YR 5/2) and sometimes trending toward gley. All cores reflect a trend toward reducing conditions with depth, exhibiting muted coloration and a pungent sulfurous odor near the base.

Minor soil development was observed in all SCC cores, with a thin organic layer at the surface (O horizon), followed by dark organic accumulation (proto-A horizon) in the upper 30 cm. Coloration becomes less saturated below the A horizon up to 120 cm depth (proto-E horizon), but transitions are gradational and reflect no distinct horizon development. No evidence of clay remobilization was observed. The soil on the St. Catherine Creek NWR floodplain is deemed an entisol (NRCS, 2024).

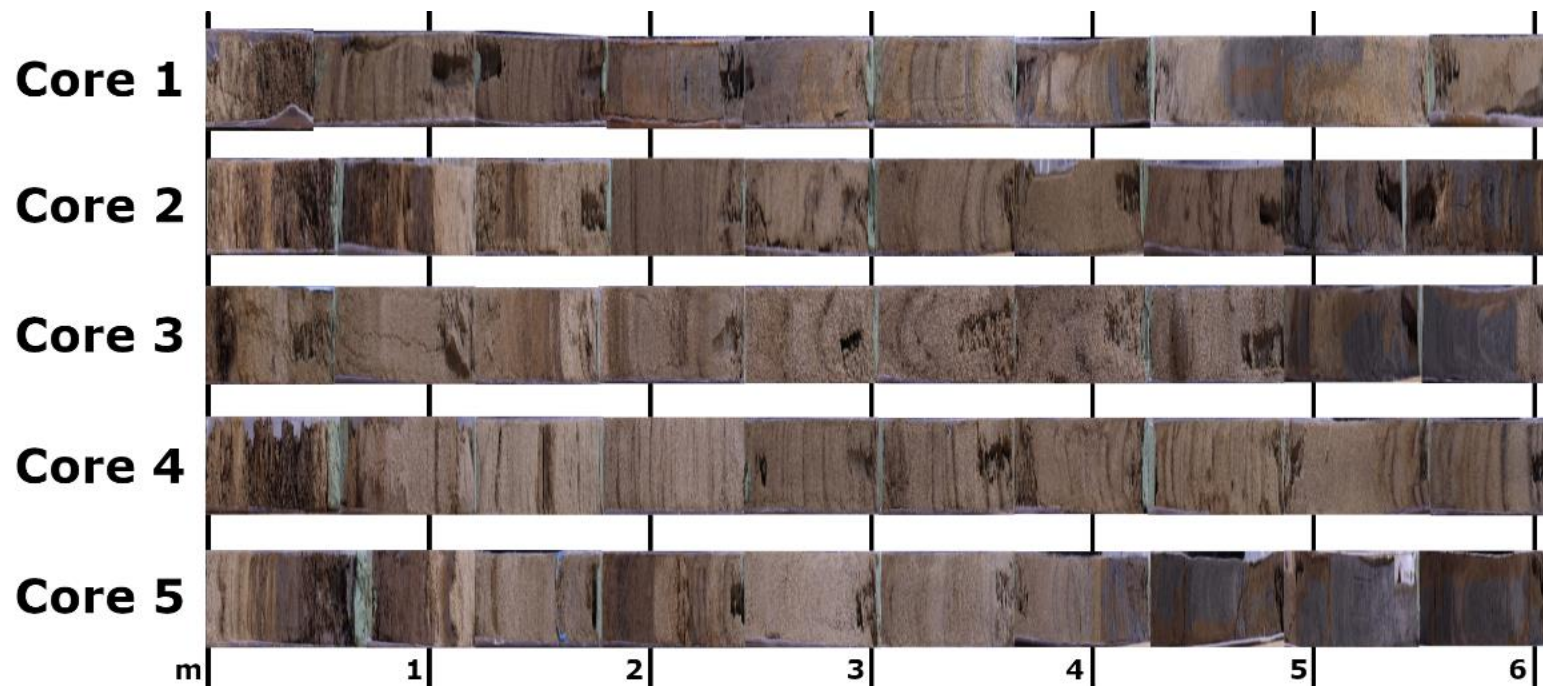
Shipland WMA

Figure 5.1 *Sediment core photos from Shipland WMA*

Core widths have been artificially extruded to increase visibility and are not true to scale. Core lengths were extruded to the assumed 6.1 meters of total recovery. Green zones are floral foam used while coring to prevent sediment loss and movement in gaps.

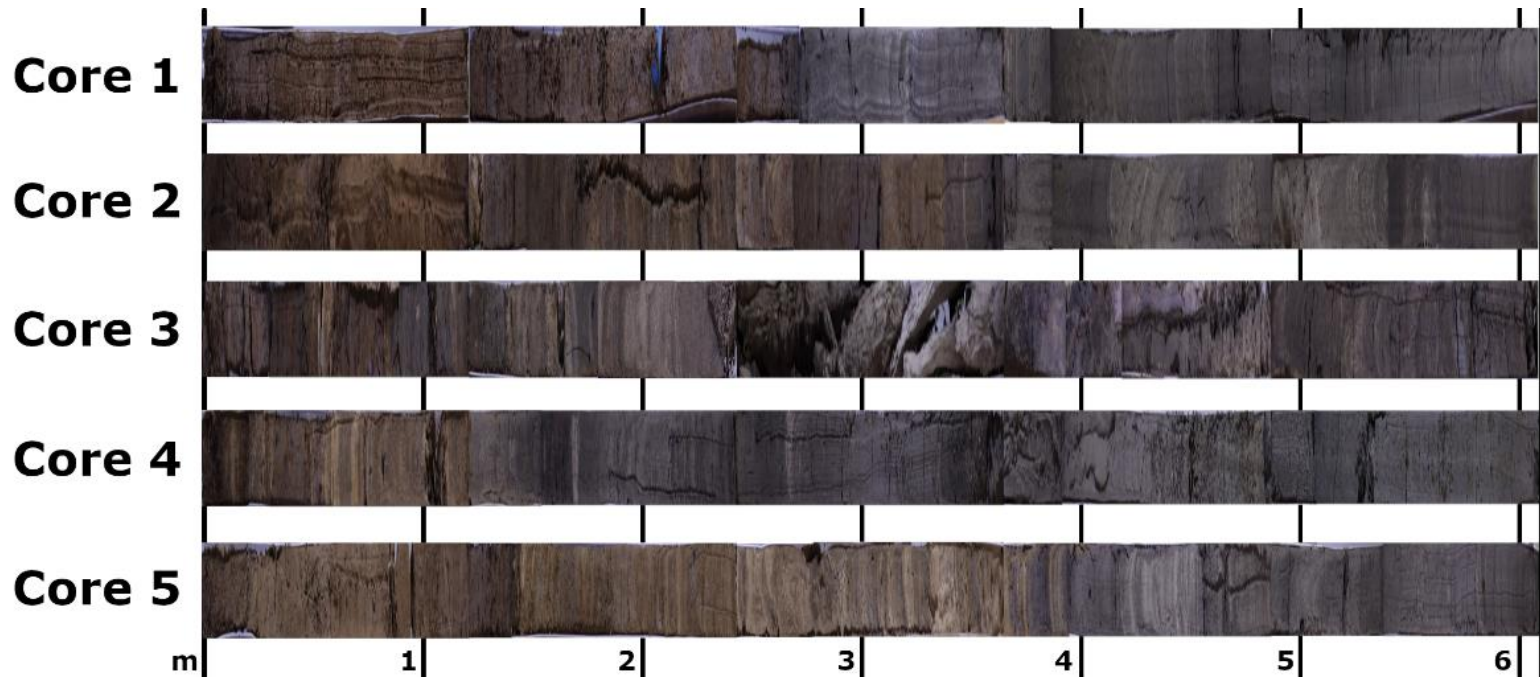
**St. Catherine
Creek NWR**

Figure 5.2 *Sediment core photos from St. Catherine Creek NWR*

Core widths have been artificially extruded to increase visibility and are not true to scale. Core lengths were extruded to the assumed 6.1 meters of total recovery.

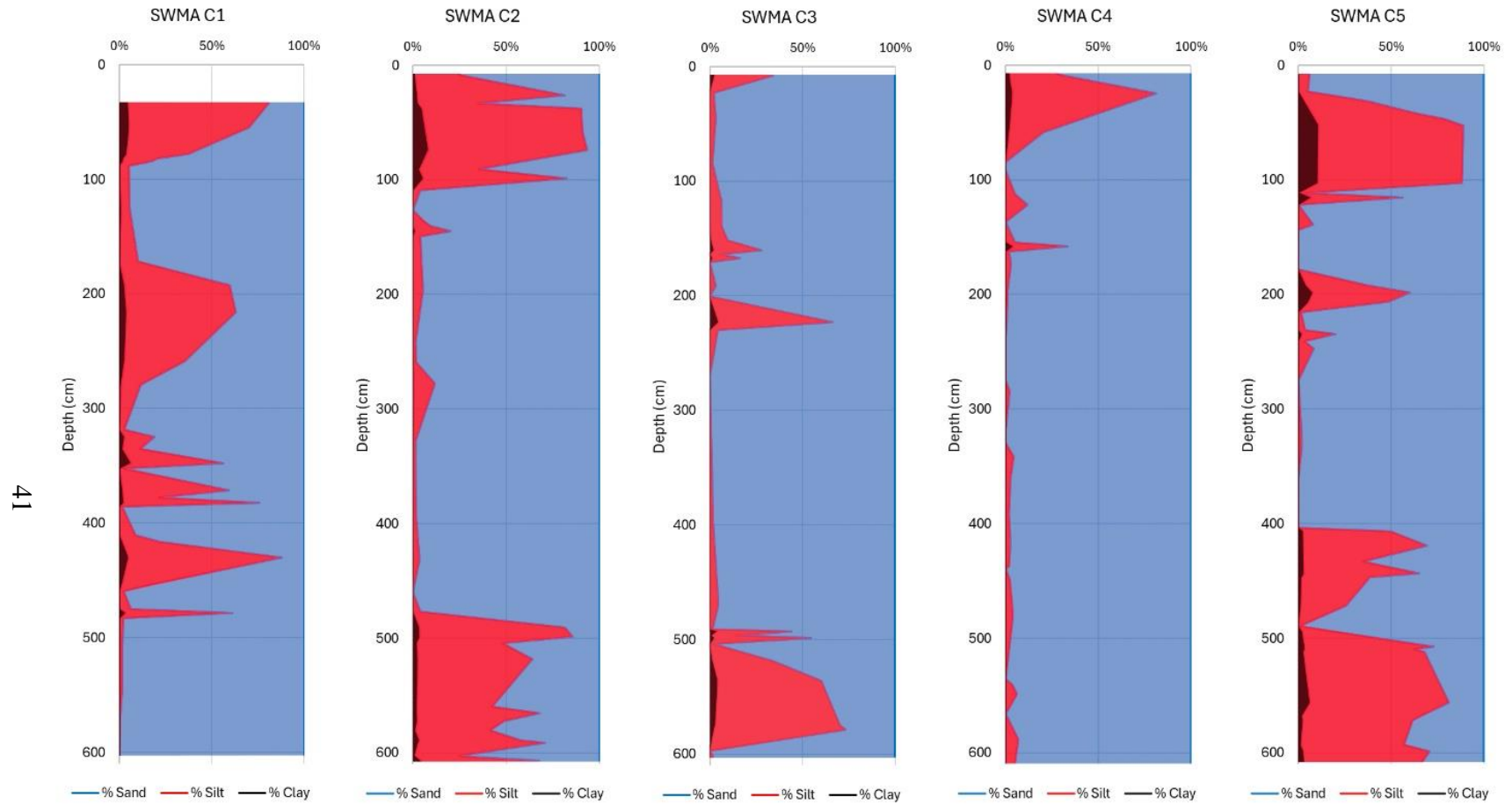


Figure 5.3 *Shipland WMA sand/silt/clay graphs*

Sand/Silt/Clay percentage diagrams displaying grain size changes through depth at Shipland WMA. Grain size statistics calculated using the Folk and Ward method via Gradistat 9.1 (Blott and Pye, 2001).

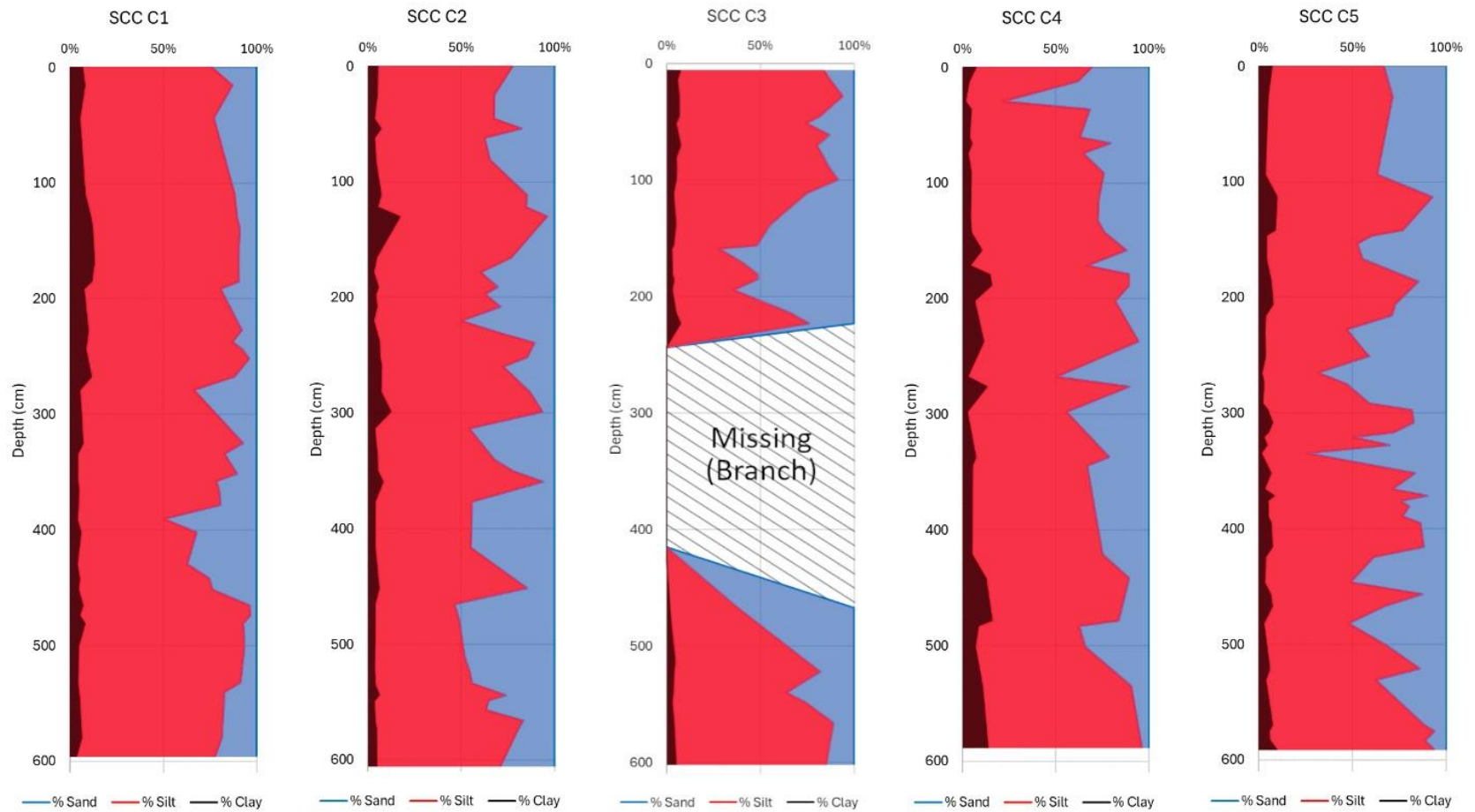


Figure 5.4 *St. Catherine Creek NWR sand/silt/clay graphs*

Sand/Silt/Clay percentage diagrams displaying grain size changes through depth at St. Catherine Creek NWR. Grain size statistics calculated using the Folk and Ward method via Gradistat 9.1 (Blott and Pye, 2001).

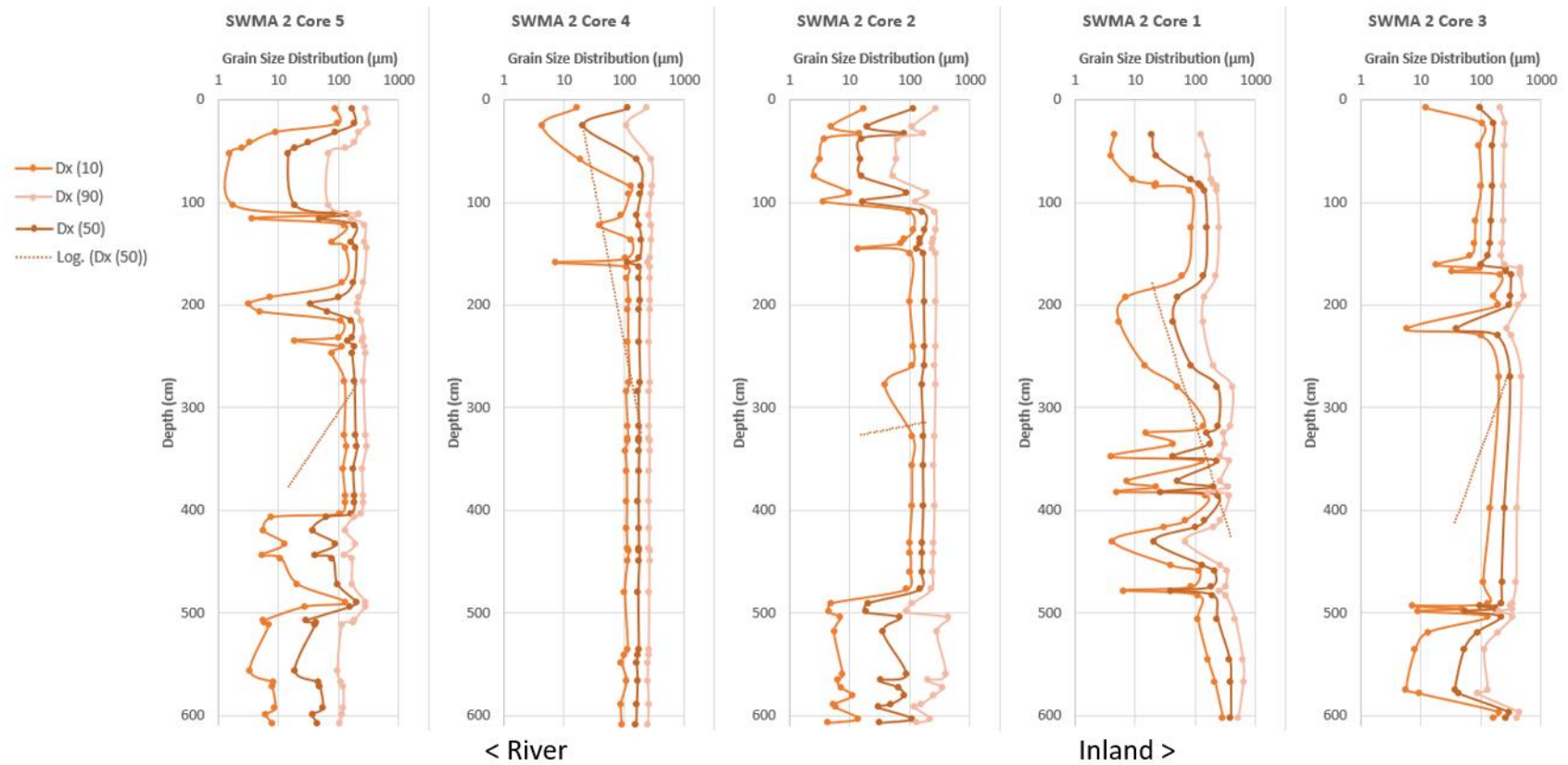


Figure 5.5 *Shipland WMA grain size percentile trends*

Changes in grain size fractions through depth at Shipland WMA, displaying 10th and 90th percentiles as well as mean grain size (Dx 50) and logarithmic trendlines for each core. Calculated via Gradistat 9.1 (Blott and Pye, 2001).

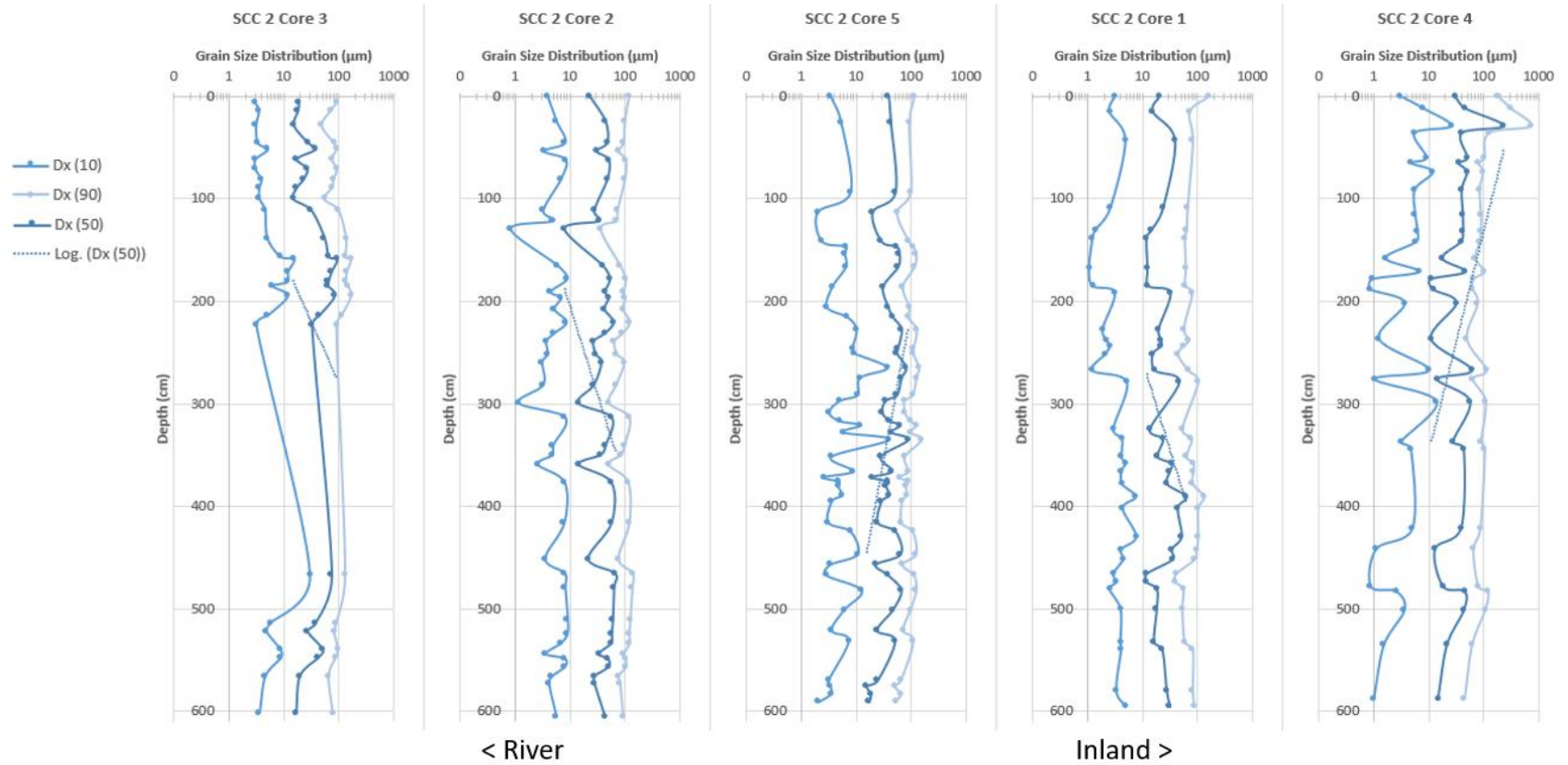


Figure 5.6 *St. Catherine Creek NWR grain size percentile trends*

Changes in grain size fractions through depth at St. Catherine Creek NWR, displaying 10th and 90th percentiles as well as mean grain size (Dx 50) and logarithmic trendlines for each core.

Calculated via Gradistat 9.1 (Blott and Pye, 2001).

5.2 ¹⁴C Dating

Forty-seven samples were collected in total for age dating. All ¹⁴C sample depths and age ranges are reported in Appendix A (Table A.2). This report addresses only the 68% confidence interval defined by NOSAMS and CALIBomb to best constrain date ranges. At SWMA, 3 samples were collected from Core 1, 6 from Core 2, 6 from Core 3, and 5 from Core 4. No samples were recovered from Core 5. At SCC, 6 were collected from Core 1, 3 from Core 2, 7 from Core 3, 8 from Core 4, and 4 from Core 5. Of the 47 samples processed, reworked material created age discrepancies, resulting in only 27 viable date estimates (9 samples from Shipland WMA, 18 samples from St. Catherine Creek NWR). These dates are shown in the core profile interpretations in Figures 6.5 and 6.6 for SWMA and 6.7 and 6.8 for SCC.

Organic material sampled from Shipland WMA was often highly fragmentary and unidentifiable. Because of the high energy sedimentation observed on the point bar, it is apparent that older/outlier dates (some on orders of millennia) recovered from Shipland derive from weathered/reworked material that was previously buried upstream. Organics are sparse in the SWMA cores, with no available samples observed from Core 5. Core 2 produced a comprehensive timeline for deposition at Shipland WMA, ranging from 1965-1966 at 603 cm to 2003-2007 at 47 cm depth; however, data is lacking between 61-502 cm from this core. Correlative horizons at other Shipland cores lack original organic material, so any dating assessments within this zone are relative to overlying or underlying strata. The age record from Core 2 indicates a sedimentation rate of roughly 10.6 cm/year at Shipland WMA for this site. These data were chosen as the basis for

depositional history because all samples occur in chronological order with depth without major outlier dates, but the degree of reworking is unknown.

Organic material was better preserved in the St. Catherine Creek NWR cores. Overall, carbon samples were more intact and identifiable as pieces of grass or bark. However, reworked material was still prevalent. In some intervals, such as 279 cm in Core 1 or 190 cm in Core 4, contain organic material that dates very recently. These outliers are assumed to have been pushed to depth through the coring process and have been disregarded. Ages recorded at the base of each core at St. Catherine Creek vary. The oldest/deepest material was found in Core 3 at 592 cm, dated between 1810-1925. In Core 5, a sample from 524 cm deep was dated 1810-1873. The oldest sediments in these cores likely date to the mid-1800s. Unfortunately, this estimate is speculative as these samples predate any control markers generated by the first atomic bomb detonations, and available ^{14}C material was still sparse. Based on the 1810-1873 date from Core 5, this site has an average sedimentation rate of 2.5-3.5 cm/year.

5.3 GPR

Table 5.1 details the specific parameters for GPR data processing. All transects received wobble removal, time zero, trim, bandpass, background removal, and auto gain filters. TGC gain and migration filters were applied when necessary to better visualize structures and strata. Dielectric constants were achieved by aligning known subsurface horizons observed in cores to distinct reflectors seen in radar scans. For example, at Shipland WMA, each core contains a muddy layer overlain by sand within the upper 1 meter of the core profile. The depths of these transitions (reflectors) were adjusted in the GPR scans to approximately the same depth as observed in the sediment cores by altering

the dielectric constant. Due to saturated conditions and/or high proportions of silt/clay content, 400 MHz loses visibility below roughly 2 meters. Within the uppermost overbank profile, beds and structures can be traced and correlated between cores.

200 MHz data is low resolution at both study sites due to sediment characteristics and water content. The maximum depth of usable data extends around 3.5-4 meters at SWMA due to saturated conditions and roughly 2.5 meters at SCC due to fine sediment content and potential saturation. Because of the poor resolution, the 200 MHz data is best utilized to identify distinct strata or potential facies changes at various depths, but these transects are not applicable to identify individual flood layers or events on a fine scale. The best approach regarding the GPR data in this study is to ground-truth depths of strata observed in sediment cores and correlate visible horizons and structures across the study areas between boreholes.

Table 5.1 *GPR parameters chosen for data processing at Shipland WMA and St. Catherine Creek NWR.*

	Shipland WMA		St. Catherine Creek NWR	
Frequency	200 MHz	400 MHz	200 MHz	400 MHz
Dielectric Constant	8	8	20	20
Velocity	0.106 m/ns	0.106 m/ns	0.067 m/ns	0.067 m/ns

5.3.2 Shipland WMA

At Shipland WMA, GPR reveals subsurface topography not visible from sediment cores alone. In the 400 and 200 MHz scans, an anomalous layer with abundant parabolic reflectors is observed just below the surface. Below this, monoclinal/inclined reflections dip toward the channel in transect A-A' from 0.5-3 m (Fig. 5.7). In transect A-A', a series of at least two distinct, strong reflectors is observed; these layers are not continuous perpendicular to the channel. These reflectors are less pronounced in B-B' (Fig. 5.8). In both transects, the inclined reflections are better pronounced in the 200 MHz data, but layer resolution is better in the 400 MHz profiles. Below 3.5-4 m, signal loss prevents succinct identification of structures.

5.3.3 St. Catherine Creek NWR

At St. Catherine Creek NWR, all visible bedding is nearly horizontal. Abundant parabolic disruptions are located from the surface to roughly 0.4 m deep. No strong reflector layers comparable to SWMA were observed, but some forms are visible in the 200 MHz data, such as 65 meters, 1 m deep in transect A-A' (Fig. 5.9). And 35 meters, 1 m deep in transect B-B' (Fig. 5.10). Horizontal tracers are prevalent across the study site in both transects.

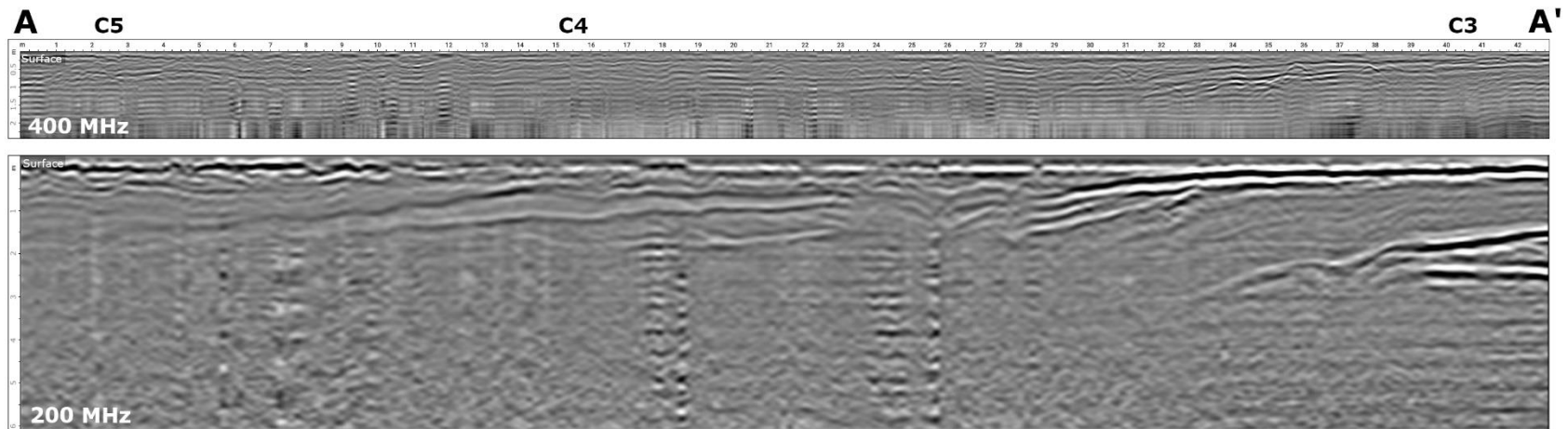


Figure 5.7 Processed GPR transect A-A' at Shipland WMA

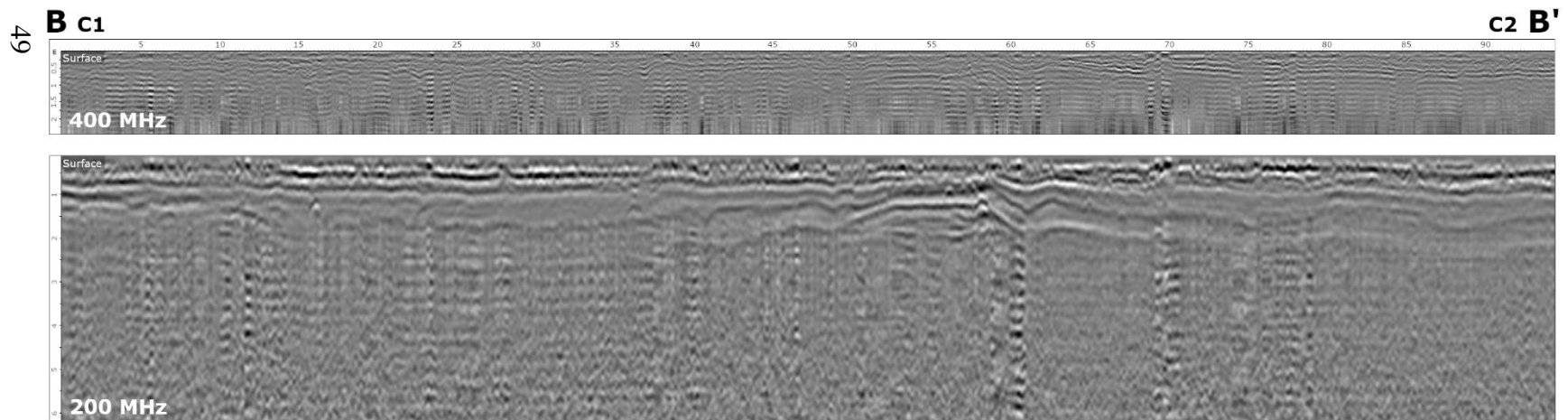


Figure 5.8 Processed GPR transect B-B' at Shipland WMA

A-A' is perpendicular to the river channel; B-B' is parallel to the channel. Approximate core locations are marked by C# at the top of the transects. Both scans are shown with Auto Gain filters.

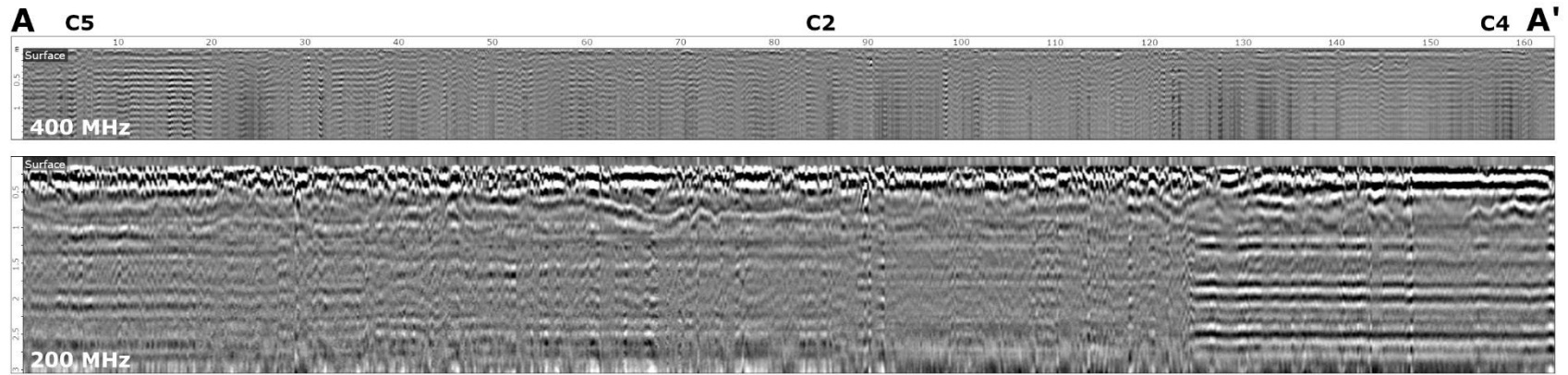


Figure 5.9 Processed GPR transect A-A' at St. Catherine Creek NWR

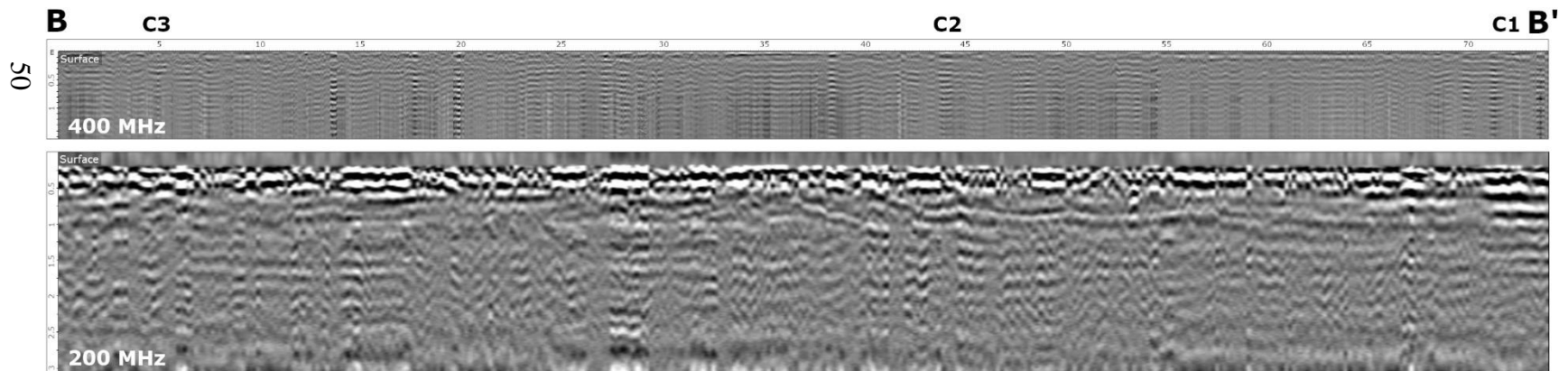


Figure 5.10 Processed GPR transect B-B' at St. Catherine Creek NWR

A-A' is parallel to the river channel; B-B' is perpendicular to the channel. Approximate core locations are marked by C# at the top of the transects. Both scans are shown with Auto Gain filters.

CHAPTER VI – DISCUSSION

Based on percentile trends (Dx 10, Dx 50, and Dx 90), distinct systematic shifts in grain size (potentially individual flood events) can be correlated among cores at each site. When laid in perspective of the elevation profile in cross section view, potential flood deposits can be traced across the cores along correlative layers.

Once aligned in cross-sectional view, correlative grain size layers make sense in the context of depth/elevation after the applied method of core length extrusion – this may be a viable option for saturated floodplain cores to correct for depth. Without access to holes or trenches for ground-truthing on site, the method of core depth extrusion utilized in this project may be the best way to correct core shortening if large-diameter core sleeves are not available. However, this method does not account for variation in saturation, organic content, or grain size that could preferentially compress certain areas of a core over others. Without ground-truthing, this facet is a necessary drawback in order to align sediment cores at correlative horizons.

6.1 Sedimentary Structures and Depositional Trends

Major and minor flood events cannot be succinctly identified without a temporal record, such as ^{14}C . Assumed flood deposits are abundant in the core profiles at each site, but there is little evidence based on lithology alone to delineate specific events in history to what is seen in the core profiles.

Flood deposits are thicker and sedimentation rate is higher at Shipland WMA than St. Catherine Creek NWR, but this does not directly imply greater degrees of flood sedimentation near Vicksburg. This does not reflect the historical trend of Natchez receiving more frequent and severe floods than Vicksburg. The sedimentation dynamics

at Shipland WMA are likely a facet of the point bar/meander scroll depositional environment presenting local topographic traps to collect sediment, thereby accentuating the degree of flood sedimentation. A more apt comparison would be between the same depositional subenvironment at each site.

Depositional changes are apparent at both sites, as seen in the percentile graphs (Fig. 5.5 and 5.6). Whether these result from river engineering or are a facet of different/separate flood dynamics (or both) is not yet known. Trendlines do not indicate an apparent trend toward coarser or finer sedimentation in the upper 6 m of the floodplain profile at either site. The best method to determine flood deposits may be to identify fining-upward layers (i.e., beds, laminations), which likely represent longer duration flood events that allowed suspended load differentiation. Many more of these fining-upward deposits can be seen at St. Catherine Creek; at Shipland, they are sporadic. This variation may be a facet of sedimentation style/environment of deposition, but St. Catherine by nature preserves a better record of all flood events compared to Shipland.

There is no immediate distinction among flood layers through time aside from any major flood event outliers – there is little evidence of systematic change to be observed using these methods due to variation between separate floods. Furthermore, not every flood may be represented as fining upward. Each flood may be different in terms of energy, erosive capacity, sediment load, etc. For example, the 2011 flood only deposited a few centimeters in some locations despite being a major flood, whereas the 1973 flood carried a greater sediment load (Kesel and others, 1974; Heitmuller and others, 2017).

Laminations are present at both study sites throughout all cores, which could result from minor flood events (both sites) or may be cross-bedding structures (Shipland)

not identifiable in the small diameter core liners used in this study. It is most likely that long inundation would create more distinctive differentiation than a short or shallow flood.

The best ^{14}C results yielding the more believable/representative dates of deposition at each site are SWMA Core 2 (1965-recent) and SCC Core 5 (mid 1800s-recent). While the 95% confidence interval is most common in ^{14}C analyses, it does not provide as narrow of a time range as the 68% confidence interval. When assessing distinct flood events from organic material, much of which having been reworked from older deposits upstream, narrow time ranges are vital. Although confidence and accuracy decline by using the 68% dataset, this tradeoff was deemed necessary to constrain chronology and identify flood event markers. The 68% confidence dataset was especially important in identifying the 2011 flood. In several cores (SWMA C3, SCC C2, C3, C4, and C5), the ^{14}C data was constrained either earlier or later than the 2011 flood by the 68% dataset, whereas these 95% dataset hinted at more general times in the early 2000's (Table A.2).

6.1.1 Shipland WMA

The Shipland site predominantly deposited via lateral accretion. In GPR, structures were observed offlapping toward the channel direction. Variation in grain size most likely derives from the ridge and swale setting, resulting in topographic lows that entrap finer grained suspended load during inundation through vertical accretion. Furthermore, grain size is determined by flow velocity of individual flood events. No evidence of soil development was observed, indicating frequent deposition and activation of the floodplain sediments and is a facet of the high sedimentation rate of around 10.6

cm/yr. No direct trend toward finer nor coarser grain size was observed through time, which may be obscured by the heterogeneity of the subsurface structures.

The Shipland WMA site is located within a meander scroll; similar features and topography are interpreted in the subsurface. Transect A-A' displays correlative silt-clay-silt sequences in Cores 3 (500 cm) and 5 (400 cm). Core 4, which is directly in between, exhibits uninterrupted sand deposits below 160 cm. This variation may represent a ridge in Core 4, with juxtaposed swales in Cores 3 and 5 that collected finer grained sediments. Splays of sand interrupt the silt lenses in Cores 3 and 5, which could represent a major flood or a particularly high-energy flood/storm event that remobilized sand from the ridge in Core 4. Although ^{14}C sample resolution is poor, this sand layer dates approximately to the late 1960s to early 1970s.

6.1.2 St. Catherine Creek NWR

Nearly every observed stratum from St. Catherine Creek NWR is laterally correlative across all cores, both parallel and perpendicular to the river, with minimal relief or change between cores. This sedimentation style is typical of a low energy backswamp setting; however, St. Catherine Creek NWR has more fine sand and less clay than expected in a backswamp. The depositional environment at the study site may be better described as a natural levee or a marginal/transition zone between the levee and backswamp given proximity to the river, potentially a levee backslope. This finding may indicate a shift from pre-disturbance natural deposition patterns to post-disturbance additions of relatively coarse sediment. All flood deposits at St. Catherine appear low energy and laminated, limiting the ability to determine major or minor floods based solely on grain size. Minor proportions of sand disrupt the silt-dominated flood deposits,

which may be event markers. However, without a well-constrained temporal record, historical flood events must be estimated based on relative ^{14}C data that has not been reworked.

Only vertical accretion processes were observed in the St. Catherine Creek overbank profile. Deposition across the study site is nearly horizontal. Grain size trends across all cores do not indicate a definitive trend toward finer or coarser sediments. The depositional environment is best defined as a levee backslope considering the proportion of fine sand observed in grain size analyses. Soil development at this site is infantile but apparent (entisol), which may be a facet of constant but slow sediment accumulation (2.5-3.5 cm/yr).

6.2 GPR Interpretation

GPR imagery beyond the upper ~1 m overbank profile is not adequate or fine enough scale to determine individual flood layers. GPR's best application in this research is to visualize structures that cannot be preserved or viewed in the core profiles, such as the ridge and swale structures seen at Shipland WMA.

Percentile grain size trends are good for indicating systematic shifts between coarser and finer sediment deposition but are problematic in assessing individual flood events. For example, in Shipland WMA Cores 3, 4, and 5, C4 does not show any change in sandy lithology at the same correlation points as C3 or C5. This variation supports the need for GPR data to supplement sediment cores, where subsurface structures can be interpreted in the GPR profile but are not readily visible in core profiles alone. Based on GPR imagery and the depositional environment, this region is interpreted as a ridge in Core 4 with corresponding swales in Cores 3 and 5 (Fig. 20). A sand splay is recorded in

Cores 3 and 5 within the swales, which likely derives from a high-energy flood event that deposited new sand or remobilized sand from the ridge in Core 4.

6.2.1 Shipland WMA

In both 400 MHz (Fig. 6.1) and 200 MHz (Fig. 6.2) transects, vertical accretion is the predominant sedimentary style. Hard inclined tracers seen in radar best reflect the lateral accretion facies (facies 3) presented by Dara and others (2019). The uppermost sediments at SWMA are fine sands that overlie an organic rich mud layer of variable thickness, defined in the radar profiles of both transects as a cap of facies 2 above organic accumulation (facies 5) (Dara and others, 2019). Beneath the organic layer, laterally accreting sands dip toward the channel, sporadically interrupted by lenses of mud.

6.2.2 St. Catherine Creek NWR

Vertical accretion is the only depositional style observed at SCC (Fig. 6.3 and 6.4). Organic material is abundant at the surface of all cores, as seen in both transects. In the 400 MHz profiles, the only facies identified are an upper organic-rich layer underlain by horizontal layers of vertically accreted material. In the 200 MHz profiles, some variable and structureless zones were observed, attributed to general muddy lenses (facies 2) or unstructured clay accumulation (facies 8) (Dara and others, 2019). These lenses may be attributed to poor 200 MHz scan quality because they are not seen in the higher-detailed 400 MHz profile at correlative depths. Regardless, the SCC overbank profile is nearly homogeneous through depth, consisting of nearly flat horizontal beds.

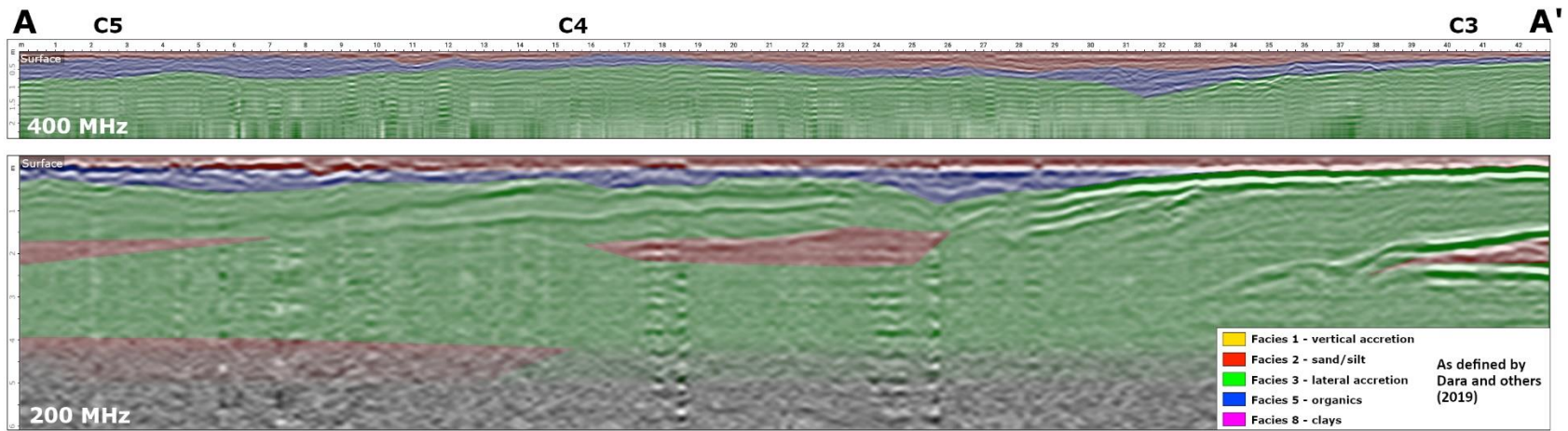


Figure 6.1 GPR interpretations of Shipland WMA transect A-A'

57

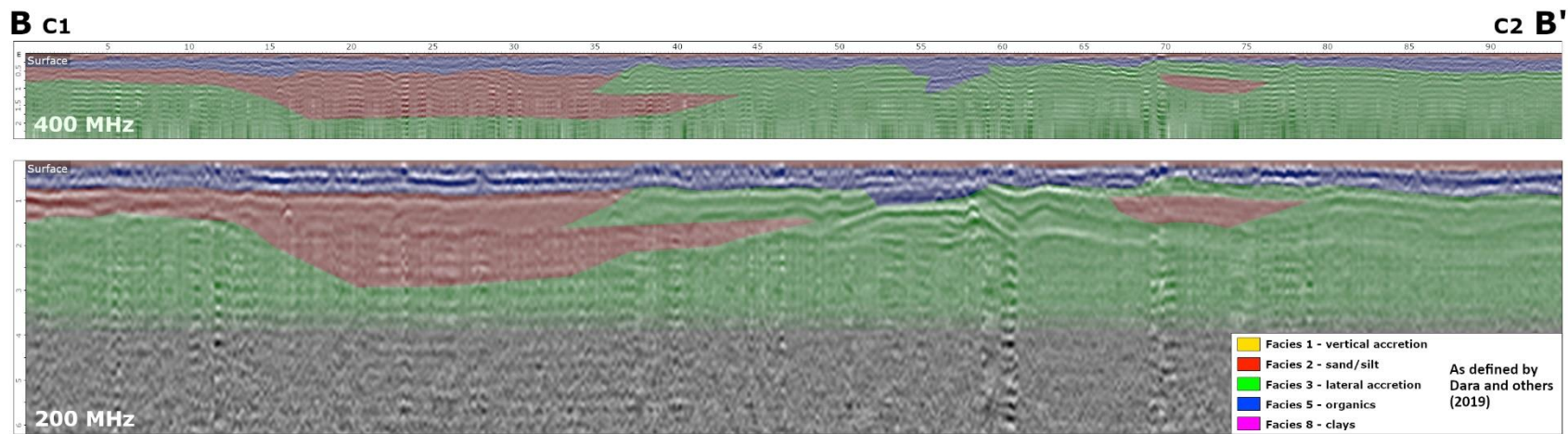


Figure 6.2 GPR interpretations of Shipland WMA transect B-B'

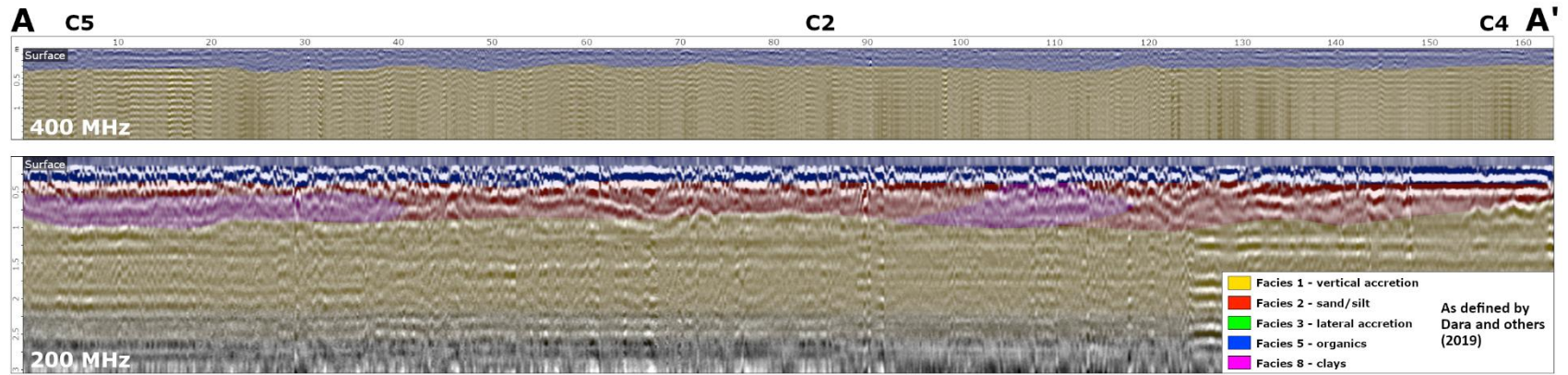


Figure 6.3 GPR interpretations of St. Catherine Creek NWR transect A-A'

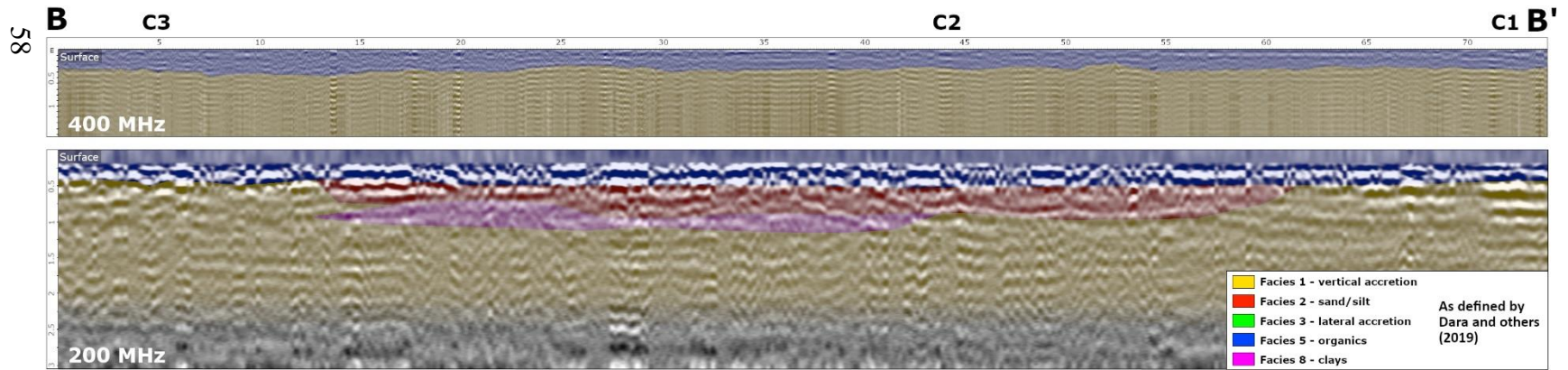


Figure 6.4 GPR interpretations of St. Catherine Creek NWR transect B-B'

6.3 Flood Event Interpretations

All sedimentary structure and flood event marker interpretations derived from core profiles and GPR are displayed in cross-section view in Figures 6.5-6.8.

6.3.1 1973 Flood

6.3.1.1 Shipland WMA

Kesel and others (1974) reported that natural levees received up to 53 cm of predominantly sand south of Natchez. It is possible that the sand stratum that blankets the Shipland site in Core 3 (500 cm) and Core 5 (400 cm) was deposited during the 1973 flood. This sand sheet is not likely a result of crevassing in this depositional environment. A high energy or major flood event may have mobilized a sand sheet across the site. Core 2 contains the best chronological record of ^{14}C data, with a sample just above this sand sheet dated to 1969-1970. This layer likely represents or directly underlies an event marker for the 1973 flood. The organic material sampled here could be reworked from recent material that was deposited in 1973. The mud drape observed overlying the sand sheet in Core 2 could also represent the 1973 flood. This event was known to deposit relatively fine-grained sediments at Natchez (Kesel and others, 1974); however, a major event would be necessary to mobilize or rework sand across the entire study site.

6.3.1.2 St. Catherine Creek NWR

Pinpointing this event in the St. Catherine Creek profile is less effective due to unconfined ^{14}C dates or outlier strata. Organic material dating to the 1980s was found between 1-1.4 m deep in St. Catherine Creek Core 3. The 1973 flood could be represented by one of the minor grain size transitions observed near 2 m depth. Some

backswamp areas south of Natchez only received 1 cm of silt and clay deposition during this flood (Kesel and others, 1974).

6.4 2011 Flood

6.4.1.1 Shipland WMA

¹⁴C data near the surface of the Shipland cores contains some discrepancies, but all dates within the upper 1 meter are from the year 2000 or later. The latest dated material from SWMA is from 2010 at the latest (Core 3, 20 cm). Unless this sample was pushed down via coring or reworked, this could be the event marker for the 2011 flood. This sample was collected from the upper portion of the organic-rich mud layer that blankets the entire SWMA site just below the surface. All organic samples recovered from this layer date from at least 2000, but the extent of reworking of older organic material during the 2011 flood is unknown. A sample collected from 218 cm in Core 1 dated to 2004-2008 from the sand layer beneath the mud blanket. If this sample was not reworked, then the sand layer directly underlying the organic-rich mud was deposited not long before the 2011 flood event. The most likely event marker for the 2011 flood is within the mud layer just below the surface of all cores (between 10-100 cm; Fig. 6.5 and 6.6).

6.4.1.2 St. Catherine Creek NWR

Sedimentation at Natchez from the 2011 flood was low, reportedly between 3-138 mm in the backswamp and natural levee, respectively (Heitmuller and others, 2017). This event was relatively high energy but carried a relatively low proportion of coarser-grained sediments compared to the 1974 flood (Heitmuller and others, 2017).

In transects A-A' (Fig.6.7) and B-B' (Fig. 6.8), a fluctuation from fine to coarser sediments is observed within the upper 1 m of all cores except Core 5. Carbon material in this zone dates to 2011-2016 (Core 2), 2006-2011 (Core 4), and 2007-2012 (Core 4). Outlier/nonconformable samples such as 2013-2019 at 190 cm in Core 4 were likely pushed down via coring. The best indicators for the 2011 flood event at SCC are grain size fluctuation and similar ^{14}C sample accumulation, around 50 cm in Core 3.

Based on the estimated sedimentation rate of 3 cm/year, the 2011 flood would be roughly 39 cm deep across the core profiles. This discrepancy could be attributed to changes in sedimentation rate from artificial effects or from fallacies in the core depth extrusion method/rate calculation it was based upon. Because these cores were length extruded to account for compaction, no assessment on change in sedimentation rate through time should be made.

6.5 2018-2019 and 2020 Floods

Between fall 2022 to summer 2023, the LMR experienced low stage flow due to drought conditions (USACE, 2024). The last major flood events prior to the time of publishing occurred during the 2018-2020 floods, which inundated both study sites (USACE, 2023c; USACE 2023d). These flood deposits likely constitute the uppermost sediments deposited at Shipland WMA and St. Catherine Creek NWR.

6.5.1.1 Shipland WMA

Published data from these events are lacking from the Shipland WMA site. These flood events are likely represented by the uppermost few centimeters at SCC. Without a reference for deposition at SWMA, it is assumed that the uppermost sediments derive from the 2018-2020 floods, but these events cannot be accurately confined beyond lying

above the 2011 event marker. The 2018-2020 floods are likely represented within the uppermost sand layer overlying the proposed 2011 organic-rich layer.

6.5.1.2 St. Catherine Creek NWR

The sedimentation dynamics of the 2018/19 and 2020 floods were reported at the St. Catherine Creek site by Kelk (2022): 3.7 cm on average for both events combined. Although minimal, this provides an estimation for the anticipated thickness of the 2018-2020 floods at this site. No ^{14}C data can be directly confined after 2018 at this site to pinpoint dates of deposition. Very recent, minor floods may have deposited very thin layers over the 2020 event marker, but low stage and drought conditions prevalent at the time of core collection (USACE, 2024) prevented the possibility for much accumulation after the 2020 flood. Given the estimated thickness, how recently these floods occurred, and the slow accumulation rate at the study site, the 2018-2020 floods are likely represented within the uppermost 5-10 cm of the core profiles.

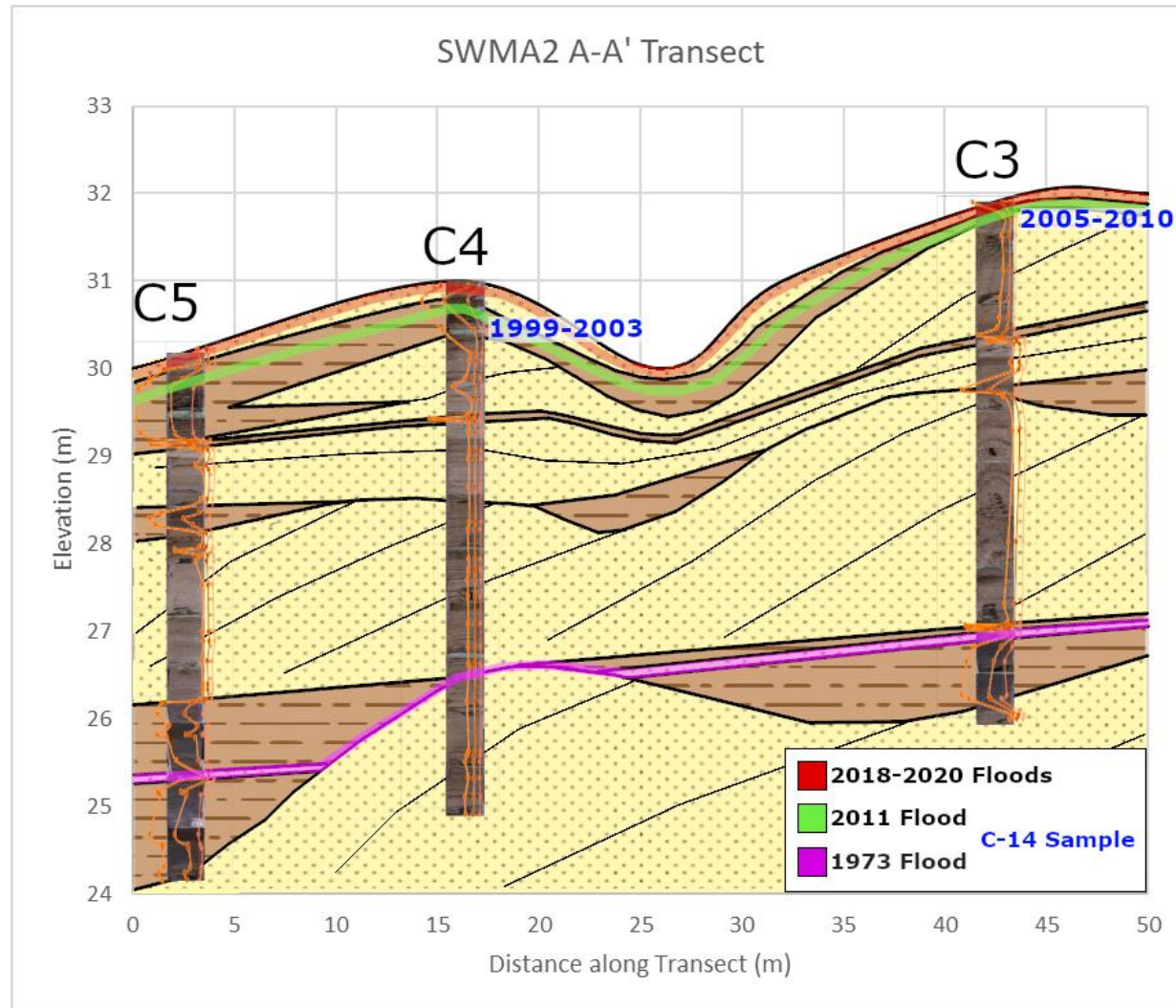


Figure 6.5 Overbank profile interpretations of Shipland WMA transect A-A'

Core photographs are overlain by Dx 10, 50, and 90 grain size data. ^{14}C dates listed are based on 68% confidence results. Only ^{14}C samples assumed in situ are included. 5x vertical exaggeration.

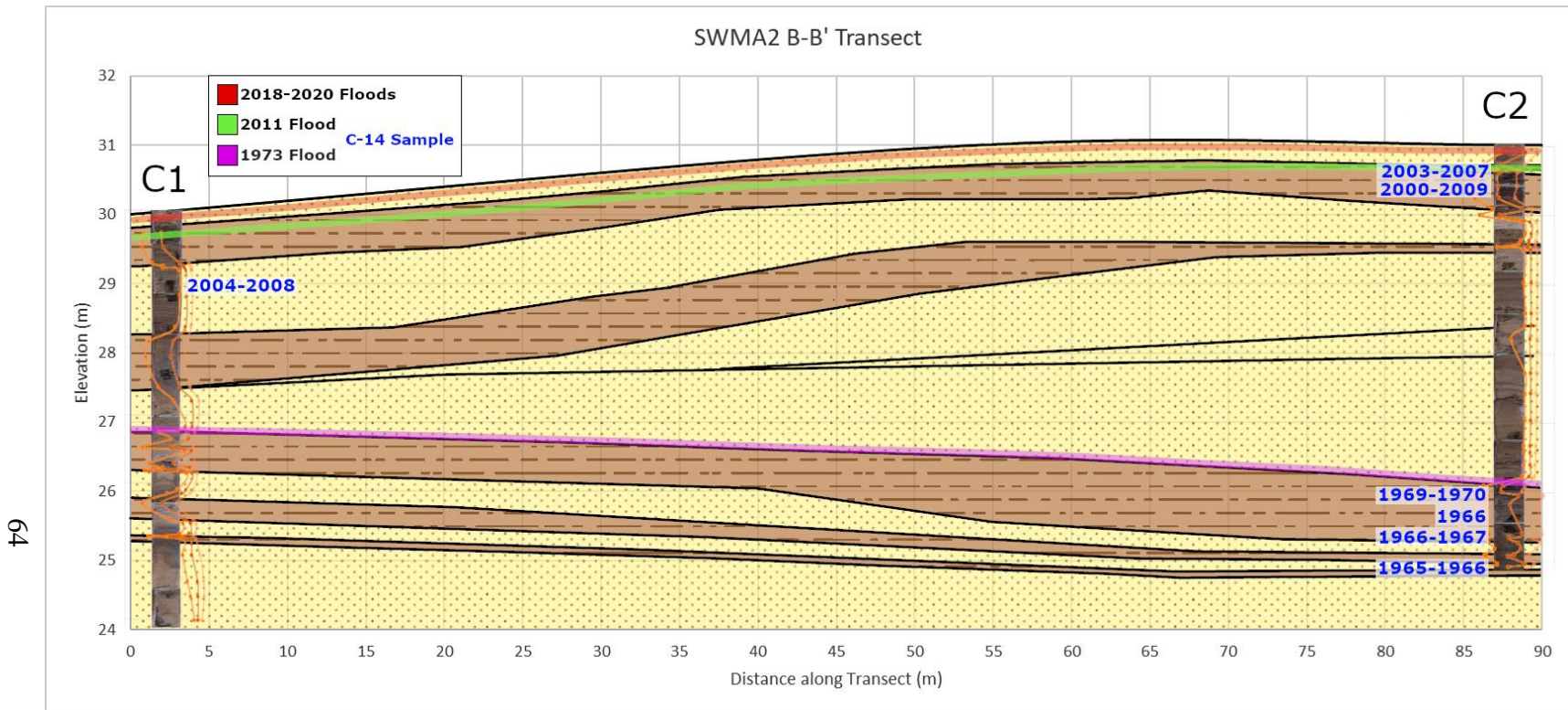


Figure 6.6 Overbank profile interpretations of Shipland WMA transect B-B'

Core photographs are overlain by Dx 10, 50, and 90 grain size data. ¹⁴C dates listed are based on 68% confidence results. Only ¹⁴C samples assumed in situ are included. 5x vertical exaggeration.

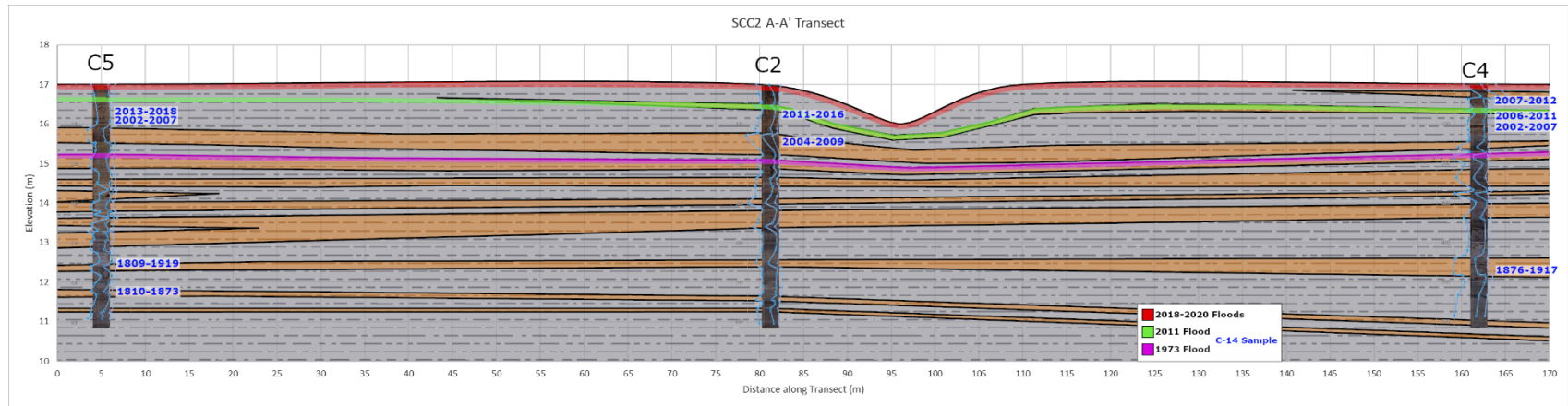


Figure 6.7 Overbank profile interpretations of St. Catherine Creek NWR transect A-A'

69

Core photographs are overlain by Dx 10, 50, and 90 grain size data. ¹⁴C dates listed are based on 68% confidence results. Only ¹⁴C samples assumed in situ are included. 5x vertical exaggeration.

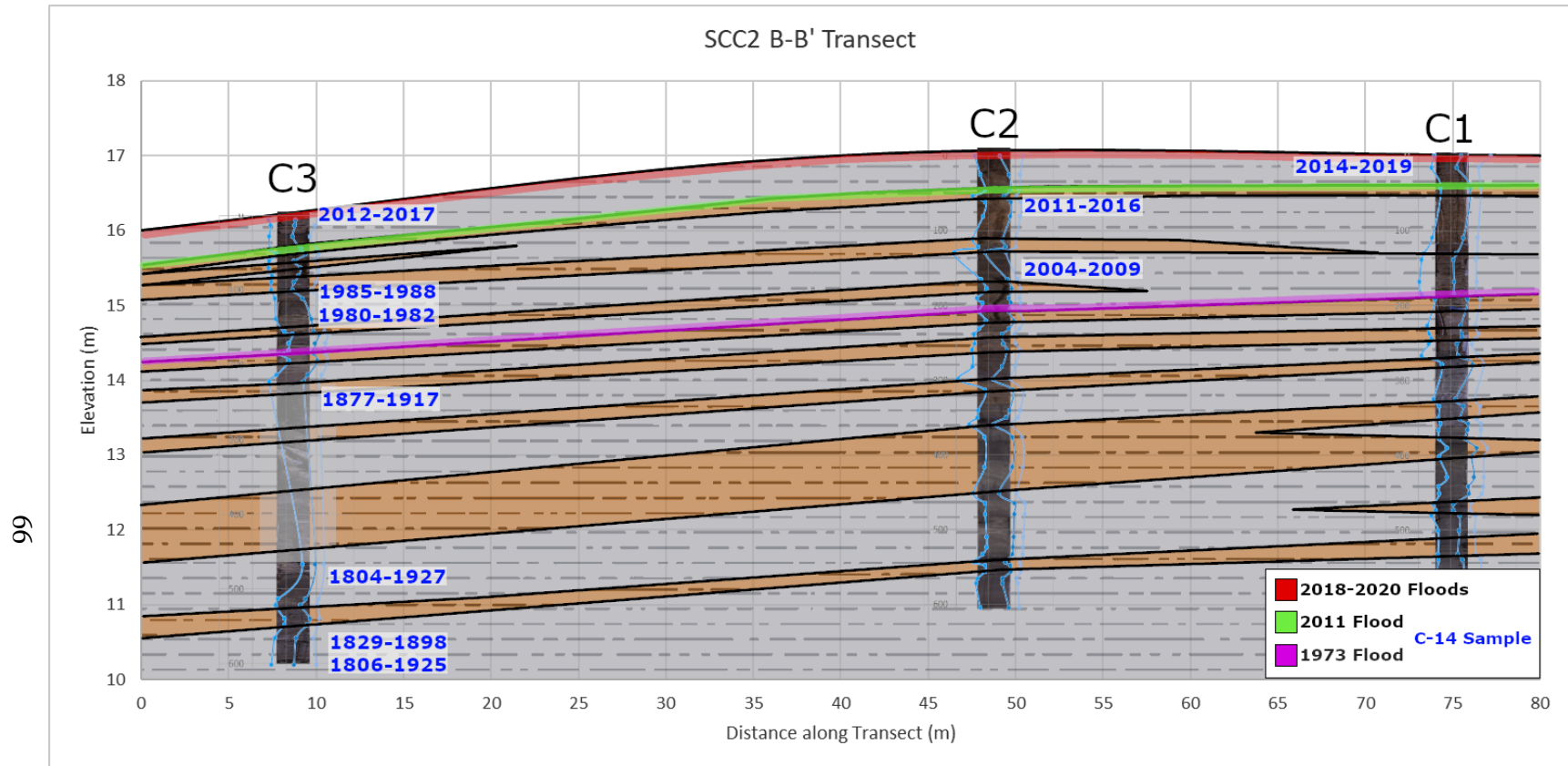


Figure 6.8 Overbank profile interpretations of St. Catherine Creek NWR transect B-B'

Core photographs are overlain by Dx 10, 50, and 90 grain size data. ¹⁴C dates listed are based on 68% confidence results. Only ¹⁴C samples assumed in situ are included. 5x vertical exaggeration.

CHAPTER VII – CONCLUSIONS

(1) Do overbank sedimentary deposits of major floods remain distinctive with progressive burial, and are major flood deposits more distinctive than minor flood deposits with progressive burial?

Flood events on the Lower Mississippi River are controlled by different parameters for each flood. For example, although the 2011 flood produced higher flood stages and longer inundation periods than the 1973 flood at Vicksburg and Natchez, 2011 characteristically deposited a fraction of the sediment in comparison. While the major floods on record have assumedly deposited more sediment per event than minor floods (which may have only deposited millimeters of laminated sediments at both study sites), pinpointing them in the overbank profile without defined date points can be subjective. Major floods can certainly remain distinctive after burial, but the limited availability of dateable organic material in the Shipland WMA and St. Catherine Creek NWR cores results in hypothetical estimations based on subsurface structures and grain size characteristics. If a major flood event deposits very little sediment at a site, it may not appear any more distinct than a minor flood containing a greater sediment load. However, if a flood has known characteristics (such as thin deposition of coarser grains in 2011), it may be possible to pinpoint the individual event marker.

Of the major flood events in question, the 1973 flood is estimated as the sandy splay observed in Shipland WMA Cores 3 and 5 at 503.8 cm and 489.9 cm, respectively. At St. Catherine Creek NWR, the 1973 flood is estimated within roughly 200 cm in Core 2. The 2011 flood is located within the uppermost mud layer observed in all Shipland cores below the sand cap. St. Catherine, the 2011 flood is marked at the subtle grain size

transition around 50 cm deep in Core 3. The 2018/2019 and 2020 floods are harder to differentiate given their close timing and recent occurrence. At SWMA, these floods are interpreted as the uppermost sands overlying organic-rich mud. SCC reportedly received very little sediment from these events, but these would have been among the last inundation periods prior to coring. These floods are assigned somewhere within the upper 10 cm of the overbank profile.

(2) How can sediment cores and ground-penetrating radar reveal how river management practices, modifications, and land use changes have affected sediment dynamics and floodplain evolution of the Mississippi River floodplains at Shipland WMA and St. Catherine Creek NWR?

GPR has limited applications in analyzing floodplain dynamics at the Shipland WMA and St. Catherine Creek NWR study sites. 400 MHz GPR is best utilized to visualize fine stratal changes in the uppermost overbank profile, whereas 200 MHz reveals more distinct tracers across the study sites up to 5 meters depth and is better for general interpretations. Due to fine-grained sediments and water saturation at both sites, GPR resolution was poor at depth. GPR alone is not an effective method to determine sedimentation changes through time; its best application lies in ground-truthing and correlation among boreholes across sites to infer subsurface structures that are not readily observable solely in the core profiles. If event markers are defined in sediment cores, GPR can be used to interpret the structure and extent of specific flood layers across an entire site. The data analyzed in this research is not conducive to determine systematic changes in floodplain dynamics through time at either study site.

Radar facies defined by Dara and others (2019) can be applied to the GPR scans collected from SWMA and SCC. At Shipland, lateral accretion appears to be the dominant depositional style, with discrete organic-rich and muddy layers. At St. Catherine Creek, vertical accretion is observed through the entire radar profile. Much of the organic material observed derives from root structures of dense contemporary vegetation and recent accumulation.

(3) What are the temporal and spatial relationships between sediment composition and grain size distribution in the Mississippi River floodplains at Shipland WMA and St. Catherine Creek NWR, and how can sediment cores and ground-penetrating radar contribute to understanding this relationship?

General grain size trends through time at Shipland WMA and St. Catherine Creek NWR are inconclusive due to the variation between individual flood events and the controls defined by topography and depositional setting on sediment accumulation (SWMA). While major flood events inundate both Shipland WMA and St. Catherine Creek NWR, the sedimentary records at both sites are obscured by minor/localized floods, observed as finely laminated deposits. Shipland WMA preserves a better record of major floods due to elevation and floodplain energy, where major/higher energy events must crest the flood stage for sediment deposition. St. Catherine Creek NWR contains a more definitive record of all flood events; however, the low-energy, fine-grained nature of the natural levee/backswamp at this location enables minor floods to deposit thin laminae of silt frequently. To compound this, St. Catherine Creek likely inundates more frequently given its proximity to Natchez, so major flood events can easily be obscured, especially if the flood in question deposits little sediment (i.e., 2011 near Natchez).

Sediment cores and GPR can be utilized to assess flood history, but tracking temporal changes is not feasible without a way to systematically date material through depth. Furthermore, this study lacks a direct comparison between equivalent depositional environments – Shipland WMA is on the point bar, whereas St. Catherine Creek NWR is a levee backslope. A direct comparison between the areas with the same sedimentation style would be ideal. From the data collected in this project, historical flood marker events can be approximated, but tracking systematic changes through time at either site would be speculative. With better constrained temporal records (Cs/Pb dating methods), variation in sedimentation rate through time may be a proxy to assess changes in historical vs. recent depositional trends. In a river as large and dynamic as the Mississippi, it may not be feasible to track sediment changes over time from these basic methods – the specifics of each individual flood are different in sediment load, water flow, and provenance, which may disrupt/mask any general trends that could be observed in a smaller tributary or watershed.

APPENDIX A – Data Tables

Table A.1 *The 50 highest flood crests recorded at Vicksburg and Natchez, MS*

Displayed in Figure 1.2. Flood stage at Vicksburg: 13.1 m/43 ft. Flood stage at Natchez: 14.6 m/48 ft (USACE, 2023d; USACE, 2023c).

Vicksburg				Natchez			
Crest (m)	Date	Crest (m)	Date	Crest (m)	Date	Crest (m)	Date
15.30	1/1/1900	15.18	4/13/1975	15.33	3/28/1903	15.15	4/27/1993
14.36	1/2/1900	14.60	4/26/1979	15.67	4/14/1912	15.15	5/19/1993
15.09	3/28/1903	15.04	5/27/1983	16.03	4/27/1913	15.16	5/20/1993
14.45	2/12/1907	13.96	5/25/1984	16.31	2/15/1916	15.97	5/7/1994
13.81	6/4/1908	13.53	1/20/1991	15.70	4/28/1920	16.18	6/14/1995
13.93	3/31/1909	13.29	5/18/1993	16.86	4/26/1922	15.09	6/3/1996
15.03	4/12/1912	14.02	5/3/1994	17.25	5/4/1927	17.16	3/26/1997
15.21	4/27/1913	14.33	6/12/1995	16.61	6/5/1929	15.24	5/16/1998
15.70	2/15/1916	14.97	3/22/1997	16.00	3/1/1932	15.70	6/4/2002
14.54	4/23/1917	13.29	5/14/1998	15.36	6/12/1933	15.59	2/1/2005
14.84	4/27/1920	13.84	6/3/2002	15.36	4/21/1935	17.38	4/23/2008
16.00	4/28/1922	13.57	1/30/2005	17.69	2/21/1937	16.59	5/30/2009
13.90	4/9/1923	15.54	4/20/2008	15.12	5/16/1944	15.19	4/2/2011
17.13	5/4/1927	14.51	5/28/2009	16.82	4/29/1945	18.88	5/19/2011
14.33	7/12/1928	13.17	3/30/2011	16.28	3/4/1950	15.45	5/25/2013
16.09	6/6/1929	17.40	5/19/2011	15.30	6/1/1961	15.25	4/2/2015
15.12	2/28/1932	13.51	5/23/2013	17.28	5/13/1973	16.07	7/27/2015
14.23	4/14/1935	14.01	7/26/2015	15.51	2/10/1974	17.30	1/17/2016
16.22	2/21/1937	15.31	1/15/2016	16.47	4/12/1975	15.61	3/20/2016
13.90	5/15/1944	13.20	3/18/2016	16.64	4/23/1979	16.74	5/26/2017
15.18	4/27/1945	14.78	5/25/2017	16.98	5/31/1983	17.41	3/18/2018
13.72	3/2/1950	15.22	3/15/2018	15.85	5/26/1984	17.65	3/12/2019
13.69	5/30/1961	15.69	3/12/2019	15.21	6/10/1990	17.54	4/15/2020
15.73	5/13/1973	15.38	4/13/2020	15.70	1/20/1991	16.09	4/15/2021
13.47	2/9/1974	13.96	4/15/2021	15.24	5/2/1991	15.17	3/19/2022

Table A.2 ¹⁴C data collected from all cores.

Dates were calibrated using CALIBomb (Reimer and others, 2004). Red represents inaccurate or reworked material. Yellow represents a questionable datum.

Sample ID	F Modern	Fm Err	Age Err	δ ¹³ C	95 % Confidence	68% Confidence
SWMA Core 1: 218 cm	1.0658	0.0107	55	-25.74	2002-2010 CAL AD 90%	2004-2008 CAL AD 82%
SWMA Core 1: 235 cm	1.5267	0.0153	45	-27.72	1969-1971 CAL AD 70%	1970-1971 CAL AD 80%
SWMA Core 1: 269 cm	0.1134	0.0037	260	-21.75	20,530-21,948 CAL BP 100%	20,800-21,480 CAL BP 96%
SWMA Core 2: 47 cm	1.0708	0.0107	55	-27.94	2001-2010 CAL AD 89%	2003-2007 CAL AD 82%
SWMA Core 2: 61 cm	1.0731	0.0107	55	-25.12	2000-2009 CAL AD 90%	2002-2006 CAL AD 79%
SWMA Core 2: 502 cm	1.5573	0.0156	45	-26.37	1968-1970 CAL AD 91%	1969-1970 CAL AD 78%
SWMA Core 2: 564 cm	1.7	0.017	45	-26.4	1965-1967 CAL AD 93%	1965.7-1966 CAL AD 65%
SWMA Core 2: 572 cm	1.6864	0.0169	45	-25.75	1966-1967 CAL AD 92%	1966-1967 CAL AD 96%
SWMA Core 2: 603 cm	1.7045	0.017	45	-28.25	1965-1966 CAL AD 81 %	1965-1966 CAL AD 95%
SWMA Core 3: 20 cm	1.0587	0.0106	55	-26.75	2003-2012 CAL AD 90%	2005-2010 CAL AD 88%
SWMA Core 3: 392 cm	0.055	0.003	430	-23.93	26,878-28,600 CAL BP 97%	27,148-27,924 CAL BP 100%
SWMA Core 3: 396 cm	0.0278	0.0027	790	-23.47	31,312-34,688 CAL BP 100%	32,120-33,980 CAL BP 100%
SWMA Core 3: 398 cm	0.0939	0.0032	280	-22.93	22,397-23,437 CAL BP 91%	22,533-23,194 CAL BP 100%
SWMA Core 3: 507 cm	0.0516	0.003	460	-22.82	27,268-29,029 CAL BP 100%	27,651-28,599 CAL BP 100%
SWMA Core 3: 513 cm	0.8732	0.0087	65	-26.77	773-1053 CAL AD 90%	878-1030 CAL AD 94%
SWMA Core 4: 49 cm	1.0902	0.0109	55	-25.12	1996-2004 CAL AD 88%	1999-2003 CAL AD 91%
SWMA Core 4: 172 cm	0.6472	0.1348	1700		7072 CAL BC-1398 CAL AD 100%	4066-34 CAL BC 98%
SWMA Core 4: 196 cm	0.2094	0.0059	220		13,606-12,118 CAL BC 100%	13,260-12,826 CAL BC 53%
SWMA Core 4: 208 cm	0.154	0.004	210	-23.13	16,842-15,937 CAL BC 100%	16,696-16,243 CAL BC 100%
SWMA Core 4: 237 cm	0.0808	0.0034	340	-23.07	22,740-21,906 CAL BC 100%	23,287-21,773 CAL BC 98%
SCC Core 1: 3 cm	1.0185	0.0102	60	-29.95	2009-2019 CAL AD 75%	2014-2019 CAL AD 86%
SCC Core 1: 49 cm	0.9962	0.01	60	-31.72	1797-1942 CAL AD 64%	1810-1874 CAL AD 43%
SCC Core 1: 149 cm	1.3804	0.1281	750		1968-1988 CAL AD 85%	1964-2019 CAL AD 74%
SCC Core 1: 186 cm	0.6711	0.025	300		2288-801 CAL BC 100%	1826-1110 CAL BC 95%
SCC Core 1: 279 cm	1.0216	0.0102	60	-27.94	2008-2019 CAL AD 84%	2013-2018 CAL AD 80%
SCC Core 1: 323 cm	1.0258	0.0103	60	-28	2010-2019 CAL AD 86%	2013-2017 CAL AD 78%
SCC Core 2: 88 cm	1.0314	0.0103	70	-28.63	2009-2019 CAL AD 86%	2011-2016 CAL AD 86%
SCC Core 2: 157 cm	1.0602	0.0106	55	-29.06	2002-2012 CAL AD 90%	2004-2009 CAL AD 81%
SCC Core 2: 409 cm	1.0052	0.0101	60	-28.66	1798-1942 CAL AD 62%	1878-1915 CAL AD 31%
SCC Core 3: 3 cm	1.0278	0.0103	60	-25.13	2010-2019 CAL AD 86%	2012-2017 CAL AD 79%
SCC Core 3: 103 cm	1.1899	0.0119	55	-27.73	1984-1989 CAL AD 77%	1985-1988 CAL AD 77%
SCC Core 3: 137 cm	1.2541	0.0125	55	-26.99	1980-1983 CAL AD 86%	1980-1982 CAL AD 90%
SCC Core 3: 230 cm	0.9993	0.01	60	-27	1798-1942 CAL AD 64%	1877-1917 CAL AD 32%
SCC Core 3: 488 cm	0.9889	0.0099	60	-27.01	1794-1949 CAL AD 61%	1804-1927 CAL AD 72%
SCC Core 3: 570 cm	0.9834	0.0098	60	-27.3	1652-1955 CAL AD 100%	1829-1898 CAL AD 35%
SCC Core 3: 592 cm	0.9904	0.0099	60	-27.98	1795-1949 CAL AD 62%	1806-1925 CAL AD 73%
SCC Core 4: 37 cm	1.0477	0.0105	60	-28.86	2004-2014 CAL AD 88%	2007-2012 CAL AD 80%
SCC Core 4: 85 cm	1.0523	0.0105	60	-28.49	2004-2013 CAL AD 90%	2006-2011 CAL AD 83%
SCC Core 4: 88 cm	1.0712	0.0107	65	-28.93	2000-2009 CAL AD 89%	2002-2007 CAL AD 82%
SCC Core 4: 190 cm	1.0174	0.0102	60	-26.32	2009-2019 CAL AD 70%	2013-2019 CAL AD 84%
SCC Core 4: 353 cm	0.9948	0.0099	55	-26.24	1797-1943 CAL AD 63%	1809-1918 CAL AD 74%
SCC Core 4: 482 cm	0.998	0.01	55	-21.91	1798-1942 CAL AD 65%	1876-1917 CAL AD 31%
SCC Core 4: 531 cm	0.9078	0.0091	60	-28.72	1118-1323 CAL AD 86%	1197-1296 CAL AD 87%
SCC Core 5: 79 cm	1.0234	0.0102	55	-30.87	2010-2019 CAL AD 85%	2013-2018 CAL AD 88%
SCC Core 5: 91 cm	1.0683	0.0107	55	-27.32	2001-2012 CAL AD 90%	2002-2007 CAL AD 83%
SCC Core 5: 458 cm	0.9938	0.0099	60	-28.93	1797-1945 CAL AD 63%	1809-1919 CAL AD 74%
SCC Core 5: 524 cm	0.9975	0.01	60	-24.54	1798-1942 CAL AD 64%	1810-1873 CAL AD 43%

APPENDIX B – Sediment Core Data

Table B.1 *Shipland WMA Core 1 grain size data*

Shipland WMA Core 1											
Depth (cm)	Description	D10 (µm):	D50 (µm):	D90 (µm):	(D90 / D10) (µm):	(D90 - D10) (µm):	(D75 / D25) (µm):	(D75 - D25) (µm):	% SAND:	% SILT	% CLAY:
33.6	Coarse Silt	4.58	19.00	125.89	27.47	121.30	4.86	35.89	0.19	0.77	0.04
54.7	Coarse Silt	4.00	22.29	163.27	40.85	159.27	9.86	77.43	0.30	0.65	0.05
77.8	Very Fine Sand	9.08	83.61	181.53	20.00	172.46	3.29	91.91	0.63	0.33	0.04
82	Very Fine Sand	22.06	112.84	204.22	9.26	182.16	2.18	85.69	0.80	0.18	0.02
84.1	Very Fine Sand	21.83	126.56	223.99	10.26	202.16	2.12	92.41	0.82	0.16	0.02
88.3	Fine Sand	80.94	142.86	229.14	2.83	148.20	1.72	77.82	0.95	0.05	0.00
124.7	Fine Sand	85.49	153.65	249.74	2.92	164.25	1.75	86.11	0.94	0.05	0.01
171.8	Fine Sand	60.97	136.69	220.58	3.62	159.61	1.77	77.59	0.90	0.10	0.00
192.6	Very Coarse Silt	6.97	51.00	142.04	20.37	135.06	3.77	63.31	0.40	0.57	0.03
216.1	Very Coarse Silt	5.42	43.14	134.57	24.81	129.15	5.63	69.89	0.37	0.60	0.04
258.7	Very Fine Sand	14.54	84.58	196.95	13.54	182.41	2.92	88.95	0.64	0.33	0.03
279.5	Fine Sand	50.51	232.10	411.37	8.14	360.86	2.16	173.32	0.88	0.11	0.01
318.2	Fine Sand	137.45	236.33	380.51	2.77	243.06	1.72	128.22	0.97	0.03	0.00
324.9	Very Fine Sand	15.02	153.65	301.43	20.07	286.41	2.57	138.56	0.81	0.17	0.02
335.3	Fine Sand	42.97	173.43	309.17	7.20	266.21	2.03	122.11	0.89	0.10	0.02
347.9	Very Coarse Silt	3.95	42.81	262.48	66.53	258.53	13.21	152.91	0.44	0.50	0.06
352.4	Fine Sand	131.30	227.55	365.29	2.78	234.00	1.73	124.91	0.97	0.03	0.00
371.6	Very Coarse Silt	7.15	50.35	262.51	36.73	255.37	4.43	84.32	0.41	0.58	0.01
377.5	Fine Sand	22.19	197.19	349.22	15.74	327.04	2.47	162.89	0.79	0.19	0.02
382.2	Coarse Silt	4.99	26.75	162.47	32.55	157.48	5.69	49.68	0.24	0.73	0.02
385.7	Fine Sand	148.75	236.47	360.61	2.42	211.86	1.60	112.34	0.98	0.02	0.00
410.3	Fine Sand	67.46	143.68	262.51	3.89	195.05	2.02	101.49	0.91	0.09	0.00
416.2	Very Fine Sand	30.76	102.58	197.44	6.42	166.68	2.19	80.27	0.78	0.21	0.01
430.2	Coarse Silt	4.22	20.36	68.50	16.22	64.28	4.48	31.30	0.12	0.83	0.05
453.7	Very Fine Sand	38.60	130.36	259.21	6.72	220.61	2.39	111.96	0.83	0.16	0.01
459.5	Fine Sand	114.81	206.77	340.56	2.97	225.76	1.78	119.31	0.98	0.02	0.00
474.8	Fine Sand	85.91	184.22	316.97	3.69	231.06	1.92	120.04	0.94	0.06	0.00
478.3	Very Coarse Silt	6.39	39.62	250.31	39.20	243.93	9.08	127.23	0.39	0.58	0.03
483	Fine Sand	109.22	196.26	323.94	2.97	214.72	1.78	113.54	0.98	0.02	0.00
506.2	Fine Sand	109.33	233.21	463.75	4.24	354.42	2.18	185.11	0.98	0.02	0.00
545.6	Medium Sand	161.11	371.30	624.56	3.88	463.45	1.90	235.73	0.98	0.02	0.00
567.7	Medium Sand	210.35	385.68	634.50	3.02	424.15	1.79	224.61	0.99	0.01	0.00
602.2	Medium Sand	284.37	389.33	527.04	1.85	242.68	1.39	128.39	1.00	0.00	0.00

Table B.2 *Shipland WMA Core 2 grain size data*

Shipland WMA Core 2											
Depth (cm)	Description	D10 (µm):	D50 (µm):	D90 (µm):	(D90 / D10) (µm):	(D90 - D10) (µm):	(D75 / D25) (µm):	(D75 - D25) (µm):	% SAND:	% SILT	% CLAY:
8.4	Very Fine Sand	17.42	117.02	277.10	15.90	259.68	2.95	122.19	0.75	0.24	0.01
26.5	Coarse Silt	5.05	19.98	110.50	21.89	105.45	4.80	36.16	0.19	0.79	0.02
33.1	Very Fine Sand	14.33	82.85	165.25	11.53	150.92	2.62	76.40	0.65	0.33	0.02
38	Medium Silt	3.86	15.46	61.64	15.96	57.77	4.13	23.52	0.10	0.86	0.05
57.8	Medium Silt	3.14	15.25	58.87	18.73	55.73	4.48	24.08	0.09	0.84	0.07
74.3	Medium Silt	2.62	15.87	52.30	19.98	49.68	4.80	24.95	0.07	0.85	0.08
90.7	Very Fine Sand	9.75	90.02	190.20	19.50	180.45	3.66	102.29	0.64	0.32	0.03
99	Coarse Silt	3.69	16.43	123.73	33.55	120.04	4.67	29.11	0.18	0.77	0.05
108.9	Fine Sand	95.10	163.80	261.90	2.75	166.80	1.70	87.29	0.96	0.04	0.00
126.6	Fine Sand	116.07	179.76	270.97	2.33	154.90	1.58	83.48	1.00	0.00	0.00
135.8	Fine Sand	83.05	151.09	246.17	2.96	163.12	1.76	85.83	0.95	0.05	0.00
140.3	Fine Sand	71.53	149.74	238.77	3.34	167.24	1.76	83.90	0.91	0.09	0.00
144.9	Very Fine Sand	14.15	131.74	235.86	16.66	221.71	2.29	103.91	0.80	0.19	0.01
149.5	Fine Sand	100.10	169.97	267.50	2.67	167.40	1.68	88.39	0.96	0.04	0.00
196.7	Fine Sand	99.25	173.28	273.71	2.76	174.46	1.69	91.84	0.95	0.05	0.00
240.9	Fine Sand	114.83	177.50	265.32	2.31	150.49	1.56	80.05	0.99	0.01	0.00
259.2	Fine Sand	108.25	172.61	264.07	2.44	155.82	1.61	82.87	0.98	0.02	0.00
277.5	Fine Sand	38.35	159.06	268.47	7.00	230.12	1.92	102.59	0.88	0.11	0.01
327.8	Fine Sand	111.61	171.66	258.42	2.32	146.81	1.57	77.46	0.99	0.01	0.00
356.7	Fine Sand	108.54	167.96	253.98	2.34	145.44	1.57	76.09	0.99	0.01	0.00
396	Fine Sand	107.91	169.83	258.49	2.40	150.57	1.59	79.08	0.98	0.02	0.00
432.2	Fine Sand	99.07	161.61	249.53	2.52	150.45	1.62	78.50	0.96	0.04	0.00
441.9	Fine Sand	102.75	161.97	245.29	2.39	142.54	1.58	75.01	0.98	0.02	0.00
460	Fine Sand	103.09	158.64	238.98	2.32	135.90	1.57	72.59	1.00	0.00	0.00
476.9	Fine Sand	89.67	148.57	230.24	2.57	140.57	1.65	74.23	0.96	0.04	0.00
490.5	Coarse Silt	4.92	20.37	110.10	22.37	105.18	4.66	35.75	0.19	0.78	0.03
498.8	Coarse Silt	4.56	18.56	86.85	19.06	82.29	4.21	29.25	0.14	0.82	0.04
504.3	Very Fine Sand	7.09	69.01	440.68	62.18	433.60	17.25	289.36	0.52	0.46	0.02
518.2	Very Coarse Silt	5.55	36.34	282.73	50.92	277.18	7.85	81.42	0.36	0.62	0.03
559.7	Very Fine Sand	7.71	89.63	399.48	51.81	391.77	10.84	240.76	0.58	0.40	0.02
565.3	Very Coarse Silt	6.27	32.14	197.89	31.57	191.63	6.39	70.27	0.32	0.66	0.02
572.2	Very Coarse Silt	7.23	65.72	348.08	48.12	340.84	10.19	195.36	0.51	0.47	0.02
580.5	Very Fine Sand	11.10	80.31	245.26	22.10	234.16	4.84	116.99	0.58	0.40	0.01
588.8	Very Coarse Silt	5.29	47.74	151.82	28.71	146.54	7.83	86.19	0.42	0.55	0.03
591.6	Coarse Silt	5.88	30.50	122.57	20.85	116.69	5.88	59.34	0.29	0.68	0.03
602.8	Very Fine Sand	13.80	110.69	219.75	15.92	205.95	2.59	100.20	0.75	0.24	0.01
606.9	Coarse Silt	4.32	31.38	132.85	30.77	128.53	7.79	69.51	0.33	0.63	0.04

Table B.3 *Shipland WMA Core 3 grain size data*

Shipland WMA Core 3											
Depth (cm)	Description	D10 (µm):	D50 (µm):	D90 (µm):	(D90 / D10) (µm):	(D90 - D10) (µm):	(D75 / D25) (µm):	(D75 - D25) (µm):	% SAND:	% SILT	% CLAY:
7.7	Very Fine Sand	12.41	96.84	210.55	16.97	198.14	3.82	113.77	0.66	0.32	0.02
22.7	Fine Sand	103.83	164.46	252.53	2.43	148.69	1.60	77.59	0.98	0.02	0.00
45.2	Fine Sand	94.31	156.28	244.10	2.59	149.79	1.66	79.72	0.97	0.03	0.00
84.6	Fine Sand	100.99	157.34	237.09	2.35	136.10	1.58	72.67	0.99	0.01	0.00
118.3	Fine Sand	81.46	147.81	234.86	2.88	153.40	1.72	80.13	0.94	0.06	0.00
139.5	Fine Sand	78.48	142.33	228.82	2.92	150.34	1.74	78.44	0.94	0.06	0.00
151.7	Fine Sand	64.60	132.42	221.92	3.44	157.32	1.85	80.86	0.91	0.09	0.00
160.4	Very Fine Sand	18.15	103.28	251.14	13.83	232.99	2.87	107.46	0.72	0.25	0.02
163.9	Fine Sand	98.39	265.01	459.35	4.67	360.96	2.03	184.44	0.94	0.06	0.00
167.3	Fine Sand	33.39	265.08	457.96	13.72	424.58	2.20	198.50	0.84	0.15	0.01
170.8	Medium Sand	213.59	318.26	462.06	2.16	248.47	1.53	135.15	1.00	0.00	0.00
191.7	Medium Sand	158.97	312.31	509.55	3.21	350.58	1.80	183.37	0.97	0.03	0.00
200.4	Medium Sand	196.43	289.72	420.02	2.14	223.59	1.50	118.47	1.00	0.00	0.00
223.1	Very Coarse Silt	5.76	39.53	271.60	47.19	265.85	5.61	86.05	0.34	0.61	0.05
230.0	Fine Sand	101.95	193.74	325.66	3.19	223.71	1.83	117.21	0.96	0.04	0.00
270.0	Medium Sand	197.09	311.05	479.89	2.43	282.81	1.62	150.41	1.00	0.00	0.00
398.1	Fine Sand	141.76	248.13	405.99	2.86	264.23	1.76	140.92	0.98	0.02	0.00
469.5	Fine Sand	108.52	224.24	392.14	3.61	283.62	1.94	148.99	0.96	0.04	0.00
491.0	Fine Sand	132.08	215.48	338.43	2.56	206.35	1.66	109.12	0.99	0.01	0.00
493.1	Very Fine Sand	7.21	95.31	313.41	43.47	306.20	8.84	196.29	0.56	0.40	0.04
496.3	Fine Sand	48.66	177.75	338.04	6.95	289.38	2.56	157.43	0.86	0.14	0.01
498.5	Very Coarse Silt	9.01	55.69	202.47	22.48	193.46	4.02	80.43	0.45	0.53	0.02
503.8	Fine Sand	132.28	215.16	334.99	2.53	202.71	1.64	107.04	0.98	0.02	0.00
518.8	Very Fine Sand	13.17	87.77	194.76	14.78	181.58	2.94	91.13	0.66	0.33	0.01
535.9	Very Coarse Silt	8.03	52.78	113.83	14.18	105.80	2.76	51.91	0.40	0.56	0.04
574.4	Coarse Silt	5.67	37.17	128.29	22.61	122.61	5.34	58.29	0.30	0.67	0.03
578.7	Very Coarse Silt	9.29	43.01	88.06	9.48	78.77	2.57	39.47	0.27	0.71	0.02
596.9	Medium Sand	200.63	295.28	428.82	2.14	228.19	1.50	121.14	1.00	0.00	0.00
602.2	Medium Sand	164.43	262.08	402.75	2.45	238.31	1.62	128.03	0.98	0.02	0.00

Table B.4 *Shipland WMA Core 4 grain size data*

Shipland WMA Core 4											
Depth (cm)	Description	D10 (µm):	D50 (µm):	D90 (µm):	(D90 / D10) (µm):	(D90 - D10) (µm):	(D75 / D25) (µm):	(D75 - D25) (µm):	% SAND:	% SILT	% CLAY:
7.7	Very Fine Sand	16.25	116.03	238.73	14.69	222.48	3.32	124.31	0.72	0.26	0.02
24.6	Coarse Silt	4.37	20.79	108.97	24.93	104.60	5.24	38.34	0.19	0.77	0.04
58.3	Very Fine Sand	18.79	160.36	283.09	15.07	264.30	2.34	127.68	0.79	0.18	0.02
84.6	Fine Sand	129.22	195.88	293.25	2.27	164.04	1.57	88.31	1.00	0.00	0.00
92.1	Fine Sand	121.69	187.74	283.44	2.33	161.75	1.58	86.59	1.00	0.00	0.00
112.7	Fine Sand	88.58	161.11	263.17	2.97	174.59	1.76	91.61	0.95	0.05	0.00
122.1	Fine Sand	39.21	175.46	288.66	7.36	249.45	1.84	106.30	0.88	0.12	0.00
136.7	Fine Sand	131.20	193.33	283.46	2.16	152.26	1.52	80.99	1.00	0.00	0.00
154.4	Fine Sand	105.84	176.16	266.79	2.52	160.96	1.61	84.55	0.95	0.05	0.00
158.0	Very Fine Sand	7.14	115.43	245.16	34.32	238.02	5.93	151.96	0.67	0.29	0.04
162.4	Fine Sand	111.92	177.08	268.11	2.40	156.18	1.60	83.71	0.98	0.02	0.00
173.4	Fine Sand	111.38	178.25	269.40	2.42	158.02	1.60	84.57	0.97	0.03	0.00
195.5	Fine Sand	117.99	182.23	272.30	2.31	154.31	1.57	82.58	0.99	0.01	0.00
204.3	Fine Sand	116.06	178.78	266.22	2.29	150.17	1.56	79.89	0.99	0.01	0.00
236.6	Fine Sand	117.12	176.69	262.61	2.24	145.49	1.54	77.23	1.00	0.00	0.00
275.6	Fine Sand	121.83	183.33	269.84	2.21	148.01	1.54	80.10	1.00	0.00	0.00
284.6	Fine Sand	107.83	172.23	263.52	2.44	155.69	1.61	82.21	0.98	0.02	0.00
317.7	Fine Sand	113.54	174.68	263.55	2.32	150.01	1.58	80.16	1.00	0.00	0.00
329.8	Fine Sand	115.90	176.29	263.58	2.27	147.68	1.56	78.69	1.00	0.00	0.00
332.8	Fine Sand	114.02	176.69	265.93	2.33	151.91	1.58	80.92	0.99	0.01	0.00
341.8	Fine Sand	105.51	175.46	268.66	2.55	163.15	1.63	86.16	0.96	0.04	0.00
361.4	Fine Sand	109.10	174.10	264.68	2.43	155.58	1.60	82.40	0.97	0.03	0.00
391.3	Fine Sand	110.15	171.66	259.95	2.36	149.80	1.58	79.12	0.98	0.02	0.00
417.8	Fine Sand	109.70	174.35	264.33	2.41	154.64	1.60	82.15	0.97	0.03	0.00
436.9	Fine Sand	112.97	175.16	262.39	2.32	149.43	1.57	79.09	0.98	0.02	0.00
439.6	Fine Sand	120.42	180.56	266.26	2.21	145.84	1.54	78.11	1.00	0.00	0.00
448.9	Fine Sand	113.98	177.61	265.54	2.33	151.56	1.57	80.49	0.98	0.02	0.00
479.7	Fine Sand	102.75	170.11	262.69	2.56	159.93	1.63	83.77	0.96	0.04	0.00
535.8	Fine Sand	115.21	173.81	259.18	2.25	143.97	1.55	76.24	1.00	0.00	0.00
540.5	Fine Sand	102.04	166.80	256.82	2.52	154.78	1.61	80.31	0.96	0.04	0.00
548.7	Fine Sand	90.62	160.19	250.63	2.77	160.01	1.67	82.67	0.94	0.06	0.00
566.3	Fine Sand	108.83	166.00	249.36	2.29	140.53	1.56	74.67	1.00	0.00	0.00
588.6	Fine Sand	87.99	160.55	257.56	2.93	169.57	1.72	86.94	0.93	0.07	0.00
608.5	Fine Sand	90.92	157.29	250.23	2.75	159.30	1.69	82.84	0.95	0.05	0.00

Table B.5 *Shipland WMA Core 5 grain size data*

Shipland WMA Core 5											
Depth (cm)	Description	D10 (µm):	D50 (µm):	D90 (µm):	(D90 / D10) (µm):	(D90 - D10) (µm):	(D75 / D25) (µm):	(D75 - D25) (µm):	% SAND:	% SILT:	% CLAY:
8.4	Fine Sand	87.99	169.05	282.45	3.21	194.46	1.82	101.66	0.94	0.06	0.00
23.1	Fine Sand	97.79	184.70	306.21	3.13	208.42	1.81	110.01	0.95	0.05	0.00
31.5	Very Fine Sand	8.90	90.51	220.60	24.78	211.70	4.57	119.77	0.62	0.34	0.03
42	Coarse Silt	3.36	31.25	181.30	53.99	177.95	10.47	99.14	0.37	0.56	0.07
47.3	Coarse Silt	2.52	18.70	132.42	52.57	129.91	6.85	42.60	0.21	0.70	0.09
52.6	Medium Silt	1.56	14.67	69.17	44.37	67.61	5.22	25.31	0.11	0.78	0.11
103	Coarse Silt	1.78	19.07	67.08	37.64	65.29	5.54	31.83	0.12	0.78	0.10
111.4	Fine Sand	81.14	136.17	215.98	2.66	134.85	1.69	71.62	0.96	0.04	0.00
115.6	Very Coarse Silt	3.70	49.21	162.58	43.89	158.88	7.54	93.61	0.44	0.49	0.07
121.9	Fine Sand	126.06	188.36	276.89	2.20	150.83	1.54	82.07	1.00	0.00	0.00
139.1	Fine Sand	76.73	161.07	271.41	3.54	194.68	1.88	101.64	0.92	0.08	0.00
143.8	Fine Sand	128.01	195.49	294.78	2.30	166.77	1.58	89.92	1.00	0.00	0.00
178.2	Fine Sand	113.31	174.85	265.00	2.34	151.69	1.59	81.28	1.00	0.00	0.00
192.3	Very Fine Sand	7.25	101.46	221.86	30.62	214.61	5.78	135.87	0.63	0.33	0.04
198.5	Very Coarse Silt	3.20	34.04	205.74	64.25	202.54	12.03	120.83	0.40	0.52	0.08
206.3	Very Coarse Silt	4.84	66.50	206.61	42.71	201.77	8.27	127.40	0.51	0.43	0.05
215.7	Fine Sand	108.79	164.87	241.76	2.22	132.97	1.53	71.10	0.98	0.02	0.00
231.3	Fine Sand	99.40	166.73	263.93	2.66	164.53	1.67	86.14	0.97	0.03	0.00
234.5	Very Fine Sand	18.64	139.82	250.38	13.43	231.74	2.28	109.85	0.80	0.18	0.02
240.7	Fine Sand	112.37	180.98	272.29	2.42	159.93	1.60	85.58	0.97	0.03	0.00
247	Fine Sand	77.54	167.08	280.02	3.61	202.48	1.87	104.07	0.92	0.08	0.00
274.7	Fine Sand	126.27	182.54	262.92	2.08	136.65	1.49	73.66	1.00	0.00	0.00
327.2	Fine Sand	125.25	190.53	283.17	2.26	157.92	1.55	83.81	0.98	0.02	0.00
338	Fine Sand	136.35	202.62	295.44	2.17	159.09	1.51	84.05	0.99	0.01	0.00
359.6	Fine Sand	119.02	173.80	252.17	2.12	133.15	1.49	69.32	1.00	0.00	0.00
385.7	Fine Sand	129.63	182.35	256.75	1.98	127.12	1.45	67.85	1.00	0.00	0.00
392	Fine Sand	129.15	183.33	260.18	2.01	131.03	1.46	70.30	1.00	0.00	0.00
403.6	Fine Sand	105.53	159.54	237.08	2.25	131.55	1.55	70.21	1.00	0.00	0.00
406.8	Very Coarse Silt	7.72	63.76	183.31	23.75	175.59	5.19	100.03	0.51	0.47	0.02
419.4	Coarse Silt	5.58	37.00	128.28	23.01	122.70	5.26	59.11	0.31	0.67	0.03
433	Very Fine Sand	12.53	89.30	193.24	15.42	180.71	3.23	97.01	0.65	0.32	0.03
443.5	Very Coarse Silt	5.35	40.61	125.33	23.44	119.98	6.02	67.03	0.35	0.62	0.03
446.7	Very Coarse Silt	10.86	79.35	168.14	15.48	157.27	3.00	81.51	0.62	0.37	0.02
471.9	Very Fine Sand	20.81	95.16	172.33	8.28	151.52	2.18	72.41	0.74	0.25	0.01
489.8	Fine Sand	131.76	197.08	288.43	2.19	156.67	1.53	83.71	0.99	0.01	0.00
494	Very Fine Sand	27.46	156.14	279.06	10.16	251.60	2.39	127.41	0.81	0.17	0.02
507.6	Coarse Silt	5.59	29.13	182.41	32.64	176.82	5.45	55.43	0.27	0.70	0.03
509.8	Very Coarse Silt	5.90	42.66	172.37	29.19	166.46	5.98	75.35	0.37	0.59	0.03
511.9	Very Coarse Silt	6.92	40.62	113.24	16.36	106.32	4.13	55.98	0.32	0.65	0.03
556	Coarse Silt	3.31	18.83	95.42	28.81	92.11	6.29	40.31	0.19	0.75	0.06
567.6	Very Coarse Silt	8.26	45.72	107.39	13.00	99.13	3.26	51.48	0.34	0.64	0.02
571.8	Very Coarse Silt	7.98	49.33	118.60	14.87	110.63	3.56	58.74	0.38	0.60	0.02
592.8	Very Coarse Silt	8.77	54.47	120.11	13.70	111.34	3.56	62.18	0.43	0.56	0.01
599.1	Coarse Silt	6.13	36.65	112.59	18.37	106.46	4.77	54.84	0.29	0.68	0.03
607.5	Very Coarse Silt	7.91	45.12	105.13	13.30	97.23	3.07	49.25	0.33	0.64	0.03

Table B.6 *St. Catherine Creek NWR Core 1 grain size data*

St. Catherine Creek NWR Core 1												
Depth (cm)	Description	D10 (µm):	D50 (µm):	D90 (µm):	(D90 / D10) (µm):	(D90 - D10) (µm):	(D75 / D25) (µm):	(D75 - D25) (µm):	% SAND:	% SILT:	% CLAY:	
0	Coarse Silt	3.19	20.39	163.22	51.23	160.03	7.68	51.44	0.24	0.69	0.07	
15.3	Medium Silt	2.57	15.49	72.00	27.97	69.42	6.51	32.86	0.13	0.79	0.08	
43.3	Coarse Silt	4.96	38.81	82.38	16.61	77.42	3.08	40.65	0.23	0.72	0.06	
109.4	Coarse Silt	2.64	23.65	66.57	25.20	63.92	4.98	34.77	0.12	0.80	0.08	
130.3	Medium Silt	1.43	14.82	63.94	44.62	62.51	6.78	30.62	0.10	0.78	0.11	
138.8	Medium Silt	1.26	11.93	59.63	47.36	58.38	7.02	28.31	0.09	0.79	0.12	
168.2	Medium Silt	1.10	12.42	61.39	55.90	60.29	7.23	28.74	0.10	0.77	0.13	
185.1	Medium Silt	1.28	12.78	60.38	47.25	59.10	6.48	26.86	0.09	0.79	0.12	
191.4	Coarse Silt	3.21	32.14	80.52	25.11	77.31	4.72	43.53	0.19	0.73	0.08	
227.2	Medium Silt	1.92	19.66	56.82	29.59	54.90	4.77	28.26	0.08	0.82	0.10	
237.7	Coarse Silt	2.23	21.64	70.46	31.59	68.23	5.99	35.91	0.13	0.78	0.09	
243.8	Coarse Silt	2.60	21.57	56.89	21.84	54.29	4.70	30.08	0.07	0.84	0.09	
251.8	Medium Silt	2.12	15.36	44.49	21.03	42.37	4.26	21.56	0.04	0.86	0.10	
267.6	Medium Silt	1.25	16.86	67.83	54.27	66.58	7.00	34.21	0.12	0.76	0.12	
278.7	Very Coarse Silt	5.27	46.42	101.82	19.31	96.55	3.30	51.01	0.34	0.61	0.05	
324.7	Medium Silt	3.01	13.70	53.62	17.84	50.62	4.63	23.27	0.07	0.86	0.07	
334.2	Coarse Silt	4.34	23.48	78.46	18.08	74.12	5.50	41.19	0.17	0.79	0.04	
351.6	Coarse Silt	4.19	18.91	63.51	15.14	59.32	4.48	29.74	0.10	0.85	0.04	
358	Coarse Silt	4.96	33.58	84.28	16.99	79.32	4.26	44.13	0.21	0.74	0.04	
365.8	Coarse Silt	4.21	31.65	84.49	20.05	80.27	4.86	44.30	0.20	0.75	0.05	
378.2	Coarse Silt	4.33	27.92	82.00	18.95	77.67	5.50	44.22	0.19	0.76	0.05	
390.7	Very Coarse Silt	7.70	62.23	131.32	17.06	123.62	2.83	61.52	0.50	0.46	0.04	
401.8	Very Coarse Silt	4.44	43.61	102.16	23.02	97.72	3.82	53.16	0.32	0.62	0.06	
429.5	Very Coarse Silt	7.83	51.08	102.31	13.07	94.48	2.49	45.21	0.37	0.59	0.04	
442	Coarse Silt	4.12	33.63	96.30	23.37	92.18	5.62	51.77	0.25	0.69	0.05	
451.7	Coarse Silt	4.52	35.46	88.11	19.51	83.59	4.37	46.79	0.24	0.72	0.05	
465.6	Medium Silt	3.00	12.09	42.14	14.03	39.13	4.04	18.28	0.04	0.89	0.07	
473.9	Medium Silt	3.39	12.04	40.12	11.82	36.73	3.70	16.97	0.03	0.91	0.06	
480.9	Medium Silt	2.59	18.45	55.71	21.54	53.12	5.22	29.04	0.07	0.85	0.08	
500.4	Coarse Silt	4.08	18.28	53.69	13.14	49.60	3.96	25.33	0.07	0.89	0.05	
532.1	Coarse Silt	4.04	16.27	58.93	14.60	54.89	4.32	26.01	0.09	0.87	0.04	
540	Coarse Silt	4.15	23.06	82.40	19.88	78.25	5.38	39.68	0.17	0.78	0.05	
579.6	Coarse Silt	3.41	27.62	82.12	24.10	78.71	5.76	43.90	0.19	0.75	0.07	
595.5	Coarse Silt	5.07	31.72	87.97	17.36	82.90	4.88	46.38	0.22	0.74	0.04	

Table B.7 *St. Catherine Creek NWR Core 2 grain size data*

St. Catherine Creek NWR Core 2											
Depth (cm)	Description	D10 (µm):	D50 (µm):	D90 (µm):	(D90 / D10) (µm):	(D90 - D10) (µm):	(D75 / D25) (µm):	(D75 - D25) (µm):	% SAND:	% SILT	% CLAY:
0	Coarse Silt	3.87	23.06	117.51	30.40	113.65	6.19	47.39	0.22	0.72	0.06
24.8	Very Coarse Silt	5.64	44.78	98.81	17.53	93.17	3.40	50.37	0.32	0.63	0.05
45.5	Very Coarse Silt	8.03	47.82	94.43	11.76	86.40	2.46	41.84	0.33	0.64	0.04
53.8	Coarse Silt	3.30	30.71	75.81	22.99	72.52	4.54	41.14	0.17	0.75	0.07
62.1	Very Coarse Silt	8.20	51.06	103.03	12.56	94.83	2.68	47.96	0.38	0.59	0.04
80.7	Very Coarse Silt	6.79	48.39	99.31	14.62	92.52	2.81	47.30	0.35	0.61	0.04
111.7	Coarse Silt	3.22	27.85	72.88	22.65	69.66	4.38	37.36	0.15	0.78	0.07
121.9	Coarse Silt	4.87	34.34	70.85	14.55	65.98	2.79	33.38	0.15	0.79	0.06
129.7	Fine Silt	0.83	8.01	36.29	43.57	35.46	5.28	14.35	0.04	0.79	0.17
165.7	Very Coarse Silt	5.97	40.22	82.34	13.80	76.38	2.70	38.14	0.23	0.72	0.05
178.2	Very Coarse Silt	8.78	53.49	102.45	11.67	93.67	2.42	45.50	0.40	0.57	0.04
190.8	Coarse Silt	4.41	43.62	94.35	21.40	89.94	3.61	49.59	0.30	0.64	0.06
197	Very Coarse Silt	6.72	50.88	101.04	15.03	94.31	2.69	47.52	0.37	0.59	0.04
208	Very Coarse Silt	5.17	42.92	92.14	17.83	86.97	3.16	45.72	0.29	0.66	0.05
220.5	Very Coarse Silt	8.51	62.60	121.62	14.30	113.12	2.52	55.23	0.50	0.46	0.04
231.4	Very Coarse Silt	5.10	43.58	90.25	17.70	85.15	3.01	44.32	0.29	0.66	0.05
239.3	Coarse Silt	3.67	27.02	64.13	17.48	60.46	3.78	32.84	0.11	0.82	0.07
251.8	Coarse Silt	3.87	29.67	70.93	18.31	67.05	3.86	36.73	0.15	0.79	0.06
259.7	Coarse Silt	3.07	37.54	96.65	31.45	93.58	6.22	55.54	0.28	0.65	0.08
281.9	Coarse Silt	3.21	27.22	68.87	21.47	65.66	4.57	36.55	0.13	0.79	0.07
299.3	Medium Silt	1.16	14.20	51.27	44.30	50.12	5.86	25.21	0.06	0.81	0.13
313.6	Very Coarse Silt	8.07	58.05	120.09	14.89	112.03	2.81	56.75	0.46	0.51	0.04
340.5	Very Coarse Silt	4.89	44.98	97.86	20.01	92.97	3.54	50.96	0.32	0.62	0.05
350	Coarse Silt	4.74	36.39	84.15	17.74	79.41	3.45	41.93	0.22	0.72	0.06
359.5	Medium Silt	2.59	14.57	50.78	19.61	48.19	4.86	23.99	0.06	0.85	0.08
376.9	Very Coarse Silt	7.83	56.89	113.29	14.47	105.46	2.58	51.78	0.44	0.52	0.04
416.5	Very Coarse Silt	7.78	57.36	118.77	15.27	110.99	2.69	54.49	0.45	0.51	0.04
451.4	Coarse Silt	3.48	21.61	75.86	21.80	72.38	5.46	36.46	0.15	0.79	0.06
465.6	Very Coarse Silt	7.93	66.70	137.49	17.33	129.55	2.81	65.02	0.54	0.42	0.04
479.9	Very Coarse Silt	8.09	63.82	134.78	16.66	126.69	2.83	63.06	0.51	0.45	0.04
510.7	Very Coarse Silt	8.95	60.78	123.78	13.83	114.83	2.51	54.44	0.48	0.48	0.04
524.5	Very Coarse Silt	8.79	57.84	118.86	13.53	110.07	2.58	53.04	0.45	0.51	0.04
533.7	Very Coarse Silt	6.72	56.64	119.59	17.80	112.87	2.81	55.62	0.44	0.52	0.04
544.1	Coarse Silt	3.60	33.36	95.92	26.65	92.32	6.50	54.25	0.26	0.68	0.06
548.7	Very Coarse Silt	7.93	48.95	101.88	12.85	93.96	2.66	46.45	0.35	0.61	0.04
556.7	Very Coarse Silt	7.89	50.48	102.94	13.04	95.05	2.60	46.60	0.37	0.59	0.04
566	Coarse Silt	4.65	28.04	75.74	16.28	71.09	4.72	40.13	0.17	0.79	0.04
572.9	Coarse Silt	4.09	28.12	81.59	19.94	77.49	5.72	44.98	0.19	0.76	0.05
605.1	Very Coarse Silt	5.58	43.60	91.47	16.40	85.89	3.00	44.49	0.29	0.66	0.05

Table B.8 *St. Catherine Creek NWR Core 3 grain size data*

St. Catherine Creek NWR Core 3												
Depth (cm)	Description	D10 (µm):	D50 (µm):	D90 (µm):	(D90 / D10) (µm):	(D90 - D10) (µm):	(D75 / D25) (µm):	(D75 - D25) (µm):	% SAND:	% SILT	% CLAY:	
6.3	Coarse Silt	3.00	18.95	91.73	30.56	88.73	5.62	34.61	0.16	0.77	0.08	
14.1	Coarse Silt	3.51	18.18	71.86	20.46	68.35	5.14	31.26	0.13	0.81	0.06	
28.2	Medium Silt	3.10	15.36	49.85	16.06	46.75	4.34	22.96	0.06	0.87	0.07	
45.4	Coarse Silt	3.34	27.83	83.22	24.94	79.88	5.03	41.70	0.18	0.74	0.07	
51.6	Coarse Silt	5.13	37.81	92.04	17.94	86.91	3.51	44.97	0.25	0.69	0.05	
61	Coarse Silt	3.05	17.35	76.24	24.96	73.19	5.57	31.24	0.13	0.80	0.07	
70.4	Coarse Silt	3.00	26.84	93.28	31.11	90.28	5.67	43.97	0.20	0.72	0.08	
81.4	Coarse Silt	3.87	22.41	81.77	21.14	77.90	5.28	37.25	0.16	0.79	0.05	
89.2	Coarse Silt	3.55	17.19	76.14	21.43	72.59	5.50	32.34	0.14	0.81	0.05	
100.1	Medium Silt	3.62	15.01	55.62	15.38	52.00	4.15	22.48	0.09	0.86	0.05	
111.1	Coarse Silt	4.54	31.57	101.16	22.27	96.62	5.82	52.04	0.25	0.71	0.04	
138.4	Very Coarse Silt	5.01	54.92	139.21	27.80	134.20	5.01	77.31	0.45	0.50	0.05	
156.2	Very Coarse Silt	8.78	64.42	134.85	15.35	126.07	2.80	63.12	0.52	0.45	0.04	
158.9	Very Fine Sand	15.63	92.37	169.98	10.88	154.35	2.28	73.82	0.72	0.25	0.03	
171.3	Very Fine Sand	12.02	72.65	143.02	11.90	131.01	2.51	64.27	0.59	0.38	0.03	
180.9	Very Coarse Silt	11.71	64.16	136.05	11.62	124.34	2.68	61.28	0.52	0.45	0.03	
185	Very Coarse Silt	6.31	64.14	149.96	23.75	143.64	3.44	73.90	0.51	0.44	0.04	
194.6	Very Fine Sand	11.91	83.46	170.39	14.30	158.47	2.87	82.61	0.64	0.33	0.03	
213.8	Very Coarse Silt	5.08	43.93	113.82	22.42	108.74	4.13	57.95	0.34	0.61	0.05	
223.4	Coarse Silt	3.15	32.42	92.22	29.31	89.07	5.78	50.24	0.24	0.69	0.08	
467.1	Very Fine Sand	30.54	73.58	133.04	4.36	102.50	2.04	52.12	0.62	0.36	0.02	
513.7	Very Coarse Silt	5.78	37.84	91.31	15.81	85.54	3.23	42.74	0.25	0.71	0.05	
521.9	Coarse Silt	4.81	27.00	83.61	17.39	78.81	4.52	39.78	0.18	0.78	0.04	
539.8	Very Coarse Silt	8.69	50.72	97.49	11.22	88.80	2.41	43.25	0.36	0.60	0.04	
547.9	Very Coarse Silt	8.85	41.67	88.63	10.01	79.78	2.59	39.04	0.26	0.71	0.03	
565.8	Coarse Silt	4.60	19.59	66.63	14.49	62.03	3.52	25.39	0.11	0.85	0.04	
601.6	Coarse Silt	3.62	16.91	79.00	21.80	75.38	5.67	34.03	0.15	0.80	0.05	

Table B.9 *St. Catherine Creek NWR Core 4 grain size data*

St. Catherine Creek NWR Core 4												
Depth (cm)	Description	D10 (µm):	D50 (µm):	D90 (µm):	(D90 / D10) (µm):	(D90 - D10) (µm):	(D75 / D25) (µm):	(D75 - D25) (µm):	% SAND:	% SILT	% CLAY:	
0	Coarse Silt	3.06	30.44	180.93	59.08	177.87	8.63	68.25	0.31	0.62	0.08	
12	Very Coarse Silt	8.03	47.30	313.18	39.01	305.15	3.80	68.35	0.38	0.58	0.04	
29.2	Fine Sand	26.08	237.43	728.97	27.96	702.89	6.71	416.78	0.78	0.20	0.02	
36.1	Very Coarse Silt	5.52	40.45	123.61	22.38	118.09	4.10	55.67	0.32	0.63	0.05	
60.2	Very Coarse Silt	9.14	50.95	102.84	11.25	93.70	2.47	45.02	0.37	0.59	0.04	
65.3	Coarse Silt	4.79	35.15	81.21	16.95	76.42	3.52	40.93	0.21	0.74	0.05	
73.9	Very Coarse Silt	11.90	50.42	96.69	8.12	84.78	2.26	40.59	0.35	0.62	0.03	
91.1	Very Coarse Silt	5.60	40.43	84.42	15.06	78.82	2.83	39.94	0.24	0.71	0.05	
115.2	Very Coarse Silt	5.72	42.45	89.07	15.58	83.35	2.85	42.08	0.27	0.68	0.05	
132.1	Very Coarse Silt	6.29	42.66	89.46	14.23	83.17	2.81	42.02	0.27	0.68	0.05	
142.3	Very Coarse Silt	5.88	38.83	85.00	14.45	79.12	3.04	40.97	0.24	0.71	0.05	
158.2	Medium Silt	1.63	17.86	69.93	42.88	68.30	6.02	31.90	0.12	0.77	0.11	
171.3	Very Coarse Silt	6.69	47.43	102.18	15.27	95.48	2.60	44.16	0.33	0.63	0.04	
178.6	Medium Silt	0.95	11.21	64.84	68.39	63.90	7.82	28.18	0.11	0.74	0.15	
188.7	Medium Silt	0.89	12.35	63.90	71.79	63.01	9.12	32.51	0.11	0.74	0.16	
201.8	Coarse Silt	3.65	32.34	78.17	21.42	74.52	3.96	40.23	0.18	0.75	0.07	
236.7	Medium Silt	1.24	11.23	49.07	39.67	47.84	5.68	21.91	0.06	0.82	0.12	
267.2	Very Coarse Silt	10.20	61.88	111.86	10.97	101.66	2.23	48.07	0.49	0.48	0.03	
276.2	Medium Silt	1.05	14.69	63.92	61.08	62.88	6.95	30.44	0.10	0.76	0.13	
297.7	Very Coarse Silt	14.03	57.72	107.28	7.65	93.25	2.18	44.44	0.44	0.53	0.03	
337.2	Coarse Silt	3.16	28.15	90.14	28.48	86.97	5.84	46.93	0.21	0.71	0.07	
344.4	Very Coarse Silt	4.76	44.09	105.12	22.07	100.35	4.01	55.17	0.33	0.61	0.06	
421.2	Coarse Silt	5.11	39.47	87.43	17.11	82.32	3.13	42.38	0.25	0.70	0.05	
441.8	Medium Silt	1.10	13.14	64.67	58.83	63.57	6.40	26.44	0.10	0.77	0.13	
478.3	Medium Silt	0.87	18.57	79.66	91.19	78.78	10.59	42.03	0.16	0.68	0.16	
483.1	Coarse Silt	2.58	46.07	119.90	46.55	117.33	5.94	67.85	0.37	0.54	0.09	
501.2	Coarse Silt	3.64	44.57	107.08	29.43	103.44	4.42	58.03	0.34	0.59	0.07	
535.1	Coarse Silt	1.53	21.85	61.34	40.06	59.81	4.99	31.67	0.10	0.80	0.11	
587.7	Medium Silt	1.00	14.98	45.00	44.95	44.00	5.48	23.46	0.04	0.82	0.14	

Table B.10 *St. Catherine Creek NWR Core 5 grain size data*

St. Catherine Creek NWR Core 5											
Depth (cm)	Description	D10 (µm):	D50 (µm):	D90 (µm):	(D90 / D10) (µm):	(D90 - D10) (µm):	(D75 / D25) (µm):	(D75 - D25) (µm):	% SAND:	% SILT	% CLAY:
0	Coarse Silt	3.45	38.81	115.08	33.37	111.63	6.45	64.49	0.33	0.60	0.07
26.2	Very Coarse Silt	5.41	42.20	92.88	17.17	87.47	3.29	46.60	0.29	0.66	0.05
93.8	Very Coarse Silt	8.03	51.10	98.40	12.26	90.37	2.46	44.26	0.37	0.60	0.04
113.4	Medium Silt	2.02	19.85	55.99	27.76	53.97	4.83	28.80	0.07	0.83	0.10
141.7	Coarse Silt	2.37	28.37	91.01	38.34	88.64	7.71	52.09	0.23	0.68	0.09
146.7	Very Coarse Silt	6.44	52.69	106.50	16.53	100.06	2.76	50.38	0.40	0.56	0.04
153.3	Very Coarse Silt	6.25	59.87	121.71	19.47	115.46	3.01	60.31	0.47	0.48	0.04
166.5	Very Coarse Silt	6.58	57.13	114.54	17.40	107.96	2.88	55.87	0.45	0.51	0.04
186.2	Coarse Silt	3.68	30.53	70.97	19.27	67.29	3.84	36.93	0.15	0.79	0.07
206	Coarse Silt	2.98	37.90	93.11	31.28	90.13	5.97	54.34	0.27	0.65	0.08
215.9	Very Coarse Silt	7.01	45.72	88.20	12.58	81.19	2.43	39.10	0.29	0.67	0.04
227.5	Very Coarse Silt	10.36	65.67	125.18	12.09	114.83	2.34	54.22	0.53	0.44	0.03
246.6	Very Coarse Silt	8.59	56.38	109.62	12.77	101.03	2.55	50.50	0.43	0.53	0.04
250.9	Very Coarse Silt	9.40	54.03	107.93	11.48	98.53	2.60	49.63	0.41	0.55	0.04
264.9	Very Fine Sand	37.24	79.46	137.65	3.70	100.41	1.91	51.20	0.68	0.30	0.02
274.7	Very Coarse Silt	11.96	65.57	124.25	10.39	112.29	2.29	53.04	0.53	0.44	0.03
291.5	Very Coarse Silt	10.72	54.37	106.78	9.96	96.06	2.42	46.90	0.41	0.57	0.02
297.1	Coarse Silt	5.11	33.96	76.25	14.92	71.14	3.18	37.23	0.18	0.77	0.05
308.4	Coarse Silt	3.23	29.07	77.74	24.04	74.50	4.79	41.03	0.17	0.75	0.07
316.8	Very Coarse Silt	4.95	40.45	96.63	19.53	91.68	3.57	48.10	0.28	0.66	0.05
321	Very Coarse Silt	12.21	62.10	125.32	10.26	113.10	2.54	56.31	0.50	0.47	0.03
328	Very Coarse Silt	5.81	43.11	96.49	16.60	90.68	3.24	47.61	0.30	0.65	0.05
335	Very Fine Sand	40.46	87.20	151.94	3.76	111.48	1.94	57.48	0.74	0.25	0.01
351.8	Coarse Silt	3.55	27.66	77.13	21.75	73.58	4.63	39.30	0.17	0.77	0.07
365.8	Very Coarse Silt	8.89	44.80	88.92	10.00	80.03	2.50	39.80	0.29	0.68	0.03
371.6	Coarse Silt	2.61	19.58	62.50	23.95	59.89	5.20	30.90	0.10	0.82	0.08
376.1	Coarse Silt	4.92	37.90	88.13	17.93	83.21	3.52	44.10	0.24	0.71	0.05
380.5	Coarse Silt	4.73	34.56	80.99	17.12	76.26	3.30	38.94	0.20	0.75	0.06
389.3	Very Coarse Silt	5.54	39.47	82.92	14.98	77.39	2.86	39.29	0.23	0.72	0.05
395.2	Coarse Silt	3.61	28.64	69.24	19.15	65.62	3.96	35.77	0.14	0.80	0.07
415.8	Coarse Silt	3.12	24.44	66.90	21.44	63.78	4.50	33.76	0.12	0.81	0.07
424.6	Very Coarse Silt	8.01	51.17	106.63	13.31	98.61	2.88	51.19	0.38	0.58	0.04
446.6	Very Coarse Silt	10.77	63.34	122.32	11.36	111.55	2.36	52.97	0.51	0.46	0.03
456.9	Coarse Silt	3.41	22.43	69.40	20.36	65.99	5.07	34.60	0.13	0.81	0.06
467.2	Coarse Silt	2.89	37.71	111.04	38.43	108.15	9.63	67.19	0.33	0.60	0.08
481.9	Very Coarse Silt	12.86	64.59	122.65	9.53	109.79	2.28	52.20	0.52	0.45	0.03
501	Very Coarse Silt	6.14	45.72	96.55	15.74	90.41	3.00	46.88	0.32	0.64	0.04
521	Coarse Silt	3.60	23.82	72.00	20.00	68.40	4.91	36.48	0.14	0.80	0.06
530.9	Very Coarse Silt	7.41	50.30	109.31	14.76	101.90	2.84	50.44	0.37	0.59	0.04
569.8	Coarse Silt	3.14	24.39	65.66	20.91	62.52	4.45	33.67	0.11	0.81	0.08
575.3	Medium Silt	3.40	15.63	51.17	15.03	47.77	4.27	23.52	0.06	0.88	0.06
583.1	Coarse Silt	3.49	18.47	65.32	18.69	61.83	5.14	31.96	0.11	0.83	0.06
590.8	Medium Silt	2.09	17.26	53.78	25.74	51.69	5.13	27.12	0.07	0.84	0.10

WORKS CITED

- Anderson, C.P., Carter, G.A., and Waldron, M.C.B., 2022, Precise evaluation thresholds associated with salt marsh-upland ecotones along the Mississippi Gulf Coast: *Annals of the American Association of Geographers*, v. 112, no. 7, pp. 1850-1865.
- Aslan, A. and Autin, W.J., 1999, Evolution of the Holocene Mississippi River Floodplain, Ferriday, Louisiana: insights on the origin of fine-grained floodplains: *Journal of Sedimentary Research*, v. 69, no. 4, p. 800–815.
- Annan, A.P., 2009, Chapter 1: Electromagnetic principles of ground penetrating radar, in *Ground Penetrating Radar: Theory and Applications*: Oxford, UK, Elsevier Science, p. 3-40.
- Benedetto, A., and Benedetto, F., 2014, application field-specific synthesizing of sensing technology: civil engineering application of ground-penetrating radar sensing technology, *in Comprehensive Materials Processing*: Elsevier, Amsterdam, p. 393–425.
- Benedetto, F. and Tosti, F., 2013, GPR spectral analysis for clay content evaluation by the frequency shift method: *Journal of Applied Geophysics*, v. 97, p. 89–96.
- Blott, S.J. and Pye, K., 2001, GRADISTAT: a grain size distribution and statistics package for the analysis of unconsolidated sediments: *Earth Surface Processes and Landforms*, v. 26, p. 1237-1248.
- Bridge, J.S., 2003, *Rivers and floodplains; forms processes, and sedimentary record*: Oxford, Blackwell Publishing, 491 p.
- Bridge, J., 2009, Advances in fluvial sedimentology using GPR, in *Ground Penetrating Radar: Theory and Applications*: Oxford, UK, Elsevier Science, p 232-360.
- Brierley, G.J. and Fryirs, K.A., 2005, *Geomorphology and river management: applications of the river styles framework*: Oxford, Blackwell Publishing, 398 p.
- Dara, R., Kettridge, N., Rivett, M.O., Krause, S., and Gomez-Ortiz, D., 2019, Identification of floodplain and riverbed sediment heterogeneity in a meandering UK lowland stream by ground penetrating radar: *Journal of Applied Geophysics*, v. 171, no. 103863.
- Davis, R.A., 1983, *Depositional Systems: A Genetic Approach to Sedimentary Geology*: Prentice-Hall, Englewood Cliffs, New Jersey, p. 232–277.
- Dong, Y. and Ansari, F., 2011, Non-destructive testing and evaluation (NDT/NDE) of civil structures rehabilitated using fiber reinforced polymer (FRP) composites, *in*

Service Life Estimation and Extension of Civil Engineering Structures:
Woodhead Publishing, Cambridge, UK, p. 193–222.

Doolittle, J.A. and Butnor, J.R., 2009, Chapter 6: Soils, peatlands, and biomonitoring, in
Ground Penetrating Radar: Theory and Applications: Oxford, UK, Elsevier
Science, p. 179-202.

Farrell, K.M., 1987, Sedimentology and facies architecture of overbank deposits of the
Mississippi River, False River region, Louisiana: SEPM Recent Developments in
Fluvial Sedimentology, v. SP39, pp. 111-120.

Fisk, H.N., 1944, Geological investigation of the alluvial valley of the Lower Mississippi
River: U.S. Army Corps of Engineers, Mississippi River Commission, Vicksburg,
MS, 170 p.

Folk, R.L. and Ward, W.C., 1957, Brazos River bar [Texas]; a study in the significance
of grain size parameters: Journal of Sedimentary Research, v. 27, no. 1, pp. 3-26.

Heitmuller, F.T., Hudson, P.F., and Kesel, R.H., 2017, Overbank sedimentation from the
historic A.D. 2011 flood along the Lower Mississippi River, USA: Geology, v.
45, no. 2, pp. 107-110.

Horowitz, A.J., 2010, A quarter century of declining suspended sediment fluxes in the
Mississippi River and the effect of the 1993 flood: Hydrological Processes, v. 24,
p. 13–34.

Hudson, P.F., Sounny-Slittine, M.A., and LaFevor, M., 2013, A new longitudinal
approach to assess hydrologic connectivity: Embanked floodplain inundation
along the lower Mississippi River: Hydrological Processes.

Hugenschmidt, J., 2010, Ground penetrating radar for the evaluation of reinforced
concrete structures, *in* Non-Destructive Evaluation of Reinforced Concrete
Structures, Woodhead Publishing, Cambridge, UK, p. 317 –333.

Kelk, R., 2022, Sedimentary characteristics and associated carbon and nutrients of
overbank sediments deposited during the 2018, 2019, and 2020 floods in
embanked floodplains along the Lower Mississippi River near Natchez,
Mississippi: The University of Southern Mississippi Master's Theses.

Keown, M.P., Dardeau, Jr., E.A., and Causey, E.M., 1986, Historic trends in the sediment
flow regime of the Mississippi River: Water Resources Research, v. 22, no. 11, p.
1555– 1564.

Kesel, R.H., 2003, Human modifications to the sediment regime of the Lower Mississippi
River flood plain: Geomorphology, v. 56, p. 325–334.

- Kesel, R.H., Dunne, K.C., McDonald, R.C., Allison, K.R., and Spicer, B.E., 1974, Lateral erosion and overbank deposition on the Mississippi River in Louisiana caused by 1973 flooding: *Geology*, v. 2, no. 9, p. 461–464.
- Mahmoodian, M., 2018, Pipeline Inspection and Maintenance, *in* Reliability and Maintainability of In-Service Pipelines, Gulf Professional Publishing, Houston, TX, p. 49–79.
- Meade, R.H. and Moody, J.A., 2010, Causes for the of suspended-sediment discharge in the Mississippi River system, 1940-2007: *Hydrological Processes*, v. 24, p. 35–49.
- Morton, R. and White, W.A., 1997, Characteristics of and corrections for core shortening in unconsolidated sediments, *Journal of Coastal Research*, v. 13, no. 3, p. 761-769.
- Munoz, S.E., Giosan, L., Therrell, M.D., Remo, J.W.F., Shen, Z., Sullivan, R.M., Wiman, C., O'Donnell, M., and Donnelly, J.P., 2018, Climatic control of Mississippi River flood hazard amplified by river engineering: *Nature*, v. 556, p. 95–98.
- National Oceanographic and Atmospheric Administration (NOAA), 2020, National Weather Service: Mississippi River at Natchez at <https://water.weather.gov/ahps2/hydrograph.php?gage=ntzm6&wfo=jan>. (Accessed Jun 23, 2023).
- National Resources Conservation Service (NRCS), 2024, Entisols: U.S. Department of Agriculture, <https://www.nrcs.usda.gov/conservation-basics/natural-resource-concerns/soils/entisols#:~:text=Entisols%20are%20soils%20that%20show,are%20sandy%20or%20very%20shallow.> (Accessed May 22, 2024).
- Nobes, D.C., Ferguson, R.J., and Brierley, G.J., 2001, Ground-penetrating radar and sedimentological analysis of Holocene floodplains: insights from the Tuross Valley, New South Wales: *Australian Journal of Earth Sciences*, v. 48, pp. 347-355.
- Okazaki, H., Kwak, Y., and Tamura, T., 2015, Depositional and erosional architectures of gravelly braid bar formed by a flood in the Abe River, central Japan, inferred from a three-dimensional ground-penetrating radar analysis: *Sedimentary Geology*, v. 324, p. 32–46.
- Patrick, D.M., Smith, L.M., and Whitten, C.B., 1982, Methods for studying accelerated fluvial change, *in* Gravel-bed Rivers: John Wiley and Sons, Ltd., New York, pp. 738-815.
- Pinter, N., Ickes, B.S., Wlosinski, J.H., van der Ploeg, R.R., 2006, Trends in flood stages: Contrasting results from the Mississippi and Rhine River systems: *Journal of Hydrology*, v. 331, p. 554–566.

- Provost, L.A., Eisemann, E.R., Anderson, C.P., and Waldron, M.C.B., 2022, Wrack placement to augment constructed dunes: a field investigation: *Frontiers in Built Environment*, v. 8, 907608.
- Reimer, P.J., Brown, T.A., and Reimer, R.W., 2004, Discussion: Reporting and calibration of post-bomb ^{14}C data: *Radiocarbon*, v. 46, no. 3, p. 1299-1304.
- Remo, J.W.F, Pinter, N., and Heine, R., 2009, The use of retro- and scenario-modeling to assess effects of 100+ years of river engineering and land-cover change on Middle and Lower Mississippi River flood stages: *Journal of Hydrology*, v. 376, p. 403–416.
- Roudi, A.M., Moussavi-Harami, R., Mahboubi, A., and Motamed, A., 2012, Using of ground penetrating radar (GPR) and sediment cores as method interpretation of sedimentary environments the estuaries of northern west Oman Sea: *Research Journal of Environmental and Earth Sciences*, v. 4, no. 5, p. 500–510.
- Russell, C., Waters, C.N., Himson, S., Holmes, R., Burns, A., Zalasiewicz, J., and Williams, M., 2021, Geological evolution of the Mississippi River into the Anthropocene: *The Anthropocene Review*, v. 8, no. 2, p. 115–140.
- Sambrook Smith, G.H., Best, J.L., Ashworth, P.J., Lane, S.N., Parker, N.O., Lunt, I.A., Thomas, R.E., and Simpson, C.J., 2010, Can we distinguish flood frequency and magnitude in the sedimentological record of rivers?: *Geology*, v. 38, no. 7, p. 579–582.
- Saucier, 1994, *Fluvial Environments and Processes, in Geomorphology and Quaternary Geologic History of the Lower Mississippi Valley*, U.S. Army Corps of Engineers, Mississippi River Commission, Vicksburg, MS, v. 2, p. 87–128.
- Svetlik, I., Jull, A.J.T., Molnar, M., Povinec, P.P., Kolar, T., Demjan, P., Pachnerova Brabcova, K., Brychova, V., Dreslerova, D., Rybnicek, M., and Simek, P., 2019, The best possible time resolution: how precise could a radiocarbon dating method be?: *Radiocarbon*, v. 61, no. 6, p. 1729–1740.
- (a) U.S. Army Corps of Engineers (USACE), 2023, Mississippi River Commission (MRC) History, <https://www.mvd.usace.army.mil/About/Mississippi-River-Commission-MRC/History/>. (Accessed Jul 5, 2023).
- (b) U.S. Army Corps of Engineers (USACE), 2023, Mississippi River Tributaries Project, <https://www.mvd.usace.army.mil/About/Mississippi-River-Commission-MRC/Mississippi-River-Tributaries-Project-MR-T/>. (Accessed Jul 5, 2023).
- (c) U.S. Army Corps of Engineers (USACE), 2023, RiverGages.com Mississippi River @ Natchez, MS, <https://rivergages.mvr.usace.army.mil/WaterControl/stationinfo2.cfm?sid=CE4103F4&fid=NTZM6&dt=S>. (Accessed Jul 21, 2023).

(d) U.S. Army Corps of Engineers (USACE), 2023, RiverGages.com Mississippi River @ Vicksburg, MS, <https://rivergages.mvr.usace.army.mil/WaterControl/stationinfo2.cfm?dt=S&sid=CE40FF58&fid=NTZM6#:~:text=Flood%20Stage%3A43.0%20Ft.,Record%20High%20Stage%3A57.1%20Ft.> (Accessed Jul 21, 2023).

U.S. Army Corps of Engineers (USACE), 2024, Mississippi Valley Division: Army Corps of Engineers announces end of low-water drought in Mississippi Valley Division, <https://www.mvd.usace.army.mil/Media/News-Releases/Article/3665123/army-corps-of-engineers-announces-end-of-low-water-drought-in-mississippi-valle/>. (Accessed May 21, 2024).

Walling, D. and Foster, I., 2016, Chapter 9: Using environmental radionuclides, mineral magnetism and sediment geochemistry for tracing and dating fine fluvial sediments, *in* Tools in Fluvial Geomorphology, John Wiley and Sons, Hoboken, NJ, p. 182–209.